Natural Product Reports

ROYAL SOCIETY OF CHEMISTRY

REVIEW

View Article Online
View Journal | View Issue

Cite this: *Nat. Prod. Rep.*, 2025, **42**, 1136

Configurational assignments of type-I polyketide synthase (PKS)-derived natural products based on spectroscopic and chemical analysis: methodologies and case studies

Jinsheng Cui,†[a] Prima F. Hillman,†[b] Geum Jin Kim,†[c] Thinh T. M. Bui,†[d] Kyuho Moon,*[d] Sang-Jip Nam,*[e] Hyukjae Choi*[f] and Dong-Chan Oh*[a]

Covering: 1992 to 2024

Type-I polyketide synthase (PKS)-derived metabolites are structurally diverse bioactive natural products containing multiple stereogenic centres. This review focuses on the configurational analysis of type-I PKS-derived natural products, emphasizing the methodologies and challenges associated with determining their stereochemistry due to their complex structures with multiple chiral centres. Key strategies include *J*-based configuration analysis (JBCA), chemical derivatizations with chiral reagents, degradation methods, NMR spectroscopic analysis, and the exploitation of chiroptical properties. Case studies demonstrate the practical applications of these methods in elucidating the stereochemistry of type-I polyketide natural products.

Received 31st October 2024

DOI: 10.1039/d4np00061g

rsc.li/npr

[a]*Natural Products Research Institute, College of Pharmacy, Seoul National University, Seoul, 08826, Republic of Korea. E-mail: dongchanoh@snu.ac.kr*

[b]*Department of Chemistry, Faculty of Mathematics and Natural Sciences, Universitas Andalas, Kampus Limau Manis, Padang, 25163, Indonesia*

[c]*Department of Pharmacology, School of Medicine, Dongguk University, Gyeongju, Gyeongsangbukdo, 38066, Republic of Korea*

[d]*College of Pharmacy, Kyung Hee University, Seoul, 02447, Republic of Korea. E-mail: kmoon@khu.ac.kr*

[e]*Department of Chemistry and Nanoscience, Ewha Womans University, Seoul, 03760, Republic of Korea. E-mail: sjnam@ewha.ac.kr*

[f]*College of Pharmacy and Research Institute of Cell Culture, Yeungnam University, Gyeongsan, Gyeongsangbukdo, 38541, Republic of Korea. E-mail: h5choi@yu.ac.kr*

† These authors contributed equally to this work.

1. Introduction

Polyketides represent a diverse and structurally complex class of secondary metabolites produced by a wide range of microorganisms (actinobacteria, cyanobacteria, and fungi), plants, and marine organisms (sponges and dinoflagellates). These compounds are synthesized through polyketide synthases (PKSs), a family of multifunctional enzymes that catalyse the stepwise polymerization of acyl-CoA precursors. Polyketides exhibit remarkable structural diversity owing to the flexibility of their biosynthetic pathways and the remarkable diversity of post-modifications mediated by tailoring enzymes.[1,2] The significance of polyketides extends not only to their structural complexity but also to their potent biological activities and their pivotal roles in medicine and biotechnology. Their utility also spans agricultural applications, where they function as natural pesticides and growth regulators.

Among the various classes of polyketides, those synthesized by type-I polyketide synthases (PKSs) have garnered considerable attention owing to their complex structures and intricate biosynthetic pathways. These type-I PKS-derived polyketides

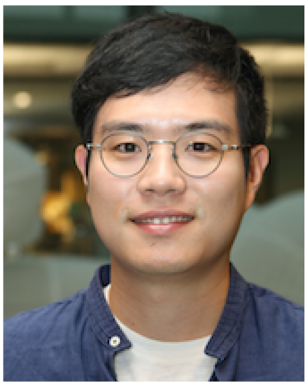

Kyuho Moon

Kyuho Moon is an assistant professor at the College of Pharmacy, Kyung Hee University, since 2024. He received his PhD degree in Seoul National University under Prof. Dong-Chan Oh's guidance in 2016. In the same year, he joined Prof. Mohammad Seyedsayamdost's group in the Department of Chemistry, Princeton University, as a postdoctoral researcher. His research is focused on microbial natural products, chemical biology, specifically discovering cryptic microbial secondary metabolites and investigation of bacteria in unreported habitats.

Sang-Jip Nam

Sang-Jip Nam is currently a professor at Chemistry and Nanoscience Department, Ewha Womans University, Korea, since 2013. He received his MS degree (2001) and PhD degree (2006) from Seoul National University, Korea. In 2007, he joined as a postdoc in the Prof. William Fenical Lab., Scripps Institution of Oceanography, University of California, San Diego. In 2012, he was appointed as an assistant professor at the College of Pharmacy, Sunchon National University. His research interests are in the discovery and development of natural products as potential treatments for diseases.

Hyukjae Choi

Hyukjae Choi earned his BS in oceanography at Seoul National University. He received his MS (2001) and PhD (2009) in marine natural products chemistry at Seoul National University under the supervision of Prof. Heonjoong Kang. After a postdoctoral fellowship (2009–2012) with Prof. William H. Gerwick at Scripps Institution of Oceanography, he joined Yeungnam University's College of Pharmacy as a faculty member in 2012. His research focuses on the discovery and structure elucidation of bioactive compounds from diverse natural sources.

Dong-Chan Oh

Dong-Chan Oh earned a BS degree in Oceanography as well as an MS degree in Marine Chemistry, from Seoul National University, Republic of Korea. He completed his doctoral studies in Marine Natural Products Chemistry in 2006 under the mentorship of Professor William Fenical at the Scripps Institution of Oceanography, University of California, San Diego. Following this, he pursued postdoctoral research in the laboratory of Professor Jon Clardy at Harvard Medical School. In 2009, he commenced his independent academic career at the College of Pharmacy, Seoul National University, where his research focuses on the discovery, structural elucidation, and stereochemical analysis of new bioactive natural products from microbial sources. From 2012 to 2017, he was recognized as a Howard Hughes Medical Institute International Early Career Scientist. Dong-Chan Oh formerly held the position of Director of the Natural Products Research Institute, Seoul National University from 2019 to 2025. Currently, he is a Full Professor in the College of Pharmacy at Seoul National University.

often contain multiple chiral centres, which result from their biosynthesis through the stepwise assembly of polyketide chains *via* elongation and modification processes mediated by PKSs. These PKSs are multi-enzyme complexes that utilize a combination of starter and extender units, typically acetyl-CoA and malonyl-CoA, to introduce chiral centres into the growing polyketide chain.[3] Furthermore, the actions of tailoring enzymes, such as oxidases, reductases, methyltransferases, and cyclases, further modify the polyketide backbone, resulting in the formation of multiple stereogenic centres. These enzymatic modifications contribute to the remarkable structural diversity and chirality of type-I PKS-derived polyketides.[4]

While the configurational diversity of type-I PKS-derived polyketides enhances their therapeutic potential, it introduces notable challenges in their structural elucidation.[3,4] This stereochemical complexity often arises from several factors, including the presence of multiple chiral centres, existence of remote stereogenic centres, unanticipated conformational changes, stereochemistry derived from hybrid biosynthetic pathways, and instability.

Consequently, analysing the absolute configurations of type-I PKS-derived polyketides is an essential but daunting task. For instance, during derivatization, eliminating alcohol groups can lead to misinterpretations, while generating multiple methoxy(trifluoromethyl)phenylacetyl (MTPA, Mosher's reagent) derivatives can complicate the analysis and yield incorrect stereochemical predictions.[5] A notable example of this complexity is gibbosol, a super carbon-chained polyketide, which features multiple hydroxy chiral centres along its extended carbon chain, making the determination of its absolute configuration particularly difficult (Fig. 1).[6] Polyketides that are unstable typically have specific structural or chemical features, making them reactive or susceptible to environmental factors. The instability of these compounds is often attributed to the presence of functional groups or molecular configurations that are highly reactive or sensitive to pH, temperature, light, or enzymatic degradation. Common features of unstable and easily degradable polyketides include epoxides, unsaturated conjugations, lactones, glycosylated polyketides, halogenated polyketides, *etc.* Hence, acquiring a comprehensive understanding of these challenges is crucial for developing reliable methods to characterize these compounds, harness their bioactive properties for pharmaceutical applications, and establish accurate synthetic targets for total synthesis.

This review aims to offer insights into the complexities and methodologies involved in the analysis of type-I PKS-derived natural products, underscoring the critical need for robust analytical techniques. We introduce several prominent methods employed by researchers in recent decades to examine the stereochemistry of type-I PKS-derived polyketides, including *J*-based configuration analysis, chiral derivatizations, chemical degradation, NMR shift comparisons with universal databases, and chiroptical analysis paired with quantum mechanical calculations. Through several case studies, we demonstrate the practical application of these techniques in resolving relative and absolute configurations, offering valuable insights into stereochemical structural elucidation.

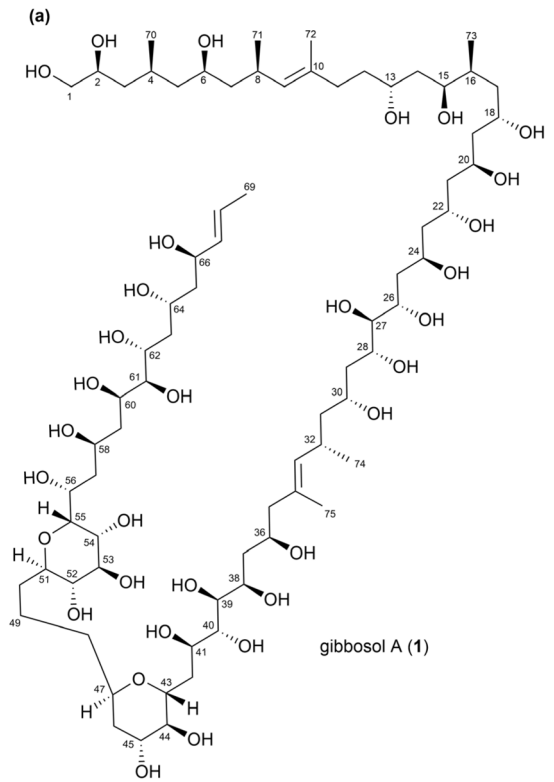

Fig. 1 (a) Structure of gibbosol A (**1**).

2. Methods and strategies for configurational analysis of type-I PKS-derived natural products

2.1. *J*-based configuration analysis (JBCA)

2.1.1. General aspects of JBCA. Nuclear magnetic resonance (NMR) spectroscopy is a non-destructive analytical technique widely used for the structure elucidation of organic compounds, including natural products. In particular, vicinal ^{1}H–^{1}H coupling constants ($^{3}J_{H,H}$) and nuclear Overhauser effects (NOEs) derived from NMR spectra offer critical insights into the relative configurations of small and rigid natural products. However, type-I PKS-derived acyclic or macrocyclic natural products typically possess highly flexible structures, leading to diverse stable conformers that complicate relative configuration analysis. To address this challenge, in 1999, Murata and colleagues introduced a JBCA strategy utilizing two- and three-bond heteronuclear coupling constants ($^{2}J_{H,C}$ and $^{3}J_{H,C}$) to enhance the completeness of relative configuration assignments, which were previously based on $^{3}J_{H,H}$ values and NOEs (Fig. 2).[7]

Notably, the value of $^{3}J_{H,H}$ depends on the dihedral angles of protons, as described by the Karplus equation.[8] Similarly, $^{3}J_{H,C}$ values also exhibit a Karplus-like dependency on dihedral angles. Although $^{2}J_{H,C}$ values are typically independent of dihedral angles, this dependence becomes relevant when the α-

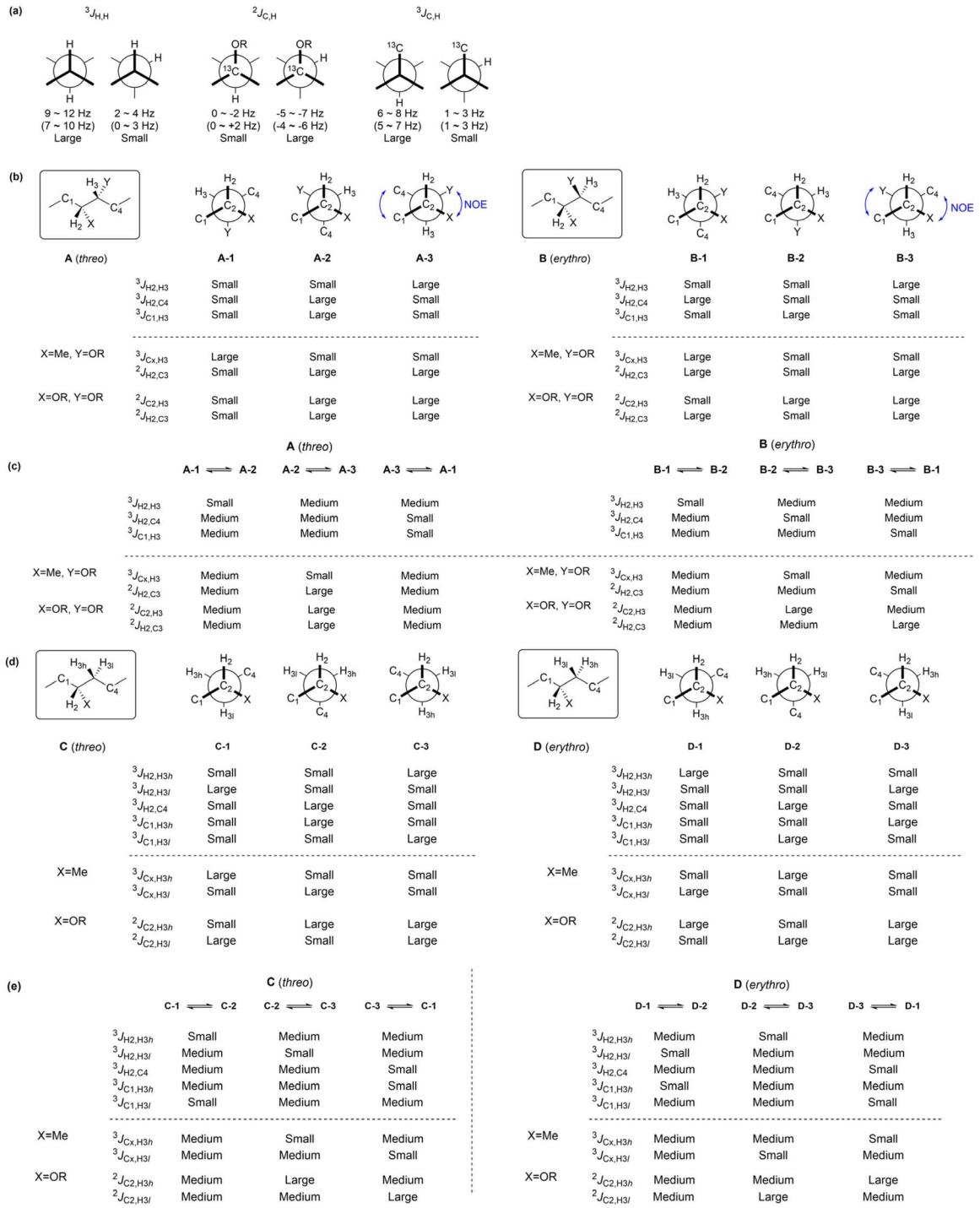

Fig. 2 Murata's JBCA strategy: (a) dihedral angle dependence of spin-coupling constants, $^3J_{H,H}$ and $^{2,3}J_{C,H}$ (values in parentheses correspond to the 1,2-dioxygenated systems. R represents H, alkyl, or acyl groups). (b) Dependence of $^3J_{H,H}$ and $^{2,3}J_{C,H}$ on the dihedral angles between vicinal methine carbons in 2,3-disubstituted butane systems. (c) Dependence of $^3J_{H,H}$, and $^{2,3}J_{C,H}$ on the dihedral angles between vicinal methine carbons in alternating butane systems. (d) Dependence of $^3J_{H,H}$ and $^{2,3}J_{C,H}$ on the dihedral angles between methine and methylene carbons in 2-substituted butane systems. (e) Dependence of $^3J_{H,H}$ and $^{2,3}J_{C,H}$ on the dihedral angles between methine and methylene carbons in alternating butane systems.

carbon is bonded to an electronegative atom, such as O, N, or a halogen. In such cases, the $^2J_{H,C}$ value depends on the dihedral angle between the proton and the electronegative atom on the α-carbon.[9,10]

Notably, Murata's JBCA strategy was originally designed to determine the relative configurations of two adjacent (1,2) or alternately positioned (1,3) stereogenic carbons substituted with hydroxy, alkoxy, or methyl groups in acyclic compounds.[7]

In 1,2-methine systems, as illustrated in Fig. 2b, six possible staggered rotamers exist for the 2,3-disubstituted butane stereoisomers. Among these, the two rotamers in the *threo* configuration (A-1 and A-2) and the two others in the *erythro* configuration (B-1 and B-2) can be distinctly identified based on the $^{3}J_{H,H}$ and $^{2,3}J_{C,H}$ values. Although rotamers A-3 (in *threo*) and B-3 (in *erythro*) cannot be uniquely assigned using only the $^{3}J_{H,H}$ and $^{2,3}J_{C,H}$ values, they can be differentiated based on the NOE (or rotating-frame Overhauser effect (ROE)) correlations among the protons located at the C1, X, Y, and C4 positions. A moderate $^{3}J_{H,H}$ value suggests that two protons are distributed between two predominant rotamers with *anti* and *gauche* orientations. As depicted in Fig. 2c, four pairs of rotamers (A-2/A-3, A-3/A-1, B-2/B-3, and B-3/B-1) can be clearly distinguished based on $^{3}J_{H,H}$ and $^{2,3}J_{C,H}$ values. However, for the rotameric pairs A-1/A-2 and B-1/B-2, which feature a *gauche* conformation between H2 and H3, the relative configurations cannot be resolved using $^{3}J_{H,H}$ and $^{2,3}J_{C,H}$ values. Notably, these unresolved rotamer pairs are thermodynamically less favored because their substituents at C2 and C3 lie on the same side. For 1,3-methine systems, the JBCA approach is applicable if the two methylene protons are magnetically distinct and thus can be stereospecifically assigned. In these cases, the relative positions of each diastereotopic methylene proton between the two adjacent methines can be distinguished among the six possible conformers using $^{3}J_{H,H}$ and $^{2,3}J_{C,H}$ values and NOE/ROE correlations, as illustrated in Fig. 2d. Similar to 1,2-methine systems, moderate $^{3}J_{H,H}$ values in 1,3-methine systems suggest the presence of multiple rotamers (Fig. 2e). Rotameric exchange is commonly observed between C-1/C-3 or D-1/D-3, while other pairs, such as C-2 and D-2, are thermodynamically less stable and hence less frequently encountered. The JBCA method is also applicable to 1,4-methine systems, provided an ethylene linker is present between the two methine carbons and all relevant proton signals in the ^{1}H NMR spectrum are stereospecifically assigned without overlapping.[11] Furthermore, previous studies have extended the application scope of the JBCA to stereogenic carbons bonded to alkyl groups or electronegative atoms such as N, S, and Cl.[10–15]

2.1.2. Measurements of vicinal ^{1}H–^{1}H coupling constants. Homonuclear coupling constants between vicinal protons ($^{3}J_{H,H}$) in acyclic compounds depend on the dihedral angle between the two protons. These constants are extensively utilized for the configurational analysis of small organic compounds. Generally, when the multiplets in ^{1}H NMR spectra are well-resolved without any overlaps, $^{3}J_{H,H}$ values can be easily determined from the spectra. However, the ^{1}H NMR spectra of type-I PKS-derived natural products often exhibit substantial signal congestion owing to overlapping proton resonances. To address these challenges, one-dimensional (1D) NMR spectroscopies using selective pulse sequences, such as 1D total correlation spectroscopy (TOCSY), 1D nuclear Overhauser effect spectroscopy (NOESY), and 1D rotating-frame Overhauser effect spectroscopy (ROESY),[16,17] are employed. Other advanced methods include homonuclear *J*-resolved NMR spectroscopy[18,19] and phase-sensitive two-dimensional NMR spectroscopies, such as phase-sensitive double-quantum filtered correlation spectroscopy (DQF-COSY) and exclusive COSY (E.COSY).[20,21]

Notably, selective irradiation pulse techniques—including 1D TOCSY, 1D NOESY, and 1D ROESY—are effective in eliminating the multiplicity associated with the irradiated proton signals,[16,17] thereby resolving overlapping signals and simplifying the ^{1}H NMR spectra for precise *J* value measurements.

Meanwhile, homonuclear *J*-resolved NMR spectroscopy separates chemical shifts (δ) along the f_2 axis and coupling constants (*J*) along the f_1 axis.[18] This separation eliminates overlapping multiplet patterns along the f_2 axis, transforming all proton signals into singlets at their corresponding chemical shifts. In this scenario, multiplicity information is retained along the f_1 axis, allowing the measurements of *J* values. Nevertheless, homonuclear *J*-resolved NMR spectroscopy often exhibits tilting patterns caused by proton couplings along both the f_1 and f_2 axes.[19] To address this issue, post-processing techniques, such as t_1-noise reduction and tilting correction at an angle of 45°, are required.

Notably, phase-sensitive DQF-COSY is a powerful technique for measuring *J* values owing to its ability to generate high-resolution crosspeak multiplets with a pure absorption lineshape.[20] Interestingly, the diagonal peaks in DQF-COSY also display an *anti*-phase absorption lineshape, suppressing the tailing commonly observed in standard COSY spectra. This suppression enhances spectral clarity near the diagonal peaks.[21]

Compared to DQF-COSY, E.COSY offers simpler crosspeak multiplet patterns. By employing E.COSY, both the magnitudes and signs of $J_{H,H}$ values can be accurately determined in complex spin systems.[22–24]

2.1.3. Measurements of two- and three-bond heteronuclear coupling constants ($^{2}J_{H,C}$ and $^{3}J_{H,C}$). Two- and three-bond heteronuclear coupling constants between protons and carbons ($^{2}J_{C,H}$ or $^{3}J_{C,H}$) are crucial for the configuration analysis of small organic compounds. These coupling constants can be determined using various 2D NMR techniques, including hetero-(ω1)-half-filtered TOCSY (HETLOC),[25] carbon-sorted HETLOC (also known as heteronuclear single quantum coherence (HSQC)–HECADE),[26] *J*-heteronuclear multiple bond correlation (*J*-HMBC),[27] in-phase anti-phase-heteronuclear single quantum multiple bond correlation (IPAP–HSQMBC),[28] HSQC–TOCSY,[29] phase-sensitive HMBC,[30–32] exclusive spin-difference experiment (EXSIDE),[33] and ^{13}C band-selective (SelEXSIDE),[34] and long-range optimized HSQC–COSY.[35]

Among these, HETLOC yields a 2D ^{1}H–^{1}H spectrum that reveals $^{n}J_{C,H}$ values through E.COSY-type splitting. This experiment enables the determination of both the magnitudes and signs of $^{1}J_{C,H}$ and $^{2,3}J_{C,H}$ based on signal displacements along the f_1 and f_2 dimensions, respectively.[25] HETLOC is relatively sensitive and can produce spectra at millimolar concentrations. Consequently, HETLOC is a popular choice for measuring $^{2,3}J_{C,H}$ values in configurational studies owing to its high sensitivity and relatively simple data analysis. However, HETLOC relies on TOCSY transfer, which limits its applicability to measuring $^{n}J_{C,H}$ values only between protons and protonated carbons. Consequently, HETLOC is incapable of measuring $^{2,3}J_{C,H}$ values for non-protonated carbons. Furthermore,

frequent signal overlap in HETLOC spectra can interfere with precise J value measurements. Moreover, if the ^{1}H–^{1}H vicinal coupling constant ($^{3}J_{H,H}$) is small, the crosspeak intensity in HETLOC may be substantially reduced.

HSQC–HECADE spectra display E.COSY-type crosspeaks, making the HSQC–HECADE technique inherently similar to HETLOC. However, in HECADE, the f_1 dimension represents the ^{13}C NMR spectrum, allowing signals to disperse over a wider spectral range compared to HETLOC,[26] thereby mitigating spectral crowding and accidental overlaps. Nevertheless, similar to HETLOC, this technique employs TOCSY transfer, which prevents the measurement of $^{2,3}J_{C,H}$ values for non-protonated carbons or heteroatoms. Furthermore, the heteronuclear coupling magnitude in HECADE depends on the ^{1}H–^{1}H vicinal coupling constant ($^{3}J_{H,H}$), similar to that in HETLOC, which is a limitation of this approach.

In contrast, J-HMBC generates a 2D ^{1}H–^{13}C spectrum, where the crosspeaks are split along the f_1 dimension, with the distance being proportional to the $^{n}J_{C,H}$ value. This distance can be adjusted by modifying J-scaling factors in experimental parameters, enabling the measurement of $^{n}J_{C,H}$ values without requiring high resolution in the f_1 dimension.[27] J-HMBC does not rely on TOCSY transfer and allows the measurement of $^{n}J_{C,H}$ values between specific protons and both protonated and non-protonated carbons not linked by TOCSY transfers. Additionally, J-HMBC can provide information on the signs of $^{n}J_{C,H}$ values in a single experiment. However, while determining $^{n}J_{C,H}$ values based on the distance between two split crosspeaks is straightforward, identifying their signs is still challenging. Other drawbacks of this technique include accidental signal overlaps owing to peak doubling and relatively lower sensitivity compared to HETLOC.

The IPAP–HSQMBC technique involves acquiring two separate 2D ^{1}H–^{13}C spectra—one with IP data and the other with AP data.[28] Once recorded, these datasets are subsequently added and subtracted to produce α- and β-HSQMBC spectra, respectively. The displacement of crosspeaks between the α/β-HSQMBC spectra along the f_2 dimension provides both the magnitudes and the signs of $^{n}J_{C,H}$ constants.[28] By examining crosspeaks from separate spectra, IPAP–HSQMBC reduces the likelihood of accidental overlaps, leading to more accurate measurements of $^{n}J_{C,H}$. Similar to J-HMBC, this technique can measure $^{n}J_{C,H}$ values independent of carbon protonation. However, it requires selective or band-selective excitation and multiple experiments, increasing the complexity of the measurement.

2.1.4. Case studies of JBCA. Formicolides A (**2**) and B (**3**) are macrolides isolated from the gut bacterium *Streptomyces* sp. BA01, which inhabits wood ants. These compounds exhibit quinone-reductase-inducing and antiangiogenic activities (Fig. 3).[36] Formicolide A (**2**) possesses a 20-membered polyene macrolide structure featuring a highly branched tetrahydropyran (THP) moiety. The relative configurations within the THP moiety at positions C21, C22, C23, and C25 were determined based on ^{1}H–^{1}H vicinal coupling constants and ROESY correlations among axially oriented protons. To extend the relative configuration assignment from C21 to C19 and C20, the

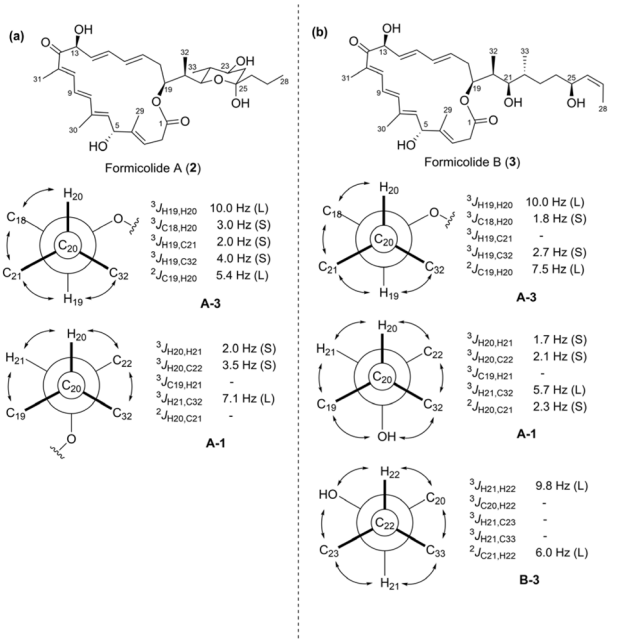

Fig. 3 Application of JBCA for the relative configuration assessment of formicolides: (a) C19–C21 of formicolide A and (b) C19–C22 of formicolide B. Newman projections were adapted from the original report and re-drawn as indicated in the JBCA models.

JBCA strategy was adopted, as illustrated in Fig. 3. Notably, both C19 and C21 are oxygenated, while C20 is attached to a methyl branch. During the JBCA, a 1,2-methine system model was employed for the configurational analyses of C19–C20 and C20–C21. The $^{3}J_{H,H}$ values for **2** were measured by inspecting the ^{1}H NMR spectrum, while the $^{2,3}J_{H,C}$ values were obtained using HETLOC and HSQC–HECADE, as C19–C21 are all protonated. The large vicinal coupling constant observed between H19 and H20 confirmed their *anti* positioning. Furthermore, the large coupling constants (5.4 Hz) between H20 and C19, alongside the small values of $^{3}J_{C18,H20}$, $^{3}J_{H19,C21}$, and $^{3}J_{H19,C32}$ aligned well with those for the A-3 and B-3 rotamers among the six model rotamers. The observed ROESY correlations of H21 with H18a and H18b eliminated the B-3 case, and the relative configurations of C19–C20 were assigned to the A-3 rotamer, as illustrated in Fig. 3a. Additional H18a/H20, H19/H21, and H19/H32 ROESY correlations further supported this A-3 assignment. The relative configurations between C20 and C21 were assigned to an A-1 rotamer based on the small $^{3}J_{H20,H21}$ and $^{3}J_{H20,C22}$ values, along with the large $^{3}J_{H21,C32}$ value. This assignment was corroborated by the H21/H19, H21/H20, H20/H22, and H22/H32 ROESY correlations. Consequently, the relative configuration of formicolide A (**2**) was assigned as 19*S**, 20*R**, and 21*R**. Formicolide B (**3**) also features a 20-membered polyene macrolide structure but lacks the THP moiety. Instead, it possesses an extended branched carbon chain. Similar to formicolide A, the relative configurations of C19–C22 in formicolide B were determined using the JBCA with a 1,2-methine system, as illustrated in Fig. 3b. Given that the $^{3}J_{H,H}$ and $^{2,3}J_{H,C}$ values for C19–C21 in formicolide B resembled those in formicolide A, the

C19–C20 and C20–C21 configurations were assigned as A-3 and A-1 rotamers, respectively. Although large $^{3}J_{H21,H22}$ and $^{2}J_{C21,H22}$ values indicated the possibility of both A-3 and B-3 rotamers for C21–C22, the observed H33/H20 and H23/21-OH ROESY correlations supported only the B-3 rotamer. Hence, the relative configurations of C19–C22 in formicolide B were assigned as 19*S**, 20*R**, 21*R**, and 22*R**. Further determination of other stereogenic centres in formicolides will be discussed in Section 2.4.3.

Strasseriolides A–D (**4**–**7**) are 18-membered macrolides isolated from the endophytic fungus *Strasseria geniculate* CF-247251. These macrolides exhibit antimalarial activity against *Plasmodium falciparum* without cytotoxic effects on the HepG2 cell line (Fig. 4a).[37] The planar structures of compounds **4**–**7** were elucidated through an integrative analysis of mass spectrometry (MS) and NMR (^{1}H, ^{13}C, HSQC, COSY, HMBC, and NOESY) data. Notably, the absolute configuration of compound **5** was determined using X-ray crystallography, while those of **4** and **6** were inferred based on similarities in NMR data, including chemical shifts and NOESY correlations. Strasseriolide D (**7**) comprises an additional stereogenic centre at C13. The relative configurations of C13 and C14 were determined using the JBCA strategy. The $^{3}J_{H,H}$ values of overlapping multiplets in compound **7** were estimated using *J*-resolved NMR spectroscopy and 1D TOCSY, while the $^{2,3}J_{H,C}$ values were accurately determined by *J*-HMBC with a scaling factor of 60. Notably, the measured $^{3}J_{H,H}$ and $^{2,3}J_{H,C}$ values between relevant nuclei indicated that the relative orientation between C13 and C14 can adopt either the A-3 or B-3 rotameric conformation. A NOESY correlation between H12a and H15 confirmed the presence of the A-3 rotameric conformation. Based on this, the absolute configurations of compound **7** were determined to be 2*R*, 3*S*, 6*S*, 8*R*, 11*R*, 13*S*, 14*S*, and 18*S*.

The authors attempted to extend the relative configuration assignment from C11 to C13 in compound **7** using a 1,3-methine system. However, this approach was unsuccessful owing to discrepancies in the $^{3}J_{H,H}$ and $^{2,3}J_{H,C}$ values around the C12–C13 bond ($^{3}J_{H12b,H13}$ = 8.0 Hz for *anti*-orientation between H12b and H13; $^{3}J_{C11,H13}$ = 6.4 Hz for *anti*-orientation between C11 and H13). These inconsistencies were attributed to a partially eclipsed relative orientation between H13 and C11, highlighting the limitations of JBCA in dealing with cyclic compounds featuring fixed conformations that include non-staggered rotamers.

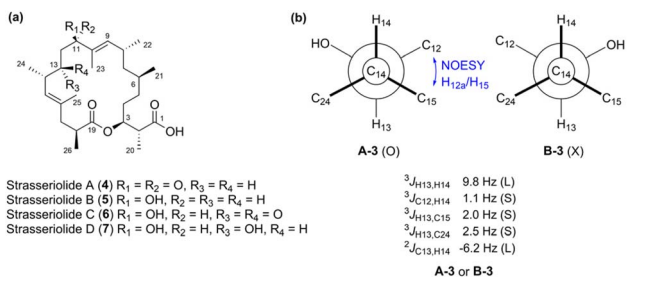

Fig. 4 Application of JBCA for the relative configuration assessment of strasseriolide D: (a) structures of strasseriolides A–D (**4**–**7**). (b) JBCA-based assessment of the relative configuration of C13–C14 in strasseriolide D (**7**).

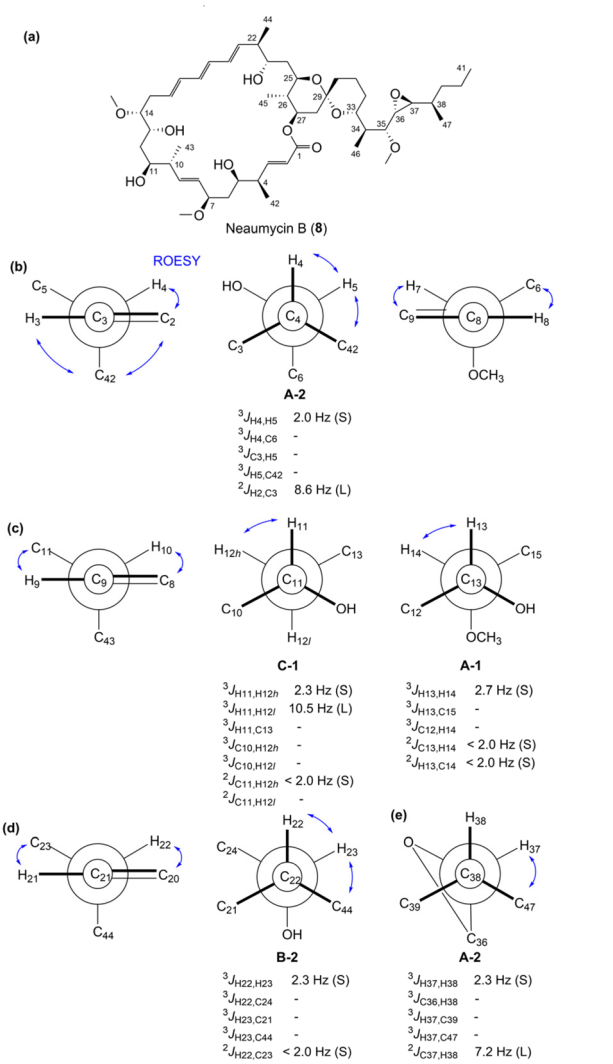

Fig. 5 Application of JBCA for the relative configuration assessment of neaumycin B: (a) Chemical structure of neaumycin B. Application of JBCA for the configurational assessment of the (b) C4–C7, (c) C10–C14, (d) C21–C23, and (e) C37–C38 positions.

Neaumycin B (**8**), a cytotoxin isolated from the marine-derived *Micromonospora* sp. CNY-010, is a polycyclic polyketide possessing a complex structure comprising an epoxide, two tetrahydropyran rings connected by a spiroketal, and a 28-membered macrolide, as depicted in Fig. 5a.[38,39] This polyketide has a highly intricate architecture with 19 chiral centres. One of its congeners, neaumycin A, was first reported in 2012,[40] and its planar structure was substantially revised in 2015.[39] Along with the structural revision of neaumycin A, the structures of neaumycins B and C were also reported in 2015. However, the absolute configurations of these neaumycins were not comprehensively assessed at that time. In 2018, Fenical and co-workers comprehensively determined the absolute configurations of neaumycin B by integrating the stereospecificities of biosynthetic enzymes with extensive NMR data analysis.[38] In

particular, the relative configurations at C4–C7, C10–C14, C22–C25, and C37–C38 were separately assigned based on the JBCA and ROESY correlations. The authors measured $^{2,3}J_{H,C}$ values using HETLOC and $^{3}J_{H,H}$ values from ^{1}H NMR data and homonuclear *J*-resolved NMR spectroscopy. In the C3–C4–C5–C6 fragment, $^{3}J_{H4,H5}$ and $^{2}J_{H2,C3}$ values were determined to be 2.0 and 8.6 Hz, respectively. In a 1,2-methine system, these coupling values indicated two possible configurations at C4–C5: the *threo* (A-2 rotamer) and *erythro* (B-1 rotamer) forms. The presence of a ROESY correlation between H5 and H42 confirmed the A-2 rotamer as the correct conformation, as depicted in Fig. 5b. Through further analyses of ROESY correlations, the relative configurations at C4, C5, and C7 were assigned as *syn*/*anti*. The relative configurations at C10–C11–C12–C13–C14 were assigned using JBCA with a 1,3-methine system, along with ROESY analyses. The $^{3}J_{H11,H12h}$ and $^{3}J_{H11,H12l}$ values were determined to be 2.3 and 10.5 Hz, respectively, while the $^{2}J_{C11,H12h}$ value was observed to be below 2.0 Hz. These observations supported the presence of a C-1 conformer at the C11–C12 position. At the C13–C14 positions, the relatively small $^{3}J_{H13,H14}$, $^{2}J_{C13,H14}$, and $^{2}J_{H13,C14}$ values indicated an A-1 rotameric configuration.

Through additional ROESY correlation analyses, the relative configurations at C10, C11, C13, and C14 were assigned as *anti*/*syn*/*syn* orientations (Fig. 5c). At the C22–C23–C25 positions, the small $^{3}J_{H22,H23}$ and $^{2}J_{H22,C23}$ values suggested two possible rotamers: A-1 and B-2. However, the observed ROESY correlations between H23 and H44 ruled out the A-1 rotameric orientation. Through further analyses of the ROESY correlations between H20/H22, H21/H24*l*, and H23/H25, the relative configuration at C22, C23, and C25 was determined as *anti*/*syn* (Fig. 5d). Next, the large values of vicinal ^{1}H–^{1}H coupling constants ($^{3}J_{H25,H26}$ and $^{3}J_{H26,H27}$) in the pyran ring allowed the extension of relative configurations from C25 to C26 and C27. ROESY correlations then confirmed the configurations within the bicyclic spiroketal structure.[38] The relative configurations at the C34–C38 positions were determined through meticulous ROESY correlation analysis and JBCA. Specifically, a small $^{3}J_{H37,H38}$ value (2.3 Hz) combined with a large $^{2}J_{C37,H38}$ value (7.2 Hz) suggested two possible rotamers: A-2 in the *threo* form and B-1 in the *erythro* form. However, the observed ROESY correlations between H37 and H47 ruled out the possibility of the B-1 rotameric configuration. Consequently, the relative configuration at the C37–C38 position was determined to be a *threo* configuration, as depicted in Fig. 5d. Additionally, the ROESY correlations between H34/H37, H36/H46, and H36/H47 facilitated the extension of relative configurations to the C34–C38 positions, which encompassed a *trans* epoxide at the C36–C37 position.

Bahamaolide A (**9**) is a polyene-polyol-type 36-membered macrocyclic lactone produced by the marine actinomycete *Streptomyces* sp. CNQ343 (Fig. 6a).[41] The relative configurations of its repeating 1,3-diol units were assigned through acetonide derivatization followed by NMR data analysis. The relative configurations of the isolated stereogenic centres at C34 and C35 were further determined using JBCA. A large $^{3}J_{H35,C39}$ value indicated two possible rotameric configurations: A-1 in the *threo* form and B-1 in the *erythro* form, both characterized by an *anti* orientation between H35 and C39. However, the observed ROESY correlations between H36 and H39 supported the existence of only the A-1 rotamer. Consequently, the relative configurations at C34 and C35 were both assigned as *S** (Fig. 6b). The absolute configurations of bahamaolide A were determined using Mosher's method, which involved analysing a tetra-acetonide derivative and its methanolysis product. Details of this analysis are provided in Section 2.3.

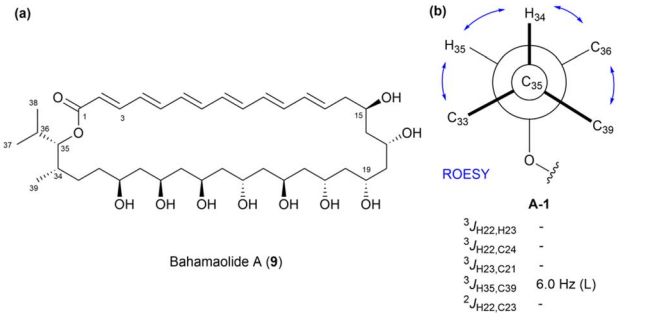

Fig. 6 Application of JBCA for relative configuration assessment at C34–C35 in bahamaolide A: (a) chemical structure of bahamaolide A. (b) Newman projection of C33–C36.

Pulvomycins are 22-membered macrolactones isolated from the bacterium *Streptomyces* sp. These macrolactones feature polyene fragments and the sugar unit labilose. Although the

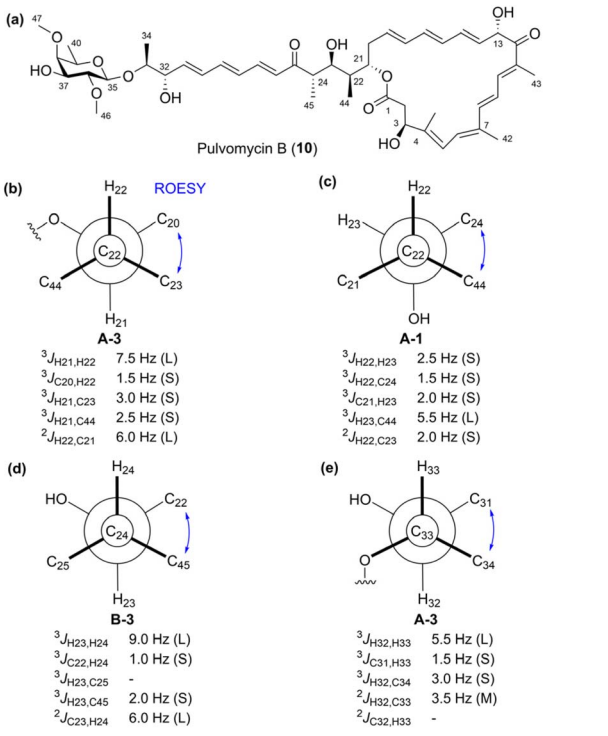

Fig. 7 Application of JBCA for the relative configuration assessment in pulvomycin B: (a) chemical structure of pulvomycin B. Application of JBCA for the configuration assessment of the (b) C21–C22, (c) C22–C23 (d) C23–C24, and (e) C32–C33 positions.

first compound of this class, pulvomycin (also known as labilomycin), was discovered in 1957, its planar structure was only fully established in 1985. The absolute configuration was later confirmed by X-ray crystallography in 2006. Pulvomycins B–D were subsequently identified as additional members of this structural class.[42] Among these, pulvomycin B (**10**) contains 13 stereogenic centres, with five located in the labilose sugar unit and eight within the polyketide moiety (Fig. 7a). The sugar unit was identified as labilose based on the $^{1}J_{C35,H35}$ and $^{3}J_{H,H}$ values, along with ROESY correlations. The relative configurations of the consecutive stereogenic centres at C21–C24 were successfully determined using JBCA. Relatively large $^{3}J_{H21,H22}$ and $^{2}J_{H22,C21}$ values, along with the small $^{3}J_{C20,H22}$, $^{3}J_{H21,C23}$, and $^{2}J_{H21,C44}$ values, indicated two possible rotamers: A-3 or B-3. The observed ROESY correlation between H20 and H23 confirmed the relative configuration at C21–C22 as the A-3 rotamer in the *threo* form, as depicted in Fig. 7b. Similarly, the relative configurations at C22–C24 were successfully identified as the *threo* form at C22–C23 and the *erythro* form at C23–C24 (Fig. 7c and d). At the C32–C33 position, JBCA analysis indicated a configuration similar to the A-3 rotamer in a 1,2-methine system. However, given that the $^{2}J_{H32,C33}$ value was moderate, the configuration was further confirmed through density functional theory (DFT) modeling and additional ROESY observations. Ultimately, the relative configuration at C32–C33 was identified as an A-3 rotamer in the *threo* form (Fig. 7e). Finally, the absolute configurations at C3, C13, C32, and C37 were determined using the modified Mosher's method. Meanwhile, the absolute configuration at C23, which was sterically hindered and inactive in Mosher's esterification, was determined using Kishi's bidentate chiral solvation technique, as will be detailed in Sections 2.2 and 2.4.

2.1.5. Limitation of JBCA. The above case studies demonstrate that JBCA is a highly effective tool for determining the relative configurations of asymmetric methine carbons adjacent to hydroxy, alkoxy, or methyl substituents. However, JBCA has limited applicability to the broad range of structural variations found in type-I polyketides. To expand its applicability, further research is needed to understand the effects of electronegative substituents and their associated dihedral angles on heteronuclear coupling constants.[43] Such attempts have already shown promising results in specific cases. For instance, extensive spectroscopic studies on the application of JBCA to chlorinated compounds—such as chlorinated hydrocarbons and chlorohydrins—have led to the development of a spectroscopic database for configurational assignments in chlorinated systems.[10,14] Another limitation of JBCA lies in its requirement for proton nuclei adjacent to chiral centres, which makes it unsuitable for proton-deficient molecules. To address this challenge and determine the configurations of proton-deficient molecules, ^{13}C NMR-based approaches, along with measurements of ^{13}C–^{13}C homonuclear coupling constants and comparisons with DFT calculations of ^{13}C chemical shifts, have been adopted.[44] A further shortcoming of JBCA arises in systems with multiple conformers in equilibrium. In such systems, the averaged NMR parameters do not entirely represent the features of individual conformers, particularly when conformer interconversion occurs faster than the NMR timescale. Consequently, conventional JBCA cannot be applied to these systems. To overcome this limitation, *ab initio* calculations are conducted for all relevant conformers of each possible diastereomer. These calculations predict molecular geometries, relative energies, Boltzmann distributions, and *J* values. The Boltzmann-averaged *J* values are then compared with experimental *J* values to study the conformational behavior of systems with multiple conformers in equilibrium.[45]

2.2. Derivatization with auxiliary chiral reagents

2.2.1. General characteristics of chiral reagents. Generally, once the relative configuration of a molecule is assigned or when the absolute configuration of one or more stereogenic centres is already known, the absolute configuration of the target molecule or compound can be determined. In NMR spectroscopic methods, assigning the absolute configuration requires the creation of a chiral environment, which can be accomplished using chiral derivatizing agents (CDAs) or chiral solvating agents (CSAs). These agents can transform an enantiomeric pair into a diastereomeric mixture. When using a CSA, the NMR spectra of the two enantiomers remain quite similar regardless of the chiral environment, as the reagent does not form a covalent bond with the substrate. Consequently, this approach encounters limitations when quantifying enantiomeric purity in racemic mixtures. In contrast, CDAs covalently bond to the substrate, resulting in larger differences in chemical shifts. Owing to these advantages, CSA or CDA derivatization is commonly employed during NMR-based absolute configuration assignment. The standard approach involves separately derivatizing a pure enantiomer of the substrate with two enantiomers of the CDA. The resulting diastereomers are then analysed using NMR spectroscopy, and the chemical shift differences ($\Delta\delta$) of the functional groups attached to the chiral centre of the substrate are evaluated. The absolute configuration is then inferred based on the positive or negative signs of these chemical shift differences, which are analysed following an appropriate empirical approach. This methodology enables the assignment of absolute configurations.[46]

2.2.2. Case studies of MTPA in Mosher's method. The traditional Mosher's method, developed by Harry S. Mosher, is a widely used technique for determining the absolute configuration of chiral secondary alcohols. This method involves derivatizing alcohol with α-methoxy-α-trifluoromethylphenylacetic acid (MTPA) to form diastereomeric esters, which are then analysed using NMR spectroscopy. The method comprises two main approaches: the ^{19}F Mosher's method, which examines the chemical shifts of the trifluoromethyl (CF_3) group, and the ^{1}H Mosher's method (OMe Mosher's method), which focuses on the proton chemical shifts of substituents near the chiral centre. The ^{19}F Mosher's method is advantageous due to its clean and well-defined spectra, as fluorine signals are distinct and unaffected by overlapping peaks. However, it is less reliable when steric-hindrance is present around the hydroxy group. In contrast, the ^{1}H Mosher's method provides broader applicability and higher accuracy for complex molecules, as it analyses

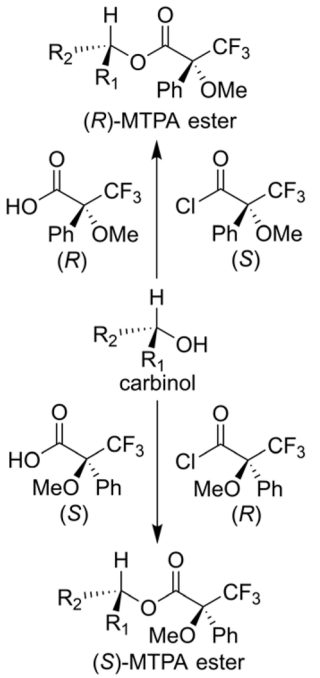

Fig. 8 Synthesis of (*R*)- and (*S*)-MTPA esters from a secondary alcohol.

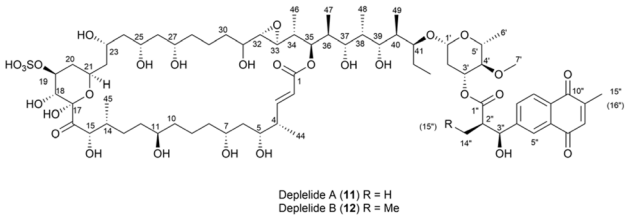

Fig. 9 Structures of deplelides A (**11**) and B (**12**).

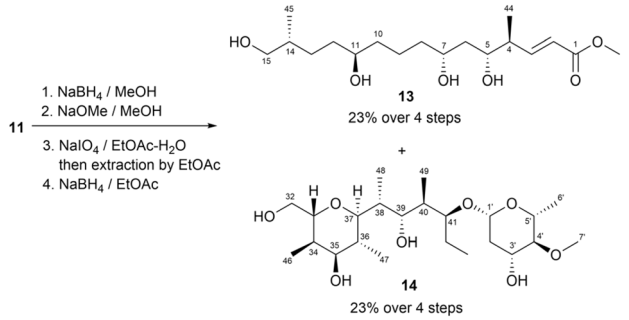

Fig. 10 Degradation of deplelide A (**11**).

detailed proton environments, but it requires advanced NMR techniques for proper interpretation.[47–49]

In the traditional Mosher's method, determination of the absolute configurations of chiral carbinol carbons through the analysis of $\Delta\delta$ values obtained from (*R*)- and (*S*)-MTPA ester derivatives was applied. However, this method has limitations when the substituents on the stereogenic centre, R_1 and R_2, are similar in size or electronic properties, resulting in ambiguous $\Delta\delta$ patterns that complicate accurate configuration assignment. Additionally, the traditional method does not systematically account for steric and electronic effects, which can lead to errors in more complex molecular environments (Fig. 8).[50]

The modified Mosher's method emerged as an evolution of the traditional approach to address its limitations, particularly when dealing with sterically hindered alcohols or molecules with complex stereochemistry. This method emphasizes the use of high-resolution ^{1}H NMR and integrates advanced multi-dimensional NMR techniques such as COSY, NOESY, and HSQC to enhance the precision of proton signal assignments. The modified Mosher's method also incorporates the use of alternative solvents like deutero-chloroform ($CDCl_3$), which improve its effectiveness for sterically hindered systems. Furthermore, it incorporates complementary validation methods, such as X-ray crystallography, to confirm the configuration of chiral centres in cases where NMR results may be ambiguous. These improvements allow the modified Mosher's method to overcome challenges associated with steric-hindrance, solvent compatibility, and the limitations of one-dimensional NMR spectroscopy. As a result, the method has become a gold standard in stereochemical analysis, offering superior versatility and accuracy compared to the traditional approach.[47,49]

In Mosher's method, MTPA is the most commonly used CDA for assigning the absolute configurations of secondary alcohols. In a previous study, deplelides A (**11**) and B (**12**) (Fig. 9), which represent 36-membered polyol macrolides, were isolated from *Streptomyces* MM581-NF15. The absolute configuration of deplelide A (**11**)[51] was determined through a degradation process followed by the application of a modified Mosher ester method. In particular, compound **11** was subjected to a four-step degradation process, involving the following steps: (1) reduction using $NaBH_4$, (2) methanolysis in the presence of NaOMe, (3) oxidative cleavage of vicinal diols using $NaIO_4$, and (4) reduction of the resulting aldehydes using $NaBH_4$ (Fig. 9). This degradation process yielded alcohols **13** (C1–C15) and **14** (C32–C43 and C1′–C6′) as the products (Fig. 10). These alcohols, **13** and **14**, were then transformed into the (*S*)- and (*R*)-MTPA esters **13a**/**13b** and **14a**/**14b**, respectively. The differences in chemical shifts ($\Delta\delta_{S-R}$) derived from the ^{1}H NMR data of **13a** and **13b** assigned the configurations at C5, C7, and C11 in **13** as *R*, *R*, and *R*, respectively (Fig. 11a). Similarly, the configurations of C35, C3′, and C5′ in **14** were determined to be *R*, *R*, and *R*, respectively (Fig. 11c). Although the $\Delta\delta_{S-R}$ values for **14a** and **14b** at C47 around C35 were inconsistent, the relative configuration between C3′ (3′*R**) and C35 (35*R**) confirmed that C35 in **14** featured the same configuration as 35*R*. Hence, the absolute configurations of the C1 to C15, C32 to C43, and C1′ to C7′ fragments in compound **11** were comprehensively determined (Fig. 11). Meanwhile, the absolute configuration of deplelide B (**12**) was inferred to be identical to that of deplelide A (**11**) given the similarity in their planar structures, except for the substitution of the methyl group at C14″ in **11** with an ethyl group in **12**.[51]

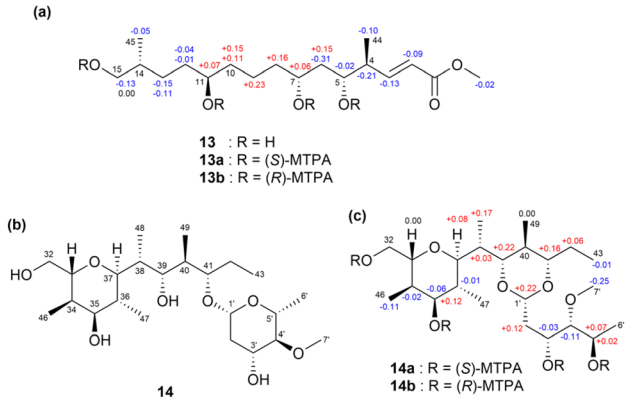

Fig. 11 (a and c) $\Delta\delta_{S-R}$ values of MTPA esters **13a** and **13b** (a) and **14a** and **14b** (c). (b) Structure of **14**.

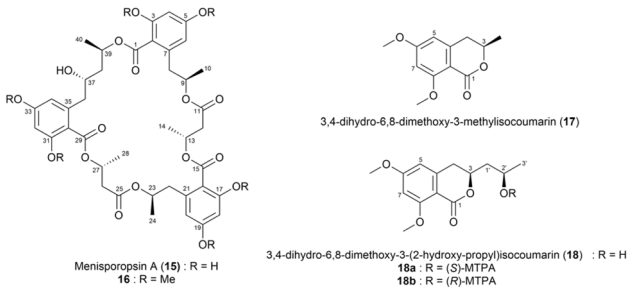

Fig. 12 Structures of menisporopsin A (**15**), its methylated derivative (**16**), 3,4-dihydro-6,8-dimethoxy-3-methylisocoumarin (**17**), 3,4-dihydro-6,8-dimethoxy-3-(2-hydroxy-propyl)isocoumarin (**18**), and the (*S*)- and (*R*)- MTPA esters of **18** (**18a** and **18b**).

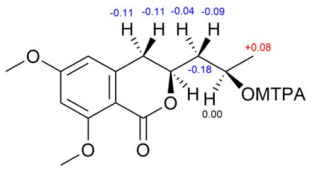

Fig. 13 $\Delta\delta_{S-R}$ values of the MTPA esters (**18a** and **18b**) of **18**.

Menisporopsin A (**15**),[52] a macrocyclic polylactone isolated from the fungus *Menisporopsis theobromae*, exhibits antimalarial activity. To determine the absolute configuration of each acid residue in compound **15**, its methylated derivative (**16**) was hydrolysed in 1 M NaOH and purified by high performance liquid chromatography (HPLC), yielding compounds (**17**) and (**18**) (Fig. 12). The absolute configuration of **18** was then determined using Mosher's method. Both the (*S*)- and (*R*)-MTPA esters of **18** (**18a** and **18b**) were prepared separately and analysed using ^{1}H NMR spectroscopy (Fig. 13). The obtained $\Delta\delta_{S-R}$ values indicated that the absolute configuration at C2′ in **18** was *R*. Consequently, the configuration at C39 in menisporopsin A (**15**) was also established as *R*. Further, the absolute configuration at C37 was determined as *S* based on spatial arrangements, in which the methyl groups at H37 and H40 of **15** are positioned in the same plane. The configuration at C3 in 3-hydroxybutyric acid was determined as *R* using chiral HPLC analysis. However, owing to the lack of a chromophore, the direct analysis of the 3-hydroxybutyric acid using chiral HPLC offered limited information regarding its identity. To address this limitation, a derivative was formed using Mosher's reagent ((*S*)-MTPA-Cl), which generated diastereomers with an aromatic chromophore. The resulting Mosher's esters, (*R*)- and (*S*)-3-hydroxybutyric acid, were successfully distinguished using chiral HPLC. Based on this analysis, the 3-hydroxybutyric acid residue in **15** was determined to be (*R*)-3-hydroxybutyric acid. Consequently, the absolute stereochemistry of all six chiral centres in menisporopsin A (**15**) was assigned as 9*R*, 13*R*, 23*R*, 27*R*, 37*S*, and 39*R*.[52]

Modiolides D-G (**19–22**)[53] were isolated from *Paraconiothyrium* sp. VK-13 (Fig. 14a). The absolute configuration at C7 in compounds **19–22** was assigned using the modified Mosher's method. Based on the $\Delta\delta_{S-R}$ values at C7, the configurations were determined as *S* for **19** and *R* for both **20** and **21** (Fig. 14b). For modiolide G (**22**), the absolute configurations at C7 and C9 were found to be inverted compared to those in modiolide A owing to the assignment of C4 as *R* using the modified Mosher's method (Fig. 14b).[53]

A previous study isolated a new tetronate-class polyketide, maklamicin (**23**),[54] from the culture extract of *Micromonospora* sp. GMKU326 (Fig. 15a). Maklamicin exhibited strong to moderate antimicrobial activity against Gram-positive bacteria. The absolute stereochemistry of the secondary hydroxy group at C31 in **23** was assigned using the modified Mosher's method. During this test, the enolic hydroxy group at C24 was protected by treating **23** with $TMSCHN_2$ in $CHCl_3$/MeOH, forming a methyl ether. The resulting methylated derivative, **24**, was then treated with (*S*)- and (*R*)-MTPA-Cl to yield the bis-(*R*)- and (*S*)-MTPA esters (**24a** and **24b**), respectively. Notably, the $\Delta\delta_{S-R}$ values for $H_3$32 were positive in the ^{1}H NMR spectra of **24a** and **24b**, while those for H30, H21, H22, H29, H19, H28, and H17 were negative (Fig. 15b). Based on these data, the absolute configuration of C31 was determined as *R*.[54]

Another successful application of Mosher's method for determining the absolute stereochemistry of chiral carbons was demonstrated in pulvomycins B–D (**10**, **25**, and **26**) (Fig. 16).[42]

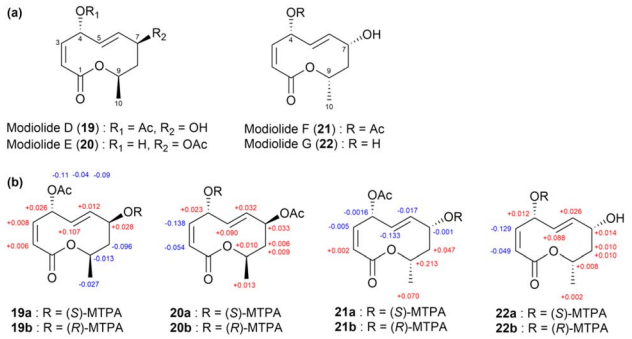

Fig. 14 (a) Structures of **19–22** and (b) $\Delta\delta_{S-R}$ values of the MTPA esters of compounds **19–22**.

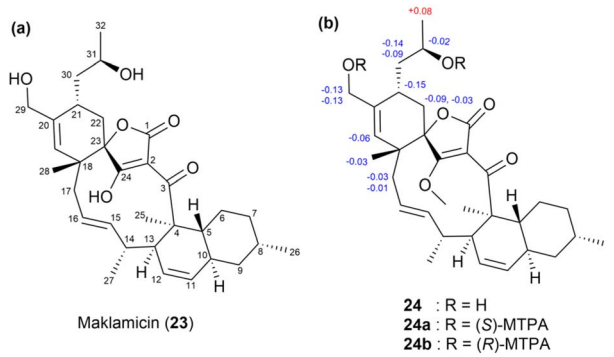

Fig. 15 (a) Structure of maklamicin (**23**) and (b) the $\Delta\delta_{S-R}$ values of the MTPA esters (**24a** and **24b**) of **24**.

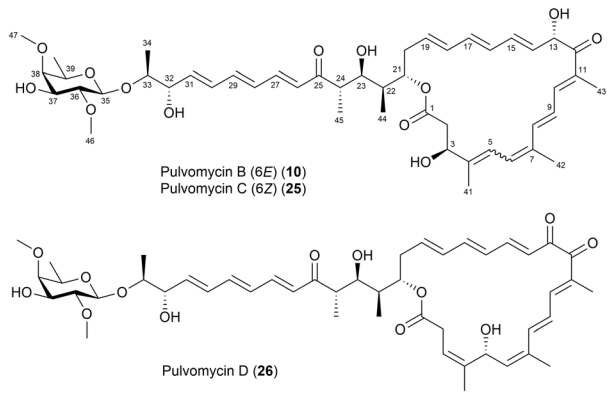

Fig. 16 Structures of pulvomycins B–D (**10**, **25** and **26**).

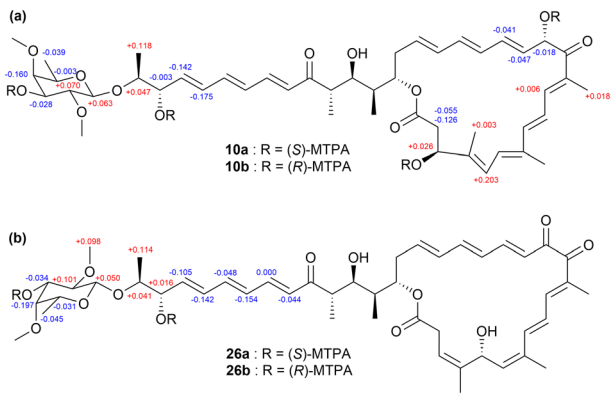

Fig. 17 (a) $\Delta\delta_{S-R}$ values of the tetra-(*S*)- and (*R*)-MTPA esters (**10a** and **10b**) of **10** and (b) $\Delta\delta_{S-R}$ values of di-(*S*)- and (*R*)-MTPA esters (**26a** and **26b**) of **26**.

The absolute configurations at C3, C13, C32, and C37 were determined using the modified Mosher's method. For this, the hydroxy groups at these positions were esterified with (*R*)- and (*S*)-MTPA-Cl to yield tetra-(*S*)- and (*R*)-MTPA esters, **10a** and **10b**, respectively. The $\Delta\delta_{S-R}$ values confirmed the absolute configurations at C3, C13, C32, and C37 as 3*S*, 13*S*, 32*S*, and 37*S*, respectively (Fig. 17). Pulvomycin C (**25**) was identified as

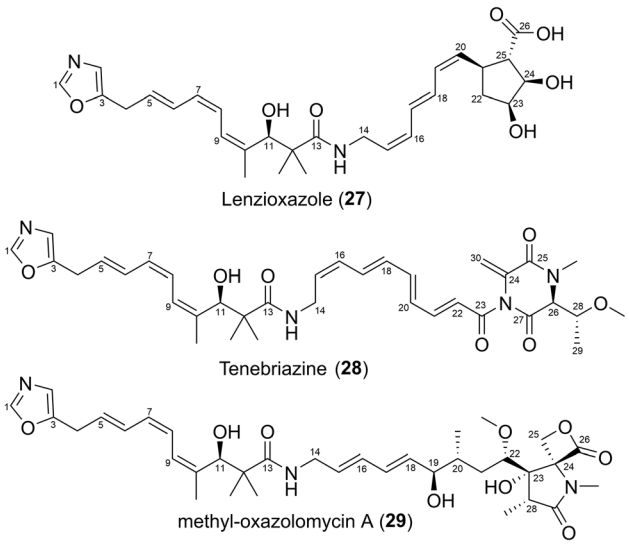

Fig. 18 Structures of lenzioxazole (**27**), tenebriazine (**28**), and methyl-oxazolomycin A (**29**).

a geometric isomer of compound **10** with a *6Z* configuration. The absolute configurations of pulvomycin D (**26**) were confirmed by analysing the ^{1}H chemical shifts of the bis-(*S*)- and (*R*)-MTPA esters (**26a** and **26b**) (Fig. 17).[42]

In a recent study, Park *et al.* described the use of Mosher's method to determine the absolute configurations of lenzioxazole (**27**), tenebriazine (**28**), and methyl-oxazolomycin A (**29**) (Fig. 18). The absolute configurations of compound **27** at positions C11, C21, C23, C24, and C25 were identified as 11*R*, 21*S*, 23*S*, 24*R*, and 25*S*, respectively, using the modified Mosher's method and NMR spectroscopic data analysis (Fig. 19a). Meanwhile, the absolute configuration of the chiral centre at C11 in compound **28** was analysed using the modified Mosher's

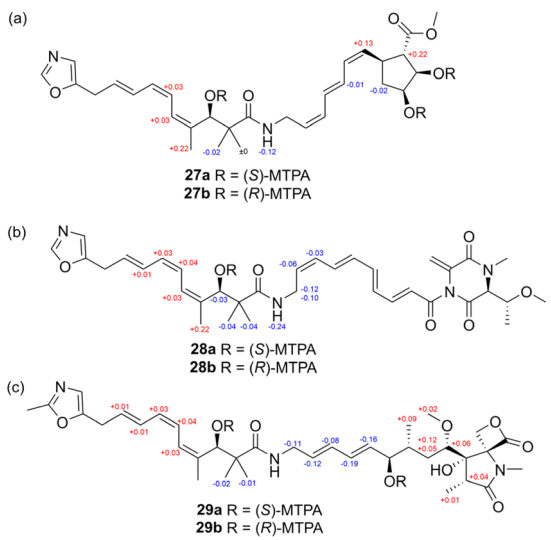

Fig. 19 (a) $\Delta\delta_{S-R}$ values of the (*S*)- and (*R*)-MTPA esters (**27a** and **27b**) of **27**; (b) $\Delta\delta_{S-R}$ values of (*S*)- and (*R*)-MTPA esters (**28a** and **28b**) of **28**; and (c) $\Delta\delta_{S-R}$ values of (*S*)- and (*R*)-MTPA esters (**29a** and **29b**) of **29**.

method with (*S*)- and (*R*)-MTPA reagents. By evaluating the chemical shift differences between the (*S*)- and (*R*)-MTPA esters, the C11 configuration was identified as *R* (Fig. 19b). Moreover, the absolute configurations of compounds **29** were identified as 11*R* and 19*R* based on the differences in chemical shifts ($\Delta\delta_{S-R}$) of (*S*)- and (*R*)-MTPA esters from the ^{1}H NMR data (Fig. 19c).[55]

2.2.3. Case studies of the phenylglycine methyl ester (PGME) method. The phenylglycine methyl ester (PGME) method is a widely utilized technique for determining the absolute configuration of chiral carboxylic acids. This method employs (*R*)- and (*S*)-phenylglycine methyl esters as chiral derivatizing agents to form diastereomeric amides with the carboxylic acid under investigation. The resulting diastereomers exhibit distinct chemical shift differences ($\Delta\delta_{S-R}$) in their ^{1}H NMR spectra, which can be analysed to deduce the absolute configuration of the original chiral centre. The PGME method, initially developed for α,α-disubstituted acetic acids, has been broadened to apply to a wider range of carboxylic acids, including α-hydroxy-, α-alkoxy-, and α-acyloxy-α,α-disubstituted acetic acids, as well as β,β-disubstituted propionic acids.[56]

The PGME method is another highly advanced approach for determining absolute configurations using CDAs. This approach is capable of determining the absolute configuration of a methine carbon adjacent to a carboxylic moiety. When dealing with carboxylic acids, the methine proton promotes an NOE interaction with the amide NH, indicating that the PGME moiety adopts a conformation that takes advantage of its anisotropic effect.[43]

In a previous study, pectenotoxins (PTXs, Fig. 20),[57] a family of polyether macrolide toxins, were isolated from the dinoflagellate genus *Dinophysis*.[58] Among the members of this family, PTX1 (**30**), PTX2 (**31**), PTX3 (**32**), and PTX6 (**33**) share the same skeleton, except for variations at the C43 position. The absolute configuration of PTX6 (**33**) was assigned using PGME-based NMR spectroscopy. Although PTX6 (**33**) lacks a methine proton at C18, the electrostatic repulsion between the lone pair electrons on the ether oxygen (O18) and the carbonyl oxygen at C43 causes the PGME moiety in PTX6-(*R*)- or PTX6-(*S*)-PGME amide to adopt a consistent conformation. This conformation enables the phenyl group of PGME to effectively extend its diamagnetic field to the protons near the chiral carbon at C18. NOEs from the amide proton to H17$_\beta$, H19$_\beta$, and H22 were clearly detected from the NOESY spectra of both (*R*)- and (*S*)-PGME amides acquired in C_5D_5N (Fig. 21). The calculated $\Delta\delta_{S-R}$ values for H42 (12-Me) to H45 (27-Me) are presented in Fig. 22. Notably, the signs of $\Delta\delta_{S-R}$ values were negative for protons from 12-Me to H17 and positive for protons from H19 to 27-Me in both C_5D_5N and $CDCl_3$ (Fig. 22). Based on these observations, the absolute configuration at C18 was determined as *S*.[57]

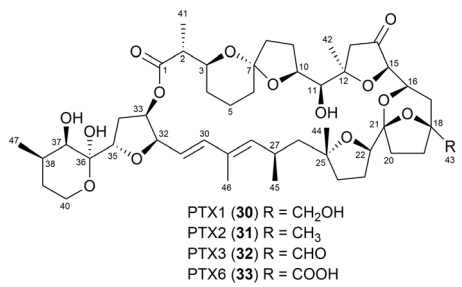

Fig. 20 Structures of PTXs.

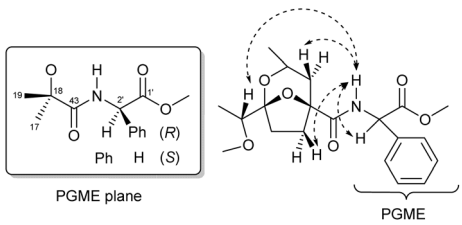

Fig. 21 PGME plane and NOE data. Dashed arrows indicate NOEs in a C_5D_5N solution at 5 °C.

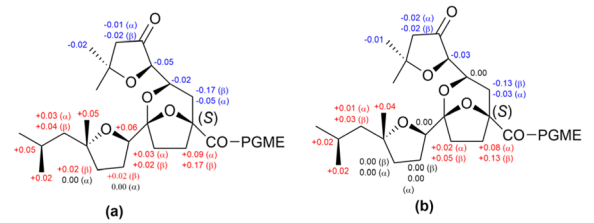

Fig. 22 Partial structures of PTX6, with $\Delta\delta_{S-R}$ values in (a) C_5D_5N and (b) $CDCl_3$ at 20 °C.

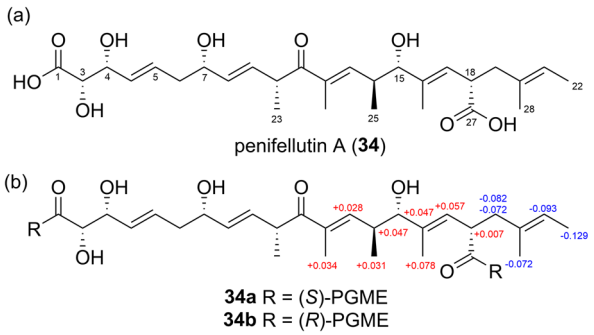

Fig. 23 (a) Structure of penifellutin A (**34**) and (b) $\Delta\delta_{S-R}$ values of the PGME derivatives (**34a** and **34b**) of **34**.

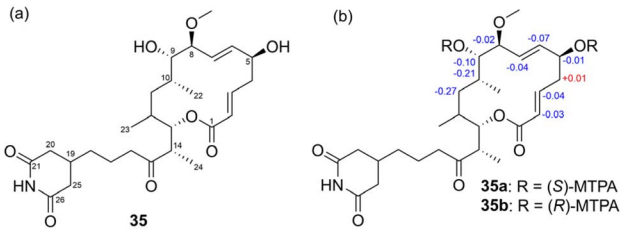

Fig. 24 (a) Structure of 5-hydroxy-migrastatin and (b) the $\Delta\delta_{S-R}$ values of the (*S*)- and (*R*)-MTPA esters of **35**.

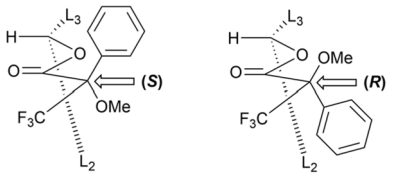

Fig. 25 Most stable conformation of (*S*)-MTPA and (*R*)-MTPA esters. L_2 and L_3 are substituents at the stereogenic centre.

In a recent study, Yu *et al.* determined the absolute configuration of penifellutin A (**34**) (Fig. 23a) at C18 using the PGME method. The calculated $\Delta\delta_{S-R}$ values derived from the (*S*)- and (*R*)-PGME amides (Fig. 23b) indicated that C18 has an *S* configuration.[59]

2.2.4. Case studies of ^{19}F-NMR in Mosher's method. A previous study isolated 5-hydroxy-migrastatin (**35**),[60] a new macrocyclic compound, from the dung beetle gut bacterium *Kitasatospora* sp. JL24 (Fig. 24a). However, determining the absolute configuration of the alcohol group at C5 in **35** proved challenging using the modified Mosher's method. The $\Delta\delta_{S-R}$ values for the MTPA ester groups at C5 and C9 in **35** could not directly confirm the absolute configuration of either carbon, as the relative configuration between these two stereogenic centres had not been established (Fig. 24b).

Notably, the absolute stereochemistry of a carbinol group or an amine centre can be inferred by comparing the chemical shifts observed in the ^{19}F-NMR spectra of (*R*)-MTPA and (*S*)-MTPA esters. This is based on a subtle conformation change caused by the interaction between the bulky phenyl group and the substituents at the stereogenic centre. When the phenyl group in a MTPA ester is ipsilateral with the relatively bulkier substituent (L_2 or L_3 in Fig. 25), the conformation is more destabilized than the most stable state and thus the CF_3 group chemical shifts in (*S*)-MTPA and (*R*)-MTPA esters can be affected. Kakisawa and Kashman's latest modification of the Mosher approach emphasizes the benefits of using more accurate proton NMR chemical shifts while highlighting the limitations of relying solely on fluorine chemical shift data for configuration assignment. The aforementioned fluorine chemical shift measurement offers only a single-point comparison. Furthermore, accurately identifying the diastereoisomer that predominates in the most stable conformation, where the CF_3 group is positioned in the carbonyl's deshielding plane, is essential (Fig. 25).[50]

Based on this, to determine the absolute stereochemistry at C5 and C9, basic Mosher-ester ^{19}F chemical shift analysis was employed. Notably, the $\Delta\delta_{S-R}$ values for ^{19}F were positive for both trifluoromethyl groups in **35a** and **35b**, suggesting that the bulky phenyl groups in the (*R*)-MTPA esters were positioned adjacent to a bulky region in **35** (specifically the carbon bearing the methoxy group), resulting in destabilization. The trifluoromethyl groups in the bis-(*R*)-MTPA esters (**35b**) were shifted upfield compared to the bis-(*S*)-MTPA esters (**35a**) owing to their shorter residence time in the MTPA carbonyl's deshielding cone. Based on this analysis, the 5*S* and 9*S* configurations were assigned, forming an *anti*-1,5 diol system.

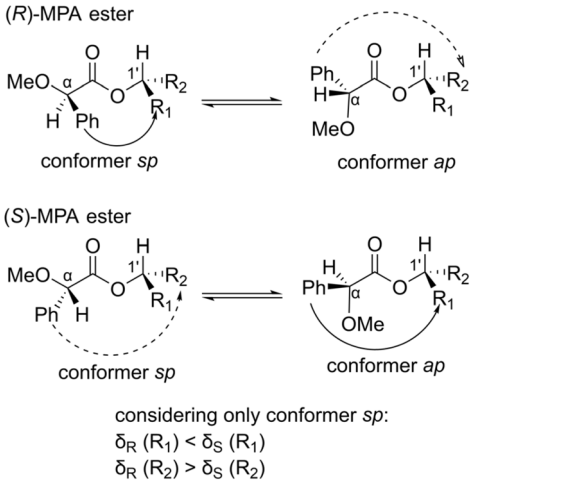

Fig. 26 Conformational equilibrium in MPA esters.

Seco *et al.*[61] established a sign distribution pattern for the $\Delta\delta_{S-R}$ values of diols, which validated these assignments based on the ^{1}H values of **35a** and **35b**.

2.2.5. Case studies of α-methoxyphenylacetic acid (MPA) in Mosher's method. Another commonly used CDA is MPA.[62] MPA esters are considered more reliable because they adopt a conformation that enhances the shielding effect of the phenyl group. Both MPA and MTPA are frequently used as CDAs for the absolute configuration assignment of secondary alcohols using NMR spectroscopy. However, owing to issues with racemization during derivatization, MPA has been less widely used compared to MTPA. Latypov *et al.*[63] discovered that MPA esters of secondary alcohols often exhibit two conformers, each with a distinct orientation relative to the Cα–CO bond (Fig. 26). Among these, the *sp* conformer is exceptionally stable, with the MeO and carbonyl groups aligned in a *syn* periplanar arrangement with C(1′)H. In practical applications, the most relevant *sp* conformer can be exclusively utilized for absolute configuration assignments, thereby aligning this approach with Mosher's empirical method.

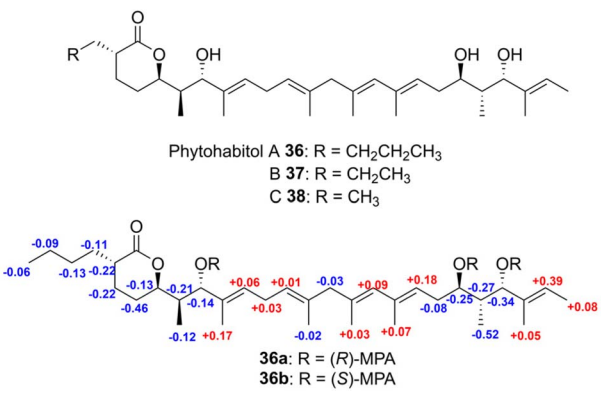

Fig. 27 Structures of phytohabitols A–C (**36**–**38**) and ^{1}H NMR $\Delta\delta_{R-S}$ values of tri (*R*)- and (*S*)-MPA esters **36a** and **36b**.

In a recent study, phytohabitols A–C (**36–38**), a novel group of linear polyketides featuring terminal δ-lactone rings, were identified in the extract of a rare actinomycete belonging to the genus *Phytohabitans* in 2022.[64] Mosher's method by applying MPA was utilized to determine the absolute configuration of the multiple secondary hydroxy groups at C7, C19 and C21 of compound **36**. Esterification of compound **36** with both (*R*)- and (*S*)-α-methoxyphenylacetic acid (MPA) in the presence of *N*,*N*′-diisopropylcarbodiimide (DIC) and *N*,*N*-dimethyl-4-aminopyridine (DMAP) yielded tri (*R*)- and (*S*)-MPA esters (**36a** and **36b**). The $\Delta\delta_{R-S}$ values were calculated, showing negative values for protons on the left side of C7 and positive values for protons on the right, confirming a 7*S*-configuration. Similarly, negative $\Delta\delta_{R-S}$ values were observed for protons between C19 and C21, while positive values were recorded for protons on the left side of C19 and the right side of C21, establishing a 19*R*,21*S*-configuration (Fig. 27).

Notably, when researchers utilize these traditional CDA approaches, they often need to conduct multiple steps, including reaction, purification, and separation, which can be time-consuming and lead to sample loss, particularly in double derivatization methods. To overcome these limitations, Riguera's research group developed a method that utilizes solid matrix-bound CDAs, deuterated NMR solvents as reaction media, and direct high-yield derivatization within NMR tubes, eliminating the need for purification or separation. In this method, the chiral substrate reacts with the CDA-resin inside the NMR tube, forming the desired derivative in solution while the resin remains out of solution.[65] This approach significantly reduces experimental time and complexity, allowing for rapid configurational analysis. Additionally, HR-MAS (High Resolution-Magic Angle Spinning) NMR was used to characterize the new CDA-resins and assess their stability and regioselectivity.

However, the application of CDA is challenging due to multiple asymmetric carbons and overlapping anisotropic effects from chiral auxiliaries. This issue is worsened by the incorrect choice of chiral auxiliaries, such as MTPA, whose high conformational flexibility leads to unpredictable results. Moreover, the chiral auxiliaries sometimes interact with each other, distorting the chemical shift patterns. As a solution, conformational studies enable the prediction of shielding effects and $\Delta\delta_{S-R}$ signs, leading to new assignment methods that utilize alternative proton chemical shifts and novel NMR parameters, including ^{13}C chemical shifts, for improved absolute configurational analysis.[66]

2.3. Degradation and chemical modification

2.3.1. General aspects of chemical degradation. Typically, the configurational analysis of type-I PKS-derived polyketides is challenging owing to several factors: first, these compounds typically possess numerous hydroxy groups, complicating the interpretation of the NMR data of their CDA derivatives. Additionally, they may incorporate non-polyketide-derived partial structures, necessitating the use of alternative methods beyond CDA derivatizations. Moreover, these compounds can contain

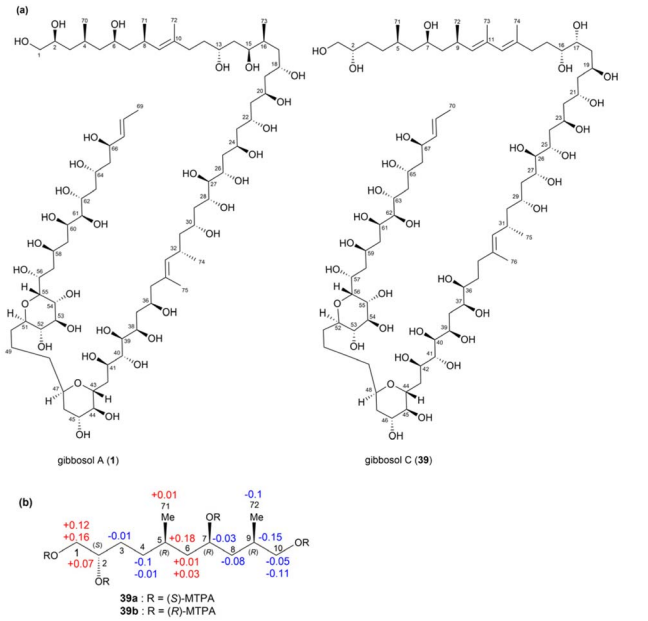

Fig. 28 (a) Structures of gibbosols A (**1**) and C (**39**). (b) $\Delta\delta_{S-R}$ values of the (*S*)- and (*R*)-MTPA esters of **39**.

remote stereogenic centres, making relative configurational analysis difficult. To address these challenges, additional degradation and chemical modifications are often required. Generally, the partial structures of type-I PKS-derived polyketides can be extracted through degradation techniques such as ozonolysis and hydrolysis and/or through chemical modifications such as acetonide and cyclization.[67,68] In the following sections, several case studies are presented to illustrate the

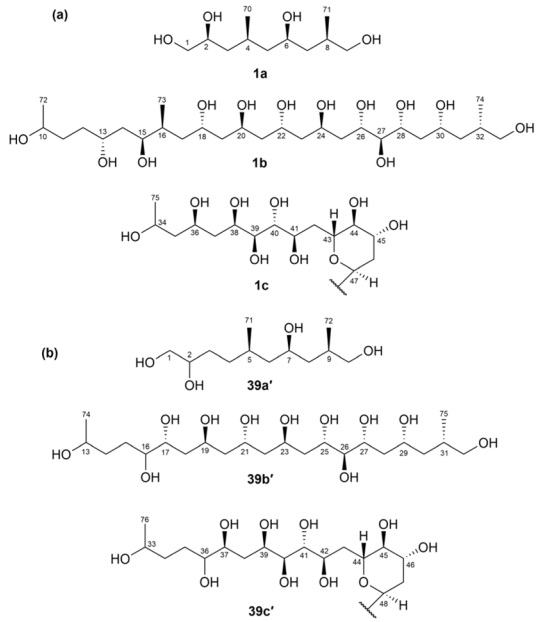

Fig. 29 (a) Structures of the ozonolysed fragments of gibbosol A (**1a–c**). (b) Structures of the ozonolysed fragments of gibbosol C (**39a′–c′**).

determination of absolute configurations using these approaches.

2.3.2. Case studies of general degradation methods. In a previous study, gibbosol C (**39**) (Fig. 28),[6] a super-carbon-chain compound, was isolated from *Amphidinium gibbosum*. The absolute configuration of compound **39** was determined by comparing the NMR data of its ozonolysis products with those of gibbosol A (**1**) (Fig. 28), in combination with Kishi's universal NMR database, *J*-based configuration analysis, and the modified Mosher's MTPA ester method. Ozonolysis was performed on compound **39**, and the resulting ozonolysis products (**39a′–c′**) (Fig. 29b) were analysed by NMR. Their data were then compared with those of the three ozonolysis fragments of gibbosol A (**1a–c**) (Fig. 29a).[6]

The absolute stereochemistry of C2, C7, and C9 in fragment **39a′** was determined using the modified Mosher's method. By comparing the $\Delta\delta_{S-R}$ values of the MTPA esters of fragments **39a** and **39b**, the absolute configurations at C2 and C7 in fragment **39a′** were determined as *S* and *R* (Fig. 29b), respectively. Meanwhile, the configuration at C9 was confirmed to be *R* based on the widely separated $H_2$10 signals of fragment **39b** (δ_H 4.29, 4.18) compared to those of fragment **39a** (δ_H 4.18, 4.13). Furthermore, the configuration of C5 in fragment **39a′** was determined to be *R* based on the *syn* relationship between Me-71 and 7-OH.

Therefore, the absolute configurations of fragment **39a′** were determined to be 2*S*, 5*R*, 7*R*, and 9*R* (Fig. 29b), resembling those of fragment **1a**. The absolute configurations at the C17–C25 and C37–C42 positions of **39** were determined as 17*R*, 19*S*, 21*S*, 23*R*, and 25*S* and 37*S*, 39*R*, 40*S*, 41*R*, and 42*R* through comparisons with gibbosol A. Meanwhile, the configurations at C16 in **39b′** and at C37 in **39c′** were confirmed to be *R* and *S*, respectively. Overall, the complete absolute configurations of gibbosol C (**39**) were determined to be 2*S*, 5*R*, 7*R*, 9*R*, 16*R*, 17*R*, 19*S*, 21*S*, 23*R*, 25*S*, 26*R*, 27*R*, 29*R*, 31*S*, 36*S*, 37*S*, 39*R*, 40*S*, 41*R*, 42*R*, 44*R*, 45*S*, 46*R*, 48*R*, 52*R*, 53*S*, 54*S*, 55*R*, 56*R*, 57*R*, 59*S*, 61*R*, 62*R*, 63*R*, 65*R*, and 67*R*.[6]

In another study, kalimantacin A (**40**)[69] (Fig. 30a) was isolated from *Alcaligenes* sp. YL-02632S. This compound exhibited activity against Gram-positive bacteria, including methicillin-resistant *Staphylococcus aureus*. Its absolute configuration was determined using a multidisciplinary approach, involving natural product isolation and chemical degradation procedures such as ozonolysis, hydrolysis, and methanolysis. In particular, the absolute configurations at C15, C17, C19, C26, and C27 were determined by comparing the NMR correlations of

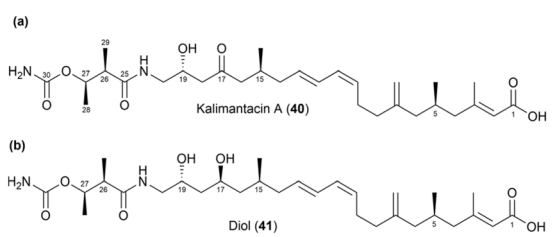

Fig. 30 (a) Structures of kalimantacin A (**40**) and (b) diol (**41**).

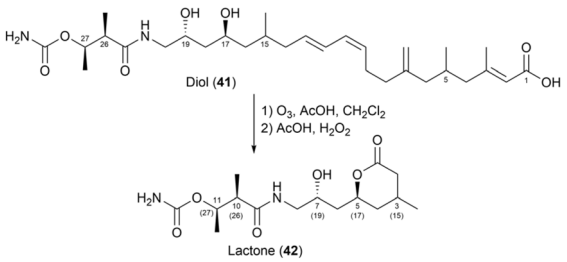

Fig. 31 Oxidative cleavage of diol (**41**).

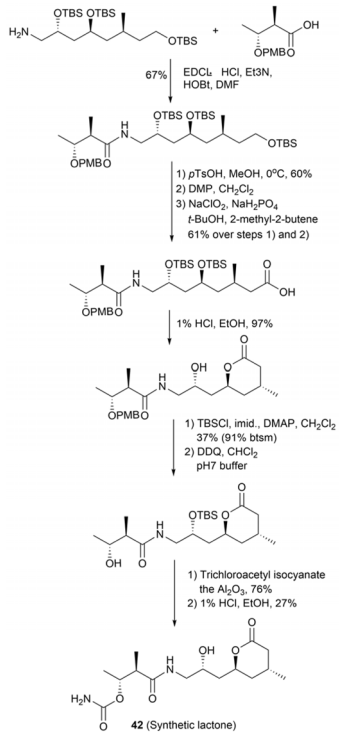

Fig. 32 Synthesis of lactone (**42**).

kalimantacin A (**40**) with those of the natural diol (**41**). Notably, the natural diol (**41**) was degraded, and its NMR data were compared with those of a synthetic standard (Fig. 31). The absolute configurations of diol **41** were determined to be 17*S*, 19*S*, 26*R*, and 27*R*. Ozonolysis of diol **41**, followed by treatment with $AcOH/H_2O_2$, resulted in the cleavage of the 12,13-double bond to yield a dihydroxy acid, which was subsequently cyclized to form lactone (**42**).

The absolute configuration at C15 was determined by comparing the NMR data of the synthetic lactone with those of compound **42**. This synthetic lactone was obtained through a five-step reaction sequence involving (2*R*,4*S*,6*S*)-2,4,8-tris((*tert*-butyldimethylsilyl)oxy)-6-methyloctan-1-amine and ethyl-(2*R*,3*R*)-3-hydroxy-2-methylbutanoate (Fig. 32). Simultaneously, degradation procedures and chemical syntheses were employed to determine the absolute configuration at C5. Diol **41** was methylated to obtain (−)-**43**, which exhibited an optical rotation value of $[\alpha]_D$ −6.8 (Fig. 33). The NMR spectra of the degradation

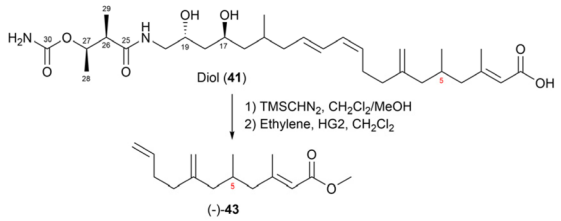

Fig. 33 Methylation of diol (**41**) followed by degradation to ester (−)-**43**.

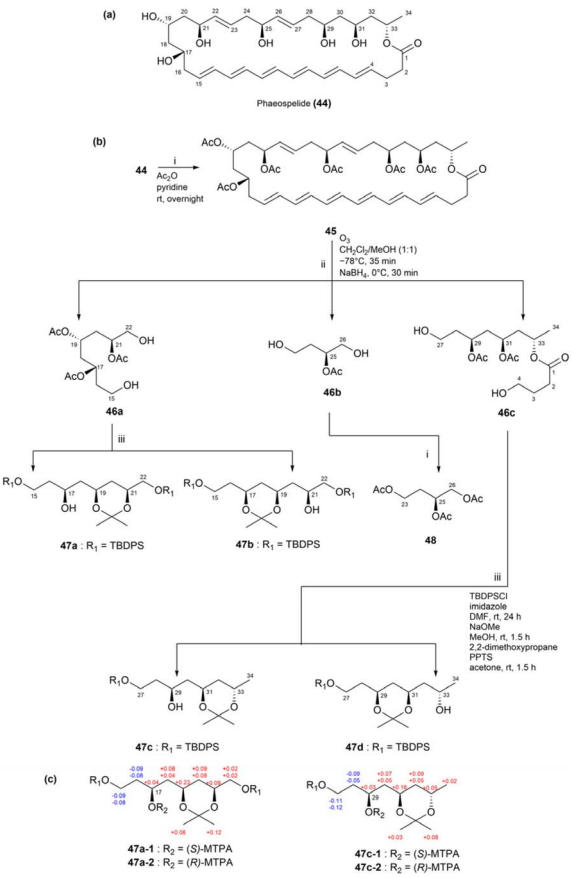

Fig. 34 (a) Structure of phaeospelide A (**44**). (b) Scheme of fragmentation and derivatization of **44**. (c) $\Delta\delta_{S-R}$ values of the MTPA derivatives.

product (−)-**43** resembled those of a synthetic unsaturated methyl ester (+)-**43**; however, the positive optical rotation value ($[\alpha]_D$ + 5.0) of (+)-**43** suggested that it was an enantiomer of the degradation product. Hence, the absolute configuration at C5 in kalimantacin A (**40**) was determined to be *R*. Overall, the absolute configurations of diol **41** were assigned as 5*R*, 15*S*, 17*S*, 19*R*, 26*R*, and 27*R* (Fig. 30b).[69]

In a previous study, phaeospelide A (**44**),[70] a novel 34-membered polyene macrolide, was isolated from *Aspergillus oryzae*. Chemical modifications were employed to determine its absolute configurations (Fig. 34a). Phaeospelide A (**44**) was first acetylated to produce compound **45** and subsequently decomposed *via* ozonolysis to yield fragments **46a–c**. Among these, fragment **46b** was further derivatized to yield triacetate (**48**), as depicted in Fig. 34b. The vibrational circular dichroism spectrum of compound **48** was compared to those of (*S*)- or (*R*)-1,2,4-butanetriols, revealing a 25*S* configuration for compound **44**. Meanwhile, fragment **46a** was subjected to a three-step reaction sequence to produce acetonides **47a** and **47b** (Fig. 34b). NOESY spectral analysis revealed that both compounds **47a** and **47b** displayed a chair conformation, with all oxygen atoms oriented along the same direction. Moreover, fragment **46c** underwent similar reactions to produce compounds **47c** and **47d**. NOESY spectral data analyses of compounds **47c** and **47d** revealed that compound **47d** adopted a chair conformation, while compound **47c** exhibited a twist-boat conformation. The oxygen atoms at C29 and C31 in compound **47d** were determined to have *cis* configurations, while that at C33 in compound **47c** was oriented in the opposite direction relative to C31. Finally, the absolute configurations at C17 and C29 were determined as *S* for both compounds **47a** and **47c** based on the $\Delta\delta_{S-R}$ values of their MTPA esters (**47a-1**, **47a-2**, **47c-1**, and **47c-2**) (Fig. 34c). Ultimately, the absolute configurations of **44** were identified as 17*S*, 19*S*, 21*S*, 25*S*, 29*S*, 31*S*, and 33*S*.[70]

In another study, four cytotoxic macrocyclic lactams, bombyxamycins A–C (**49–51**) and piceamycin (**52**) (Fig. 35), were isolated from the intestinal *Streptomyces* sp. SD53 of the silkworm *Bombyx mori*.[71] Among the bombyxamycins, compound **49** was subjected to ozonolysis and acid hydrolysis to determine the stereochemistry at C24. During this process, following step-by-step reaction sequences, the resulting β-amino acid, 3-amino-2-methylpropanoic acid, was derivatized using Sanger's reagent to yield 3-(2,4-dinitrophenylamino)-2-methylpropanoic acid (**53**). This derivative was further reacted with (*S*)- and (*R*)-PGME to produce (*S*)- and (*R*)-PGME amides (**53a** and **53b**), respectively. Analyses of the $\Delta\delta_{S-R}$ values in the ^{1}H NMR spectra of these PGME derivatives revealed that the absolute configuration of compound **53** was *S* (Fig. 36). Consequently, the absolute configuration at C24 in compound **49** was established as 24*R*. Subsequently, the secondary alcohol at C11 was derivatized with (*R*)- and (*S*)-MTPA-Cl, yielding (*S*)- and (*R*)-MTPA esters. The $\Delta\delta_{S-R}$ values of these esters were determined by analysing the ^{1}H and COSY NMR spectra of the MTPA esters.

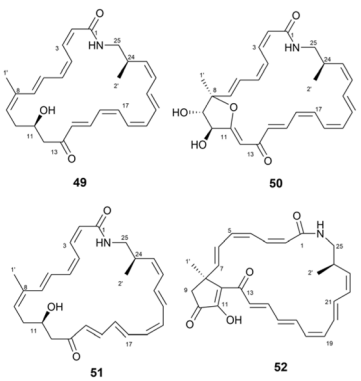

Fig. 35 Structures of bombyxamycins A–C (**49–51**) and piceamycin (**52**).

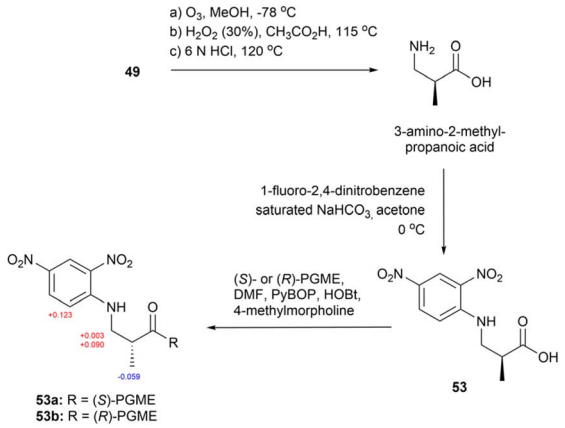

Fig. 36 Schemes for the ozonolysis, hydrolysis, and PGME treatment of compound **49**.

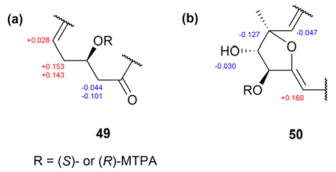

Fig. 37 $\Delta\delta_{S-R}$ values of the (*S*)- and (*R*)-MTPA esters of compounds **49** and **50**. (a) Partial assignment of C9–C13 in **49**. (b) Partial assignment of C7–C12 in **50**.

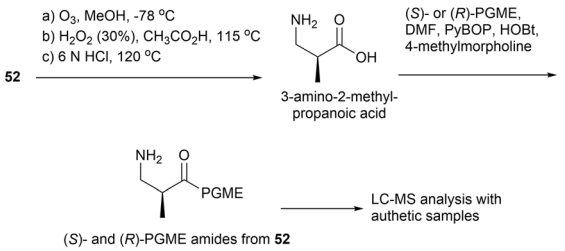

Fig. 38 Improved chemical reactions for compound **52**.

Consequently, the absolute configuration at C11 was determined as 11*R* (Fig. 37). Adopting the same procedure, the absolute configuration of **50** was determined as 8*R*, 9*S*, 10*S*, and 24*R*.[71]

Meanwhile, for piceamycin (**52**), the authors refined the entire process by introducing a liquid chromatography-mass

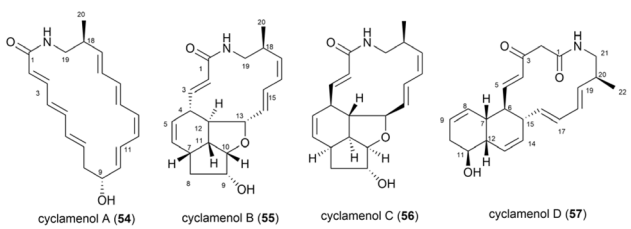

Fig. 39 Structures of cyclamenols A–D (**54–57**).

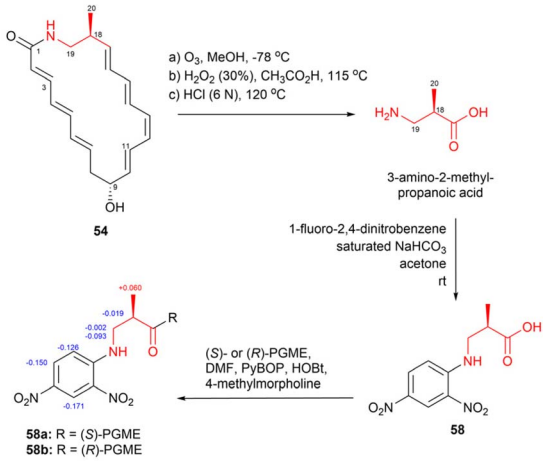

Fig. 40 Schemes for the ozonolysis, hydrolysis, and PGME treatment of compound **54**.

spectrometry (LC-MS) analysis step to compare the retention times of the (*S*)- and (*R*)-PGME amides derived from **52** with those derived from the authentic (2*S*)- and (2*R*)-3-amino-2-methylpropanoic acids (Fig. 38).[72] This approach eliminated the need for lengthy chemical derivatization, purification, and ^{1}H NMR spectroscopic analysis of the products.

Another study isolated four polycyclic macrolactams, cyclamenols A–D (**54–57**), from the Antarctic *Streptomyces* sp. OUCMDZ-4348 (Fig. 39).[73] To determine the stereochemistry at C18 in cyclamenol A (**54**), the authors performed ozonolysis followed by acid hydrolysis, which yielded 3-amino-2-methylpropanoic acid (Fig. 40). This compound was then derivatized using Sanger's reagent to yield derivative **58**. Subsequently, compound **58** was reacted with (*S*)- and (*R*)-PGME to form (*S*)- and (*R*)-PGME amides (**58a** and **58b**), respectively. The observed chemical shift differences ($\Delta\delta_{S-R}$) in the NMR spectra of these amides confirmed the *R* configuration at the stereogenic centre C18 of compound **58** (Fig. 40). Based on these results, the absolute configuration at C18 in cyclamenol A (**54**) was determined to be *S*. Furthermore, the absolute configuration at C9 in **54** was established as *R* based on the modified Mosher's method (Fig. 41). Subsequently, the absolute configurations of compounds **55–57** were also determined by adopting the same procedures.[73]

In another study, arenicolides A–C (**59–61**), a series of 26-membered macrolides, were isolated from the saline fermentation broth of the marine actinomycete *Salinispora arenicola* (Fig. 42).[74] To confirm whether compound **59** contained a 26- or

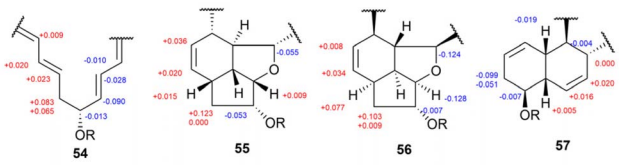

Fig. 41 $\Delta\delta_{S-R}$ values of the (*S*)- and (*R*)-MTPA esters of **54–57**.

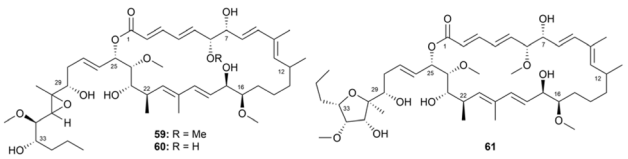

Fig. 42 Structures of arenicolides A–C (**59**–**61**).

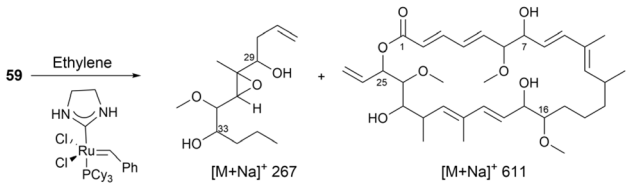

Fig. 43 Olefin cross-metathesis reaction of compound **59** and its products.

27-membered macrocycle, the authors performed degradation *via* olefin cross metathesis, inspired by a previous study on a simpler polyacetylenic oxylipid. The authors then mixed compound **59** with a second-generation Grubbs catalyst in dichloromethane under a 5 atm pressure of ethylene gas. Although the rate of the reaction was slow, LC-MS analysis detected a small amount of a macrocyclic product with a 27-carbon backbone (Fig. 43). Simultaneously, the structure of compound **61** was elucidated, providing clear NMR spectroscopic data to confirm its carbon backbone. Based on this information, the researchers concluded that compound **59** was a 26-membered macrolide. Consequently, they opted not to pursue further analysis of the metathesis reaction products.

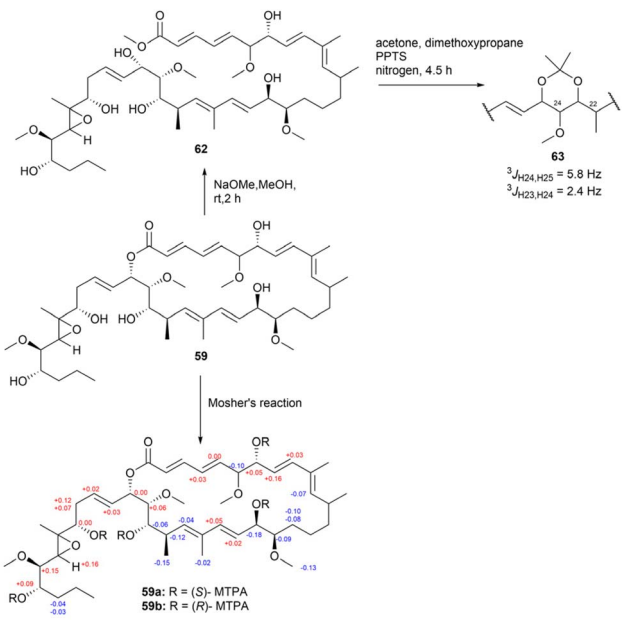

Fig. 44 Methanolysis, acetonide formation, and Mosher's reaction of compound 59.

The configurations of the stereogenic centres in compound **59**, a poly-hydroxy macrolide, were primarily determined using the modified Mosher's method, revealing arrangements of 7*R*, 17*R*, 23*S*, 29*S*, and 33*S* (Fig. 44). To determine the configuration at C25, compound **59** was initially subjected to a methanolysis reaction, yielding compound **62**. Acetonide formation produced compound **63**. Based on this, the 1,3-dioxane ring was determined to exhibit a twist-boat conformation, given the identical chemical shifts of the gem-dimethyl carbons (25.2 ppm and 24.8 ppm). The *anti*-configuration between H23 and H25 in compound **63** was confirmed by analysing the proton–proton coupling constants, specifically $^3J_{H23,H24} = 2.4$ Hz and $^3J_{H24,H25} = 5.8$ Hz, within the 1,3-dioxane ring. This deduction was further supported by comparisons with models of compound **63** established by previous studies. The findings confirmed the *anti* and *syn* stereochemical relationships in compound **63**, with H24/H25 exhibiting an *anti* relationship and H23/H24 showing a *syn* relationship.[74] However, the absolute configurations of the epoxide group in the side chain and the C12 chiral centre remained unidentified.

In another study, a pair of trisoxazole macrolides, miuramides A and B (**64** and **65**), were isolated from a marine sponge, *Mycale* sp.[75] Both compounds **64** and **65** exhibited potent cytotoxicity against 3Y1 cells. To determine the absolute configurations at the C25–C35 segment, the authors leveraged the similarity between miuramide A (**64**) and kabiramide C (**66**),

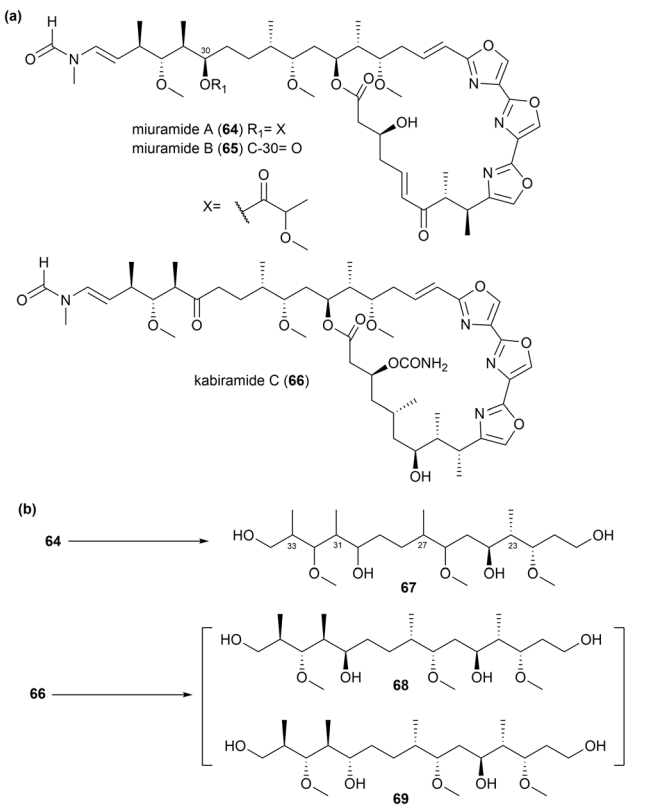

Fig. 45 (a) Structures of miuramides A and B (**64** and **65**) and kabiramide C (**66**). (b) Chemical reactions of compounds **64** and **66** to yield fragments **67**–**69**.

both of which contain a C32-methoxy group (Fig. 45a). Miuramide A (**64**) was subjected to oxidation with RuO_4, followed by reduction using a borane dimethyl sulfide complex and alkaline hydrolysis, yielding compound **67** (Fig. 45b). Further, a comparable fragment was synthesized from kabiramide C (**66**) through the following steps: $NaBH_4$ reduction, acetylation of the resulting C30 alcohol, oxidation with RuO_4, and reduction of the resulting dicarboxylic acid, yielding compounds **68** and **69**, which are epimeric at C30. The relative configurations at C30 in compounds **68** and **69** were determined based on selective decoupling NMR experiments. The ^{1}H NMR spectrum of compound **67** was superimposable with that of compound **68**, confirming that both compounds **67** and **68** shared the same total relative configuration. Given the established (22*S*, 23*R*, 24*S*) absolute configurations of compound **64**, the authors inferred that the absolute configurations of the remaining stereogenic centres in compounds **67** and **68** were also identical.[75]

2.3.3. Case studies of the acetonide method. Another popular chemical modification technique adopted to determine the absolute stereochemistry of type-I PKS compounds is the [^{13}C]acetonide method. This method relies on the distinct conformations of *anti* and *syn* 1,3-diol acetonides. Among these, *anti* 1,3-diol acetonides are anticipated to adopt twist-boat conformations, where the environments of the two acetal methyl groups are similar and the ^{13}C chemical shifts for both carbons are approximately 25 ppm. In contrast, *syn* 1,3-diol acetonides adopt chair conformations, with one acetal methyl group in an axial position and the other in an equatorial position (Fig. 46). The ^{13}C chemical shift for the axial methyl group is 20 ppm, while that for the equatorial methyl group is 30 ppm. These differences in chemical shifts between *anti* and *syn* 1,3-diol acetonides allow the relative configurations of 1,3-diol acetonides to be determined using their ^{13}C NMR chemical shifts.[76]

Macrolactin B (**70**)[76] was the first natural product whose absolute configuration was determined using the [^{13}C]acetonide method. Here, macrolactin B was subjected to hydrogenation and hydrolysis in HCl–methanol before the formation of the acetonide derivative. The ^{13}C chemical shift observed at 24.8 ppm for the acetonide methyl groups in compound **71** indicated an *anti*-configuration for the C13–C15 diols (Fig. 47).[76] The configuration of macrolactin B was further confirmed

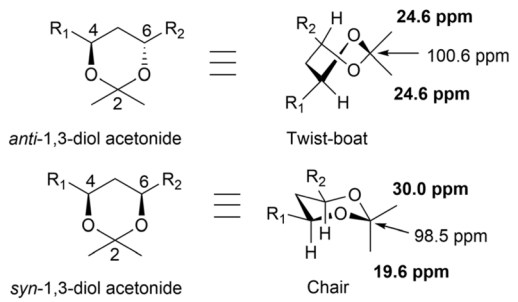

Fig. 46 NMR chemical shift correlations of *anti* and *syn* 1,3-diol acetonides (*trans*- and *cis*-4,6 dialkyl-2,2-dimethyl-1,3-dioxanes).

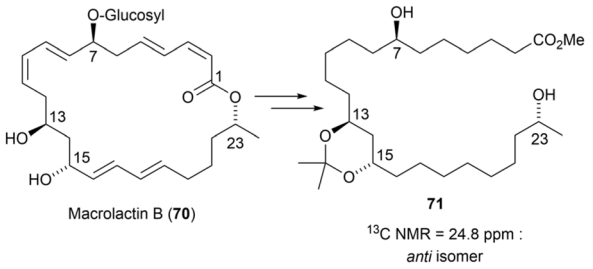

Fig. 47 Relative configurations of C13–C15 diols in macrolactin B, obtained from the [^{13}C]acetonide analysis.

through degradation and Mosher's analysis, as illustrated in Fig. 47.

Roflamycoin (**72**)[76] is a polyene macrolide derived from *Streptomyces roseoflavus*. Its stereochemistry was determined by synthesizing several polyacetonide derivatives and evaluating their relative configurations (Fig. 48).[76] Notably, roflamycoin, a cyclic hemiacetal, readily undergoes cyclization to form a spiroacetal upon acid treatment. The NMR data analysis of the configuration at C15–C19 was assigned as *syn*. The primary acetonide derivative obtained from the spiroacetal (compound **73**) contained acetonide groups at C23–C25 and C29–C31, both of which were identified as *syn* through [^{13}C]acetonide analysis. Degrading compound **72** yielded tetrahydropyran **76**, which subsequently formed the diacetonide derivative **78**. The ^{13}C NMR spectral data analysis of compound **78** indicated that its C23–C25 and C27–C29 segments exhibited *syn* conformations. Meanwhile, the ^{13}C NMR data analysis of pentaacetonide **74** revealed the presence of four *anti* rings and one *syn* ring. Despite five possible configurations for the arrangement of one *syn* and four *anti* acetonides, the [^{13}C]acetonide analysis was unable to pinpoint which acetonide ring adopted the *syn* conformation, necessitating additional analysis. Further assessments revealed that the C29–C31 acetonide in compound **73** exhibited a *syn* conformation, suggesting that compound **74** must also adopt this same *syn* configuration. The remaining acetonides, including the C21–C23 and C25–C27 rings, exhibited *anti* conformations. The stereochemical assignment of roflamycoin was successfully completed by confirming the relative stereochemical assignments of C21–C23 and C25–C27, and the absolute configuration of the C35 alcohol was established using Mosher's analysis.

In another study, filipin III (**80**),[76] a polyene macrolide isolated from *Streptomyces filipinensis*, was structurally analysed using the [^{13}C]acetonide method. Its polyacetonide derivatives of compound **80** were obtained by reacting it with acetone, 2,2-dimethoxypropane and pyridinium *p*-toluenesulfonate (PPTS) (see Fig. 49). [^{13}C]acetonide analysis of polyacetonides **82**, **83** and **84** provided key stereochemical details essential for the structural determination of filipin III. The analysis revealed that tetraacetonide **82** possessed three *syn* acetonide rings and one *anti* acetonide ring, triacetonide **83** comprised three *syn* acetonides, and triacetonide **84** contained two *syn* acetonide rings and one *anti* acetonide ring. Given that compound **83** only contained *syn* acetonide rings, the stereochemical assignments

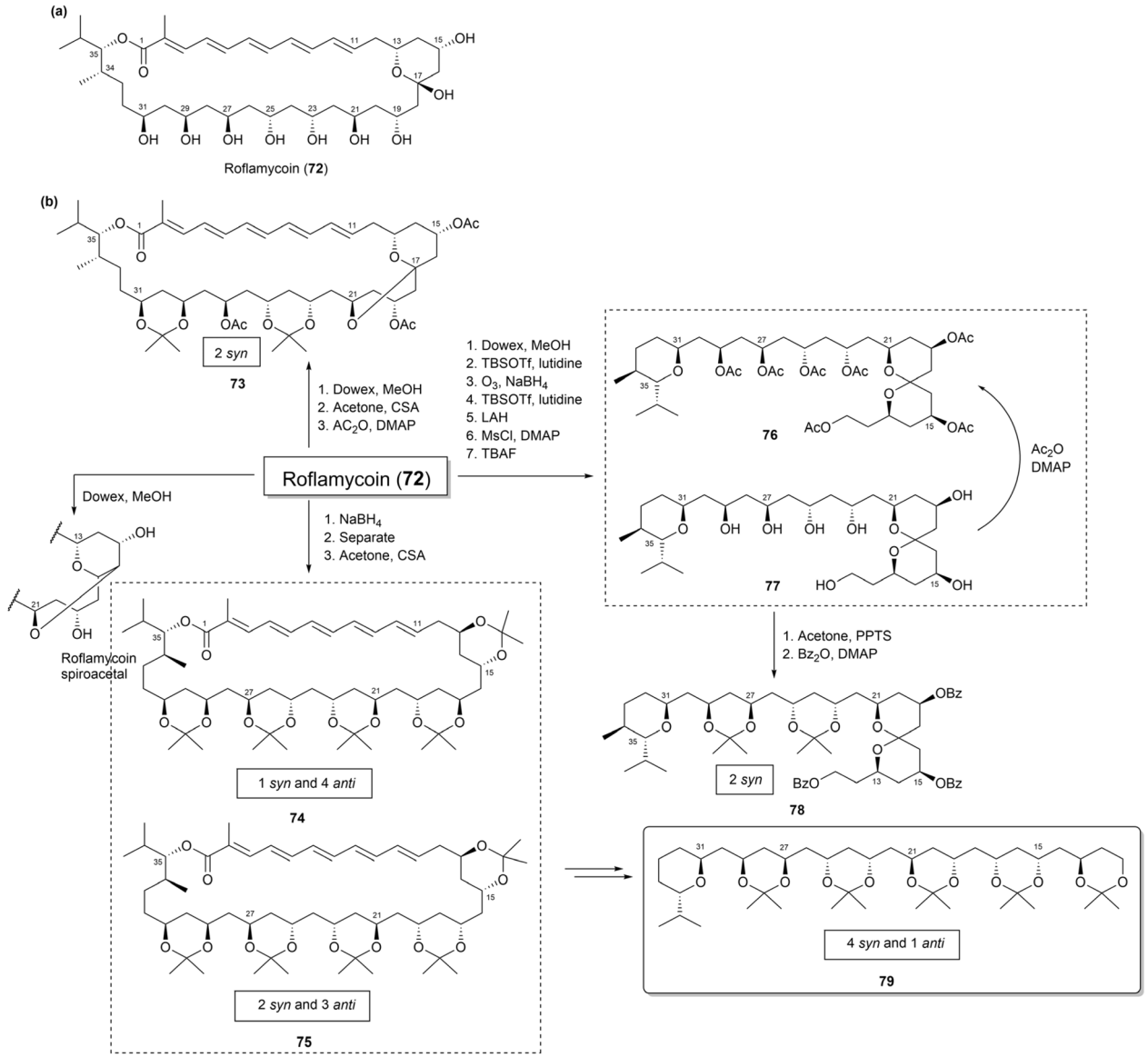

Fig. 48 (a) Structures of roflamycoin (**72**). (b) Polyacetonide derivatives of **72**.

at C3–C5, C7–C9, and C11–C13 were confirmed as *syn*. Both **82** and **84** contained one *anti* acetonide ring, and because the C3–C5 region was assigned as *syn* based on compound **83**, the *anti* acetonide ring common to both **82** and **84** must be located at either C9–C11 or C13–C15. The remaining acetonide rings in **82**, specifically at C1′–C3 and C5–C7, were confirmed to have a *syn* configuration. This narrowed the possible configurations to two locations for the single *anti* relationship in the polyol chain: C13–C15 or C9–C11.

To confirm the location of the *anti*-diol in filipin III at C13–C15, compounds **82** and **84** were degraded as illustrated in Fig. 49b, yielding compounds **85** and **86**, respectively. The methyl peaks observed at 25.69 and 24.78 ppm in **85** and at 25.94 and 24.32 ppm in **86** clearly indicated the presence of an *anti*-1,3-diol acetonide. This confirmed that the *anti* acetonide ring in both compounds **82** and **84** is positioned at C13–C15. The relative configurations of the stereogenic centres in the C1′–C15 region are illustrated in Fig. 49c. Additionally, derivatization of compounds **87** and **88** using MTPA, followed by the calculation of $\Delta\delta_{S-R}$ values for the resulting MTPA derivatives (**87a**, **87b**, **88a**, and **88b**), revealed that the absolute configurations at C1′ and C27 were both *R* (Fig. 50b). Consequently, the absolute stereochemistry of filipin III was determined to be 1′*R*, 2*R*, 3*S*, 5*S*, 7*S*, 9*R*, 11*R*, 13*R*, 15*S*, 26*S*, and 27*R*.[76]

Marinisporolides A and B (**89** and **90**), 34-membered conjugated pentaene macrolides, were isolated from the saline culture of the marine actinomycete strain *Marinispora* CNQ-140.[77] However, the presence of multiple pairs of 1,3-dihydroxy groups in the marinisporolides complicated their absolute configuration assignment.

Methanolysis of compound **89** produced the methyl ester **91** (Fig. 51). Based on the Kishi database, the relative configurations of the hydroxy groups at C25, C27, C29, and C31 were determined as either *syn*/*anti*/*syn* or *anti*/*syn*/*anti*. Fig. 51 illustrates the

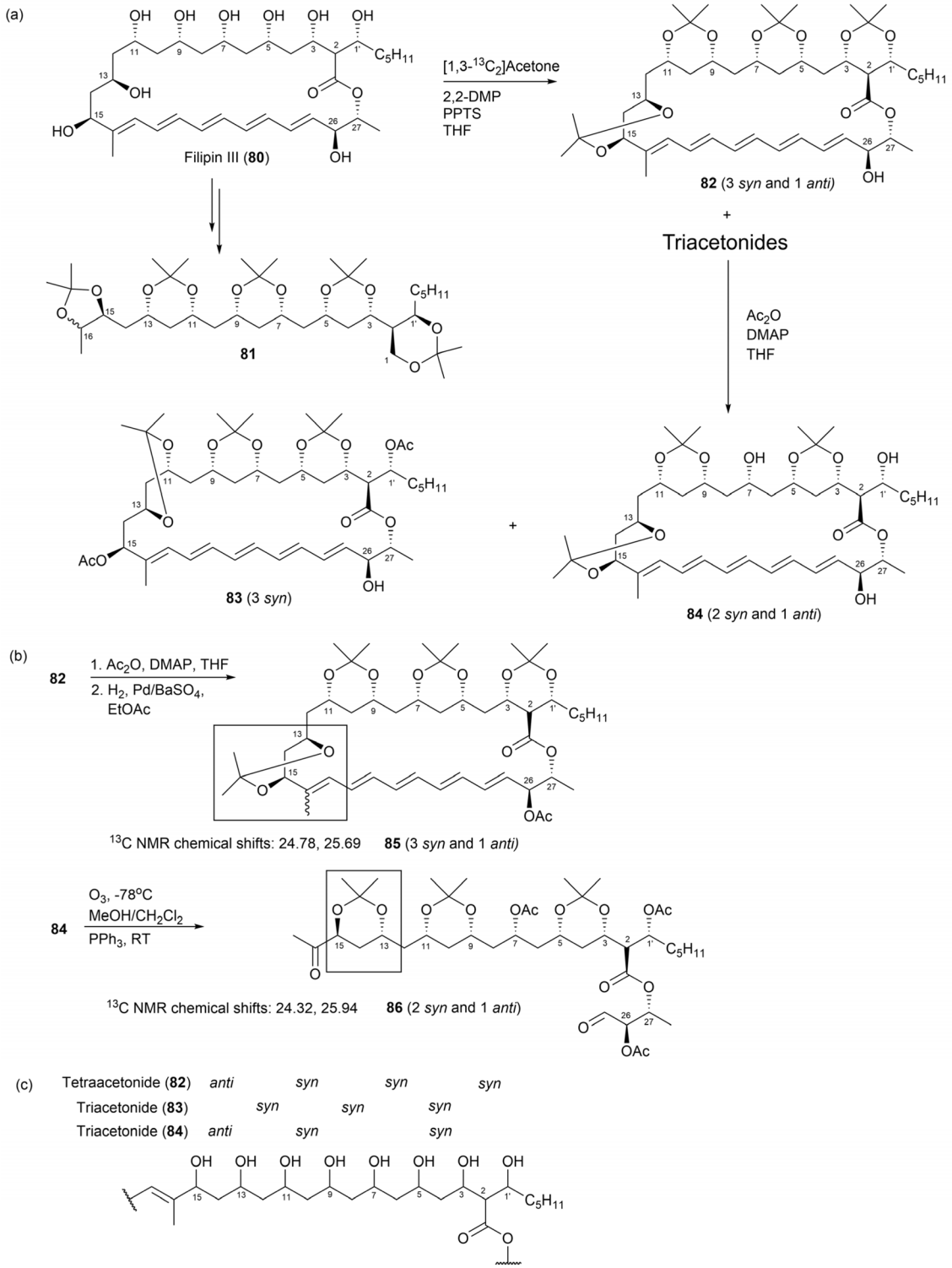

Fig. 49 (a) Polyacetonide derivatives of filipin III (**80**). (b) Degradation of compounds **82** and **84**. (c) Overview of the configurational assignment of filipin III.

synthesis of bis-acetonide **92** from compound **89** through acetonide formation, resulting in the formation of ketals on the C25, C27, C29, and C31 hydroxy groups. Based on the chemical shifts (δ_C 20.2, 30.6, 20.5 and 30.6), the configurations of the hydroxy groups at C25 and C27 and at C29 and C31 were determined as *syn*. Further characterization using NOE correlations revealed the relative configurations of other chiral centres. Specifically, the relative configurations of the 1,3-diols were obtained as 25,27-

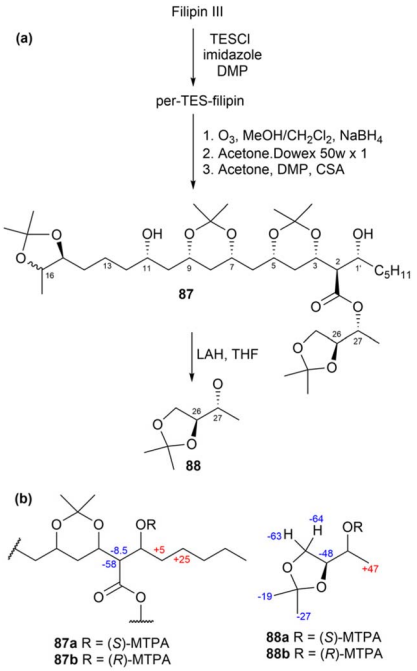

Fig. 50 (a) Degradation products (**87** and **88**) of filipin III. (b) $\Delta\delta_{S-R}$ values of the MTPA derivatives.

syn, 27,29-*anti*, 29,31-*syn*, 31,32-*anti*, and 32,33-*syn*. The absolute stereochemistry of compound **89** was established using the modified Mosher's method with the methanolysis product **93** utilized in this analysis.

Methanolysis of compound **90** with NaOMe in MeOH yielded a methyl ester (Fig. 52). HMQC NMR spectroscopy analysis of the resulting compound **94** enabled the assignment of the relative configurations at C19, C21, C25, C27, C29, C31, C32, and C33 through comparisons of the observed carbon chemical shifts with those of the methanolysis product **91**. Notably, the carbon chemical shifts at C25, C27, C29, C31, C32, and C33 in **94** aligned with those observed in compound **91**, indicating identical relative configurations at C25–C33 in both compounds. To confirm these assignments, compound **90** was treated with Dowex X2-100 resin in MeOH for 10 min, which yielded marinisporolide A (**89**) as the major product. The ^{1}H and CD spectra of compound **89**, derived from **90**, matched those of compound **89**, confirming their identical absolute configurations.[77]

To determine the relative and absolute configurations of bahamaolides A (**9**) and B (**95**, with a 13*Z* configuration), the authors of a previous study subjected the 1,3-diols to acetonide formation.[41] The resulting tetraacetonide products were analysed using various NMR techniques to determine the stereochemistry of the hydroxy groups. The absolute configuration was further confirmed using the modified Mosher's method and chemical derivatizations (Fig. 53).

Tetraacetonide **96** featured a free alcohol at C15 and displayed characteristic methyl group chemical shifts, indicating the presence of two *syn* and two *anti* 1,3-diols. ROESY correlations revealed that the hydroxy groups at C17 and C19 exhibited a *syn* configuration, while those at C21 and C23 displayed an

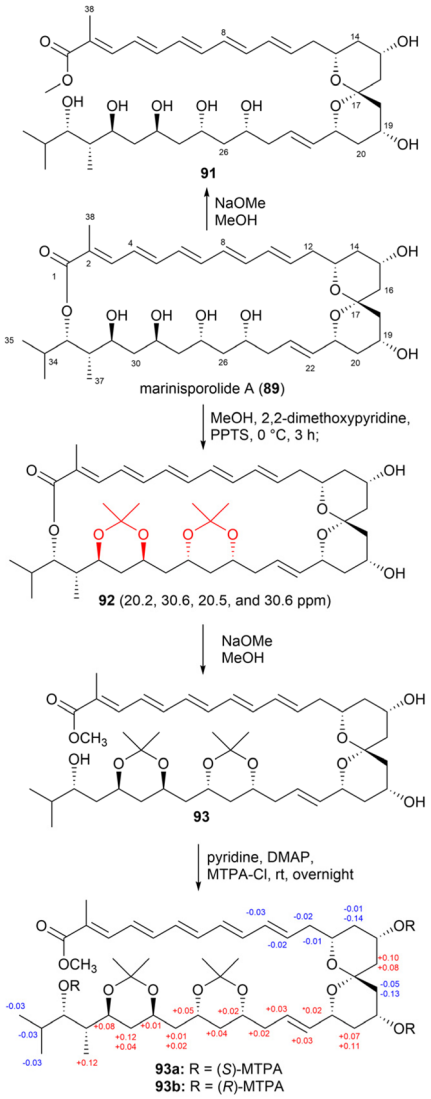

Fig. 51 Chemical reactions of marinisporolide A (**89**).

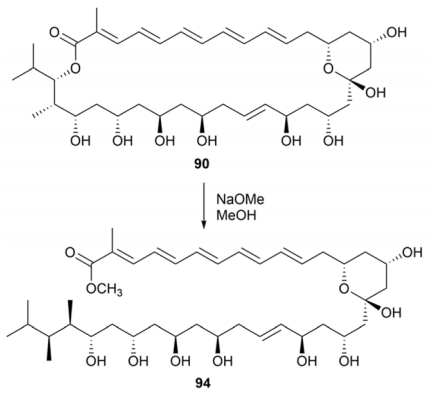

Fig. 52 Methanolysis of marinisporolide B (**90**).

anti configuration. Tetraacetonide **97** comprised a free hydroxy group at C31. In this compound, the configuration at C19 and C21 was *syn*, while that at C23 and C25 was *anti*. Notably, the

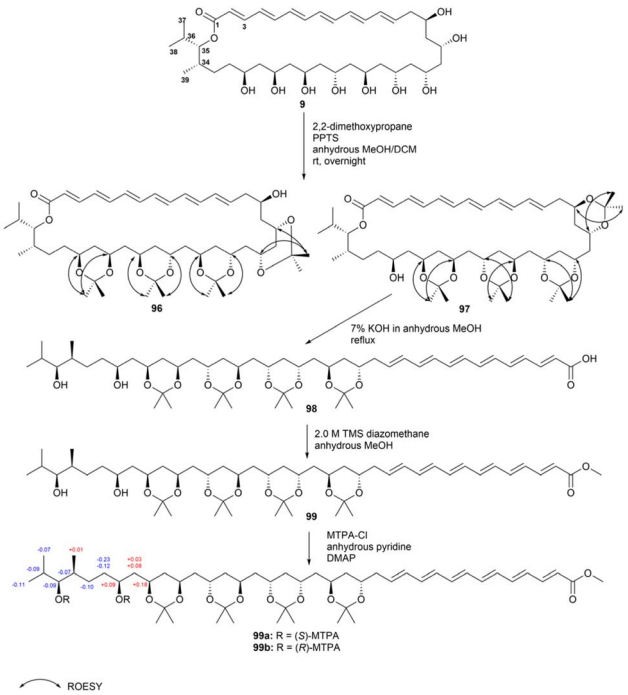

Fig. 53 Acetonide formation, hydrolysis, methylation, and Mosher's reaction of bahamaolide A (**9**).

configurations at C25, C27, and C29 were classified as *syn* or *anti* based on the appearance of distinct NMR peaks. JBCA revealed that the stereogenic centres at C34 and C35 exhibited an *anti* relationship. The application of the modified Mosher's method to tetraacetonide **97** and its linear methyl ester **99** revealed that the absolute configuration at C31 was *S*. Ultimately, the polyol configuration was confirmed to be 15*R*, 17*S*, 19*S*, 21*S*, 23*S*, 25*R*, 27*S*, 29*S*, and 31*S*, with the stereogenic centres at C34 and C35 being assigned as *S* and *S*, respectively.[41]

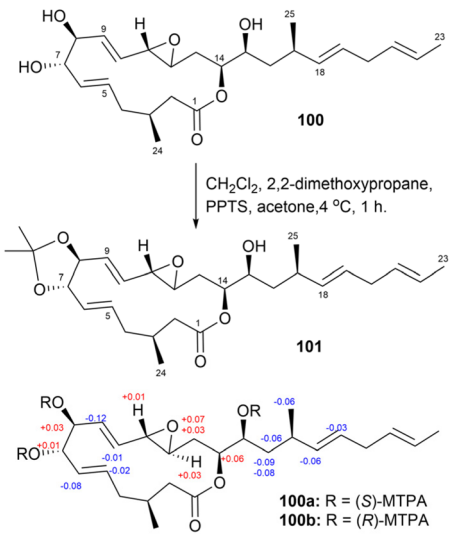

Fig. 54 Acetonide formation of iriomoteolide-3a (**100**) and its MTPA ester products (**100a** and **100b**).

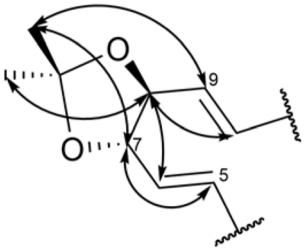

Fig. 55 Key ROESY correlations for the C4–C11 region in the derivative (**101**).

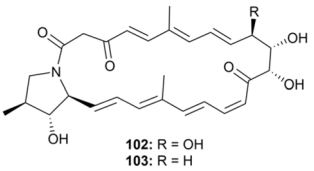

Fig. 56 Structures of niizalactams A and B (**102** and **103**).

Iriomoteolide-3a (**100**), a 15-membered macrolide featuring an allyl epoxide, was isolated from a marine benthic dinoflagellate-derived strain, *Amphidinium* sp. HYA024.[78] Determining the stereochemical configuration of compound **100** was particularly complex in the C6–C9 region, where overlapping signals from H7 and H8 complicated the assignment of the relative configuration.

To overcome these challenges, iriomoteolide-3a (**100**) was converted into the 7,8-*O*-isopropylidene derivative (**101**) through acetonide formation (Fig. 54). ROESY correlations confirmed a *trans* configuration between H7 and H8 (Fig. 55). Furthermore, the values of coupling constants ($^3J_{H6,H7}$, $^3J_{H7,H8}$, and $^3J_{H8,H9}$) for derivative **101**, all measured at 8.6 Hz, suggested *anti* relationships among these hydrogen atoms. The absolute

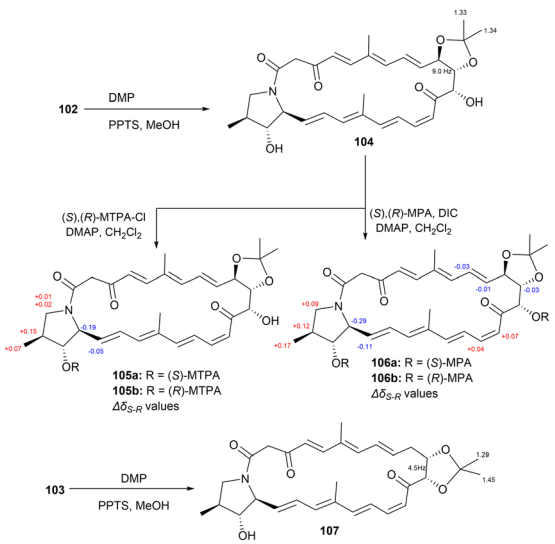

Fig. 57 Chemical modifications of niizalactams A and B (**102** and **103**).

configuration of compound **100** was ultimately determined using the modified Mosher's method.

Niizalactams A and B (**102** and **103**, Fig. 56) belong to the same structural family as niizalactam C, but both compounds **102** and **103** possess bicyclic skeletons. These compounds were isolated from a terrestrial bacterium, *Streptomyces* sp. NZ-6, and co-cultured with the mycolic acid-containing bacterium *Tsukamurella pulmonis* TP-B0596.[79]

The relative stereochemistries of the pyrrolidinol rings (C22 to C25) in compounds **102** and **103** were determined as (22*S**, 23*R**, and 24*S**) based on NOESY correlations. However, the NOESY data did not clearly resolve the stereochemistries of the 1,2,3-triol (in **102**) and 1,2-diol (in **103**) moieties. To address this, acetonide derivatives **104** and **107** were synthesized from compounds **102** and **103** using 2,2-dimethoxypropane and PPTS (Fig. 57).

The similar chemical shifts of the isopropylidene methyl groups and a large value of the coupling constant ($^3J_{H10,H11}$ = 9.0 Hz) indicated an *anti* configuration for the 10,11-diol in compound **102**. Meanwhile, dissimilar chemical shifts ($\Delta\delta_H$ = 0.16) and a small value of the coupling constant ($^3J_{H11,H12}$ = 4.5 Hz) confirmed a *syn* configuration for the 11,12-diol in compound **103**. Consequently, the relative configurations of the triol moiety in compound **102** were assigned as (10*R**, 11*S**, and 12*S**), and the corresponding moiety in compound **103** was inferred to share the same configuration.

The absolute configurations of compound **102** were further determined using the modified Mosher's method and Trost's method (Fig. 57). First, derivative **104** was treated with MTPA-Cl to yield MTPA esters (**105a** and **105b**), which established the pyrrolidinol configurations as (22*S*, 23*R*, 24*S*). Next, the absolute configurations of the 1,2,3-triol moiety were determined using bis-MPA derivatives (**106a** and **106b**), resulting in the assignments (10*R*, 11*S*, 12*S*). Structural comparisons between compounds **102** and **103** allowed the absolute configuration of compound **103** to be identified as (11*S*, 12*S*, 22*S*, 23*R*, and 24*S*).[79]

In another study, marinomycins were isolated from the saline culture of a newly discovered group of marine actinomycetes called *Marinispora*.[80] Structural elucidation revealed that marinomycins are unusual macrodiolides composed of dimeric 2-hydroxy-6-alkenyl-benzoic acid lactones, featuring conjugated tetraene-pentahydroxy polyketide chains (Fig. 58). Biological evaluation demonstrated that these compounds exhibit potent antimicrobial activity against drug-resistant bacterial pathogens and impressive selective cytotoxicity.

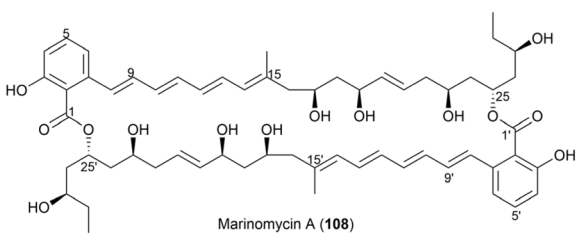

Fig. 58 Structure of marinomycin A (**108**).

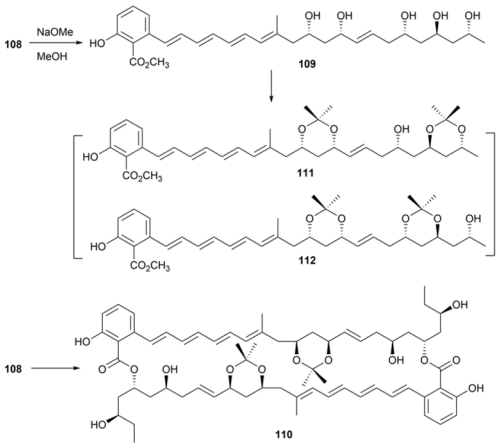

Fig. 59 Methanolysis and acetonide formation of marinomycin A (**108**).

Methanolysis of marinomycin A (**108**) resulted in the cleavage of both lactone linkages, yielding the monomeric methyl ester (compound **109**). This product was characterized using LC-MS and NMR spectroscopic analyses, confirming compound **108** to be a dimeric macrodiolide with a unique 44-membered ring structure (Fig. 58). NMR spectral analysis of **109** enabled the assignment of the relative stereochemistry of the polyol functionalities at C17, C19, C23, C25, and C27 in compound **108**.

Acetonide formation of **108** yielded a bis-acetone ketal (**110**, Fig. 59). NMR data analysis of this compound revealed chemical shifts of the acetonide methyl groups at δ_C 19.6 and 30.1, indicating that the 1,3-dioxane ring adopts a chair conformation. Based on these shifts, the authors assigned the hydroxy

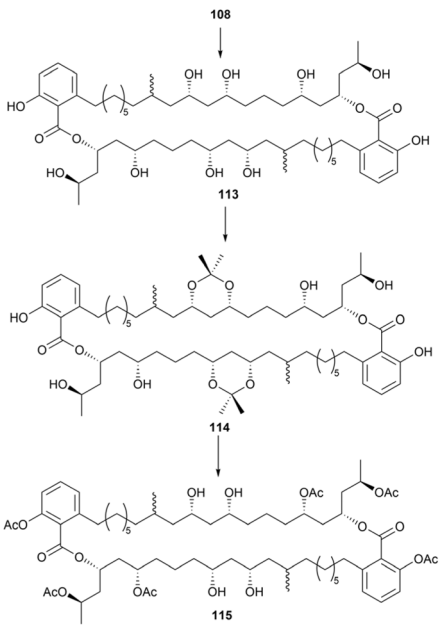

Fig. 60 Hydrogenation of olefinic bonds in **108**, acetonide formation, acetylation, and acetonide deprotection to form **115**.

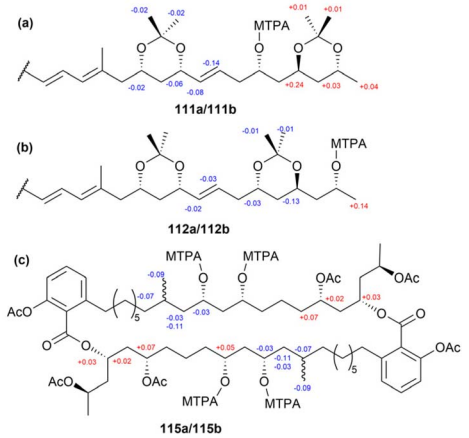

Fig. 61 Chemical shift differences ($\Delta\delta_{S-R}$) between (*S*)- and (*R*)-MTPA esters. (a) Partial assignment of (*S*)- and (*R*)-MTPA esters (**111a**/**111b**). (b) Partial assignment of (*S*)- and (*R*)-MTPA esters (**112a**/**112b**). (c) Assignment of (*S*)- and (*R*)-MTPA esters (**115a**/**115b**).

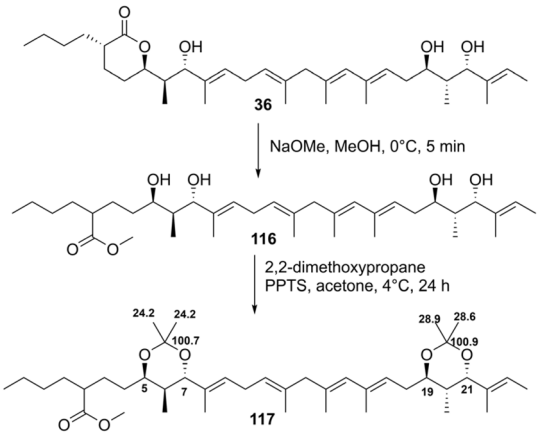

Fig. 62 Preparation of bisacetonide (**117**).

groups at C17 and C19 (and their symmetry equivalents, C17′ and C19′) to a *syn* configuration. Methanolysis product **109** was subjected to acetonide formation, resulting in two diacetonides, labeled compounds **111** and **112**. NMR data analysis of these bis-ketals confirmed the relative stereochemistry of the three 1,3-diols in **108** as follows: 17,19-*syn* (and 17′,19′-*syn*), 23,25-*anti* (and 23′,25′-*anti*), and 25,27-*anti* (and 25′,27′-*anti*).

To determine the absolute stereochemistry of marinomycin A, the modified Mosher's method was employed, using acetonides **111** and **112** (Fig. 61). Analysis of the ^{1}H NMR chemical shift differences ($\Delta\delta_{S-R}$) between the (*S*)- and (*R*)-MTPA esters (**111a** and **111b**) revealed that the absolute stereochemistry at C23 is *S*. Similarly, the preparation of (*S*)-MTPA ester (**112a**) and (*R*)-MTPA ester (**112b**) from compound **112**, followed by NMR data analysis, confirmed that the absolute stereochemistry at C27 is *R*.

To resolve the absolute configuration at C19, various derivatives were synthesized. For instance, hydrogenation of the olefinic bonds in compound **108** produced compound **113**, which was further modified through acetonide formation, acetylation, and subsequent acetonide deprotection, yielding derivative **115** with six acetyl groups (Fig. 60). Treating compound **115** with (*R*)-MTPA-Cl and (*S*)-MTPA-Cl under standard acylation conditions yielded tetra-(*S*)-MTPA ester (**115a**) and tetra-(*R*)-MTPA ester (**115b**), respectively. Using both of the conventional Mosher ester ^{19}F NMR approach and the modified Mosher's analysis, the absolute configurations of C17, C17′, C19, and C19′ were determined. The negative $\Delta\delta_{S-R}$ values observed for the four fluorine signals of compounds **115a** and **115b** (Fig. 61) indicated that the absolute configurations at C17, C17′, C19, and C19′ are all *S*.

Consequently, the absolute configurations at C17, C17′, C19, C19′, C23, and C25 were assigned as *S*, while those at C27 and C27′ were determined as *R*.[80]

For the phytohabitols A–C (**36–38**) mentioned in Section 2.2.5, the absolute configuration at C5 was determined using [^{13}C] acetonide analysis.[64] Methanolysis of the lactone with NaOMe in methanol produced methyl ester **116**, which was subsequently reacted with 2,2-dimethoxypropane in the presence of PPTS as a catalyst, yielding bisacetonide **117** (Fig. 62). Analysis of the HSQC and HMBC spectra enabled the assignment of the ^{13}C NMR chemical shifts for the acetonide methyl groups and acetal carbons: 24.2 ppm (×2) and 100.7 ppm for the 5,7-acetonide, and 28.6, 28.9, and 100.9 ppm for the 19,21-acetonide. These chemical shifts were consistent with a six-membered 1,3-dioxane ring in a twist-boat conformation, confirming *anti* relationships for the 5,7- and 19,21-diols. Consequently, the *R*-configuration at C5 was established.

2.4. Comparisons of chemical shifts without chemical derivatization

2.4.1. Application of Kishi's NMR database. Determining the absolute configurations of all chiral centres in compounds with multiple stereogenic centres can be simplified through relative configurational analysis. Relative configurational analysis is a crucial step in determining the absolute configurations of organic compounds. To facilitate this, Yoshito Kishi's research team developed an NMR database for common structural motifs found in natural products, particularly polyketides. Utilizing this database allows for the rapid and straightforward determination of relative configurations with minimal or no chemical degradation or modification. These advantages are particularly valuable for natural product research because the quantities of compounds isolated from natural sources are often limited. Noticeably, Kishi's database provides not only a dataset but also empirical rules that serve as a robust framework for configurational assignment. Generally, Kishi's method is based on an NMR database of stereoisomers of model compounds that share the same carbon connectivity as the selected stereocluster, whose NMR properties are assumed to depend on the configuration of the stereocluster but to be independent of the rest of the molecule.[81,82] Kishi's NMR database was initially developed for the chemical shifts of contiguous propionate motifs and later extended to diol, triol, and polyol systems. In addition to chemical shifts, *J*-coupling data

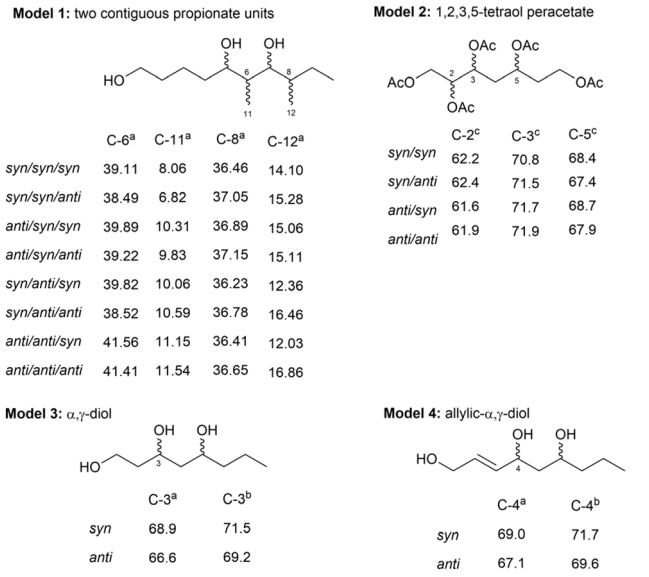

Model 1	C-6[a]	C-11[a]	C-8[a]	C-12[a]
syn/syn/syn	39.11	8.06	36.46	14.10
syn/syn/anti	38.49	6.82	37.05	15.28
anti/syn/syn	39.89	10.31	36.89	15.06
anti/syn/anti	39.22	9.83	37.15	15.11
syn/anti/syn	39.82	10.06	36.23	12.36
syn/anti/anti	38.52	10.59	36.78	16.46
anti/anti/syn	41.56	11.15	36.41	12.03
anti/anti/anti	41.41	11.54	36.65	16.86

Model 2	C-2[c]	C-3[c]	C-5[c]
syn/syn	62.2	70.8	68.4
syn/anti	62.4	71.5	67.4
anti/syn	61.6	71.7	68.7
anti/anti	61.9	71.9	67.9

Model 3	C-3[a]	C-3[b]
syn	68.9	71.5
anti	66.6	69.2

Model 4	C-4[a]	C-4[b]
syn	69.0	71.7
anti	67.1	69.6

Fig. 63 Kishi's NMR database for common motifs found in natural products, including two contiguous propionate units (model 1); α,β,γ,ε-tetraol peracetate (model 2); α,γ-diol (model 3); and allylic α,γ-diol (model 4). (a) Recorded in DMSO-d_6, (b) recorded in CD_3OD, and (c) recorded in $CDCl_3$.

were incorporated into the database to enable more precise and direct configurational assignments.[83]

Kishi's NMR database was constructed using small model molecules containing partial structures commonly found in natural products, such as α,γ,ε-triol motifs[84] and contiguous propionate units.[85] All Kishi's model molecules share an α,γ-diol core structure. This is attributed to not only the frequent occurrence of the α,γ-diol motif in natural products but also its

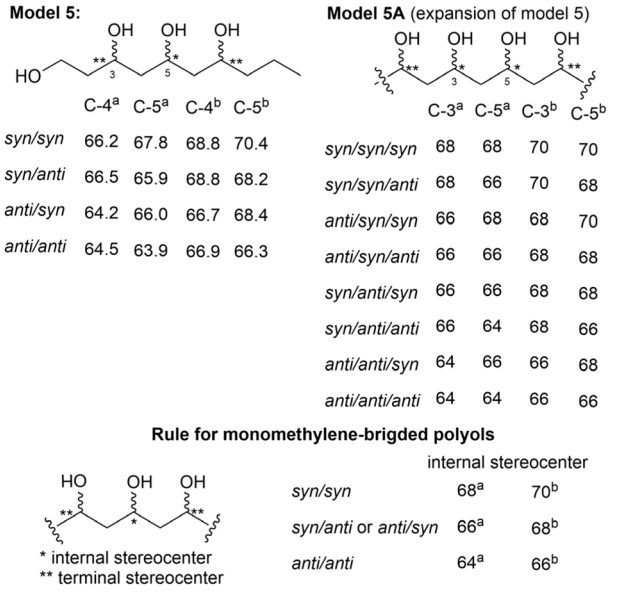

Model 5	C-4[a]	C-5[a]	C-4[b]	C-5[b]
syn/syn	66.2	67.8	68.8	70.4
syn/anti	66.5	65.9	68.8	68.2
anti/syn	64.2	66.0	66.7	68.4
anti/anti	64.5	63.9	66.9	66.3

Model 5A	C-3[a]	C-5[a]	C-3[b]	C-5[b]
syn/syn/syn	68	68	70	70
syn/syn/anti	68	66	70	68
anti/syn/syn	66	68	68	70
anti/syn/anti	66	66	68	68
syn/anti/syn	66	66	68	68
syn/anti/anti	66	64	68	66
anti/anti/syn	64	66	66	68
anti/anti/anti	64	64	66	66

Rule for monomethylene-brigded polyols	internal stereocenter	
syn/syn	68[a]	70[b]
syn/anti or anti/syn	66[a]	68[b]
anti/anti	64[a]	66[b]

Fig. 64 Kishi's NMR database for additional motifs found in natural products, including α,γ,ε-triol (model 5), along with the empirical rule for monomethylene-bridged polyols. (a) recorded in DMSO-d_6 and (b) recorded in CD_3OD.

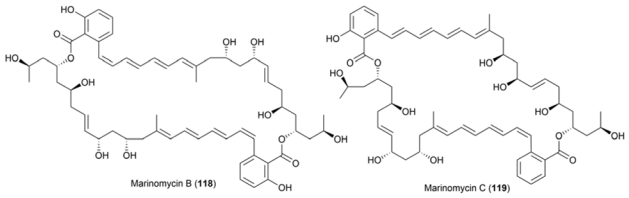

Fig. 65 Structures of marinomycins B and C (**118** and **119**).

distinctive spectroscopic features. The ^{13}C NMR chemical shifts of the α,γ-diol motif recorded in DMSO-d_6 revealed shifts of approximately 68 ppm and 66 ppm for the *syn* isomer and *anti* isomer, respectively. These results indicated a consistent trend: the ^{13}C NMR chemical shift of the *syn* diol was approximately 2 ppm higher than that of the *anti* diol (Fig. 63).[84] Additional ^{13}C NMR data from an expanded structural motif, the α,γ,ε-triol motif (model 5), confirmed this trend. A comparison between the NMR data of α,γ-diol and allylic α,γ-diol demonstrated that functional groups attached to the motif could influence chemical shifts; however, the 2 ppm difference between the *syn* and *anti* diol isomers remained unaffected. Thus, monomethylene-spaced polyols exhibit a unique characteristic: the chemical shifts of internal carbons and their corresponding hydrogen atoms are independent of the functional groups outside the motif but depend on the relative configurations at C_α/C_γ and C_γ/C_ε. This behavior remains consistent even for higher polyol systems, such as tetraols and pentaols (Fig. 64).[84]

As detailed in Section 2.3, to determine the configuration of marinomycin A (**108**), methanolysis of **108** was performed to

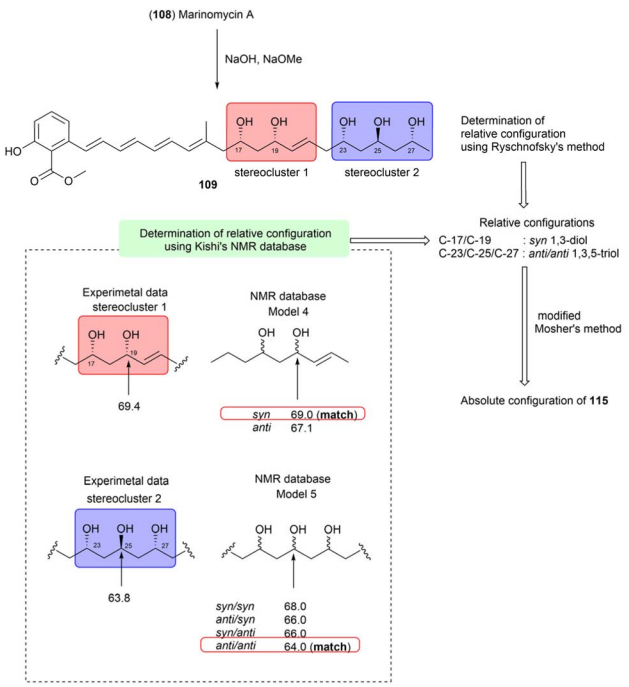

Fig. 66 Comparison of the experimental ^{13}C NMR data of stereocluster A in the degradation product (**109**) with the corresponding carbons in model 1. Data recorded in DMSO-d_6.

obtain the ester derivative (**109**), and the ^{13}C NMR spectrum of this derivative (**109**) was recorded in DMSO-d_6 (Fig. 59).[80] Notably, the alkenyl chain in (**109**) comprises two stereoclusters: the first from C16 to C20 and the second from C22 to C28 (Fig. 66). The relative configurations of these stereoclusters (stereocluster 1 and stereocluster 2) were determined by comparing the experimental ^{13}C NMR data with those of model 4 and model 5, respectively. Consequently, stereocluster 1 was determined to have a *syn* orientation, while the three hydroxy groups at C23, C25, and C27 were determined to exhibit *anti*/*anti* orientations.

To confirm the configurations assigned by the Kishi's database, acetonide derivatives of **108** and **109** were prepared. The ^{13}C NMR spectra of these derivatives were analysed following the method described by Rychnovsky, enabling the assignment of the relative configurations of the two stereoclusters. The results of Rychnovsky's method demonstrated good agreement with the configurations predicted by Kishi's NMR database. Finally, the absolute configuration of marinomycin A was assigned as illustrated in Fig. 58. This assignment was achieved by determining the *S* configurations at C17, C19, and C23 through a combination of chemical modifications and both classical and modified Mosher's methods. Marinomycins B (**118**) and C (**119**), geometric isomers of marinomycin A, were identified as photoconversion products of **108**. Hence, the stereochemistry of **118** and **119** was assumed to be identical to that of **108** (Fig. 65).[80]

Oasomycins and desertomycins are 42-membered macrolactones isolated from *Streptoverticillium baldacii* subsp. *netropse* (Fig. 67).[86] These compounds typically undergo natural structural modifications on the side chains at C22 and C50, while the macrolactone core remains preserved. Given that these compounds share the same macro-ring skeleton, oasomycin A (**120**) was selected as a representative compound for the stereochemical analysis of the macrolactone moiety. Notably, the ring structure consists of two stereoclusters: stereocluster A

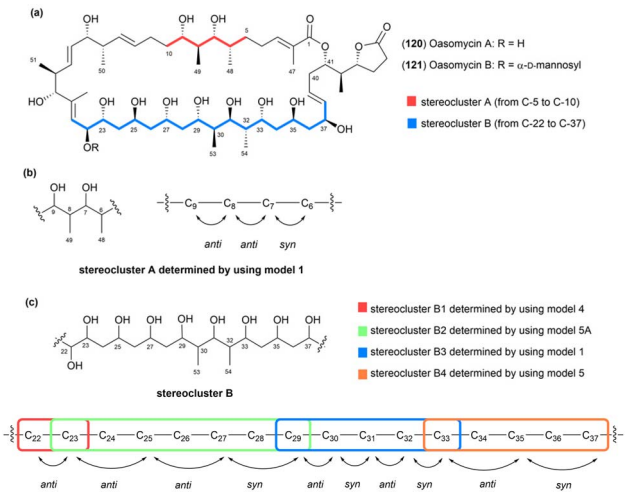

Fig. 67 (a) Structures of oasomycins A (**120**) and B (**121**). (b) Relative configurations of stereocluster A (from C5 to C10). (c) Relative configurations of stereocluster B (from C21 to C38).

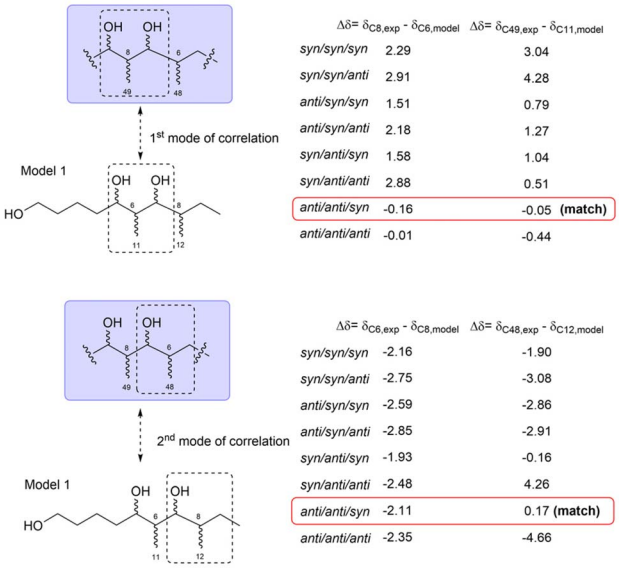

Fig. 68 Comparison of the experimental ^{13}C NMR data of stereocluster A in compound **120** with the data of corresponding carbons in model 1. NMR data were recorded in DMSO-d_6.

(from C5 to C10) and stereocluster B (from C21 to C38). The relative configuration of stereocluster A was determined by comparing the ^{13}C NMR chemical shifts of the C5–C10 fragment with those of model 1, which contains a two-contiguous-propionate-unit motif. As illustrated in Fig. 68, C6, C8, C48, and C49 in stereocluster A corresponded to C8, C6, C12, and C11 in model 1, respectively. The differences in the ^{13}C NMR chemical shifts between the corresponding carbons revealed that stereocluster A exhibits *anti*/*anti*/*syn* configurations (Fig. 68).[81]

Next, stereocluster B (Fig. 67a) of compound **120** was divided into four parts: part B1 (red box, from C22 to C23), part B2 (green box, from C23 to C29), part B3 (blue box, from C29 to C33), and part B4 (orange box, from C33 to C37) (Fig. 67c). Parts B2 and B4 were compared with model molecules 5 and 5A owing to the presence of monomethylene-spaced polyol motifs. Notably, the ^{13}C NMR chemical shifts of C25 and C27 in part B2 were similar to those of the internal carbons in model 5A, suggesting that the relative configurations at C23/C25/C27/C29 are *anti*/*anti*/*syn* (Fig. 69). Similarly, the triol in part B4 was assigned an *anti*/*anti* configuration, as the chemical shift of C25 matched that of the internal carbon of the *anti*/*anti* isomer in model 5 (Fig. 69).[87]

For part B3, which contains a two-contiguous-propionate-unit motif, comparison with model 1 revealed two correlation modes. The first mode (C29–C31) and the second mode (C31–C33) corresponded to the C5–C7 fragment of model 1. The relative configurations of C29/C30/C31/C32 were assigned as *anti*/*syn*/*anti* based on the similarities in the ^{13}C NMR chemical shifts of C30 and C53 and their corresponding carbons, C6 and C11, in model 1. However, determining the configuration of the substituents in the C31–C33 fragment proved more challenging. This was because comparisons between the ^{13}C NMR data of

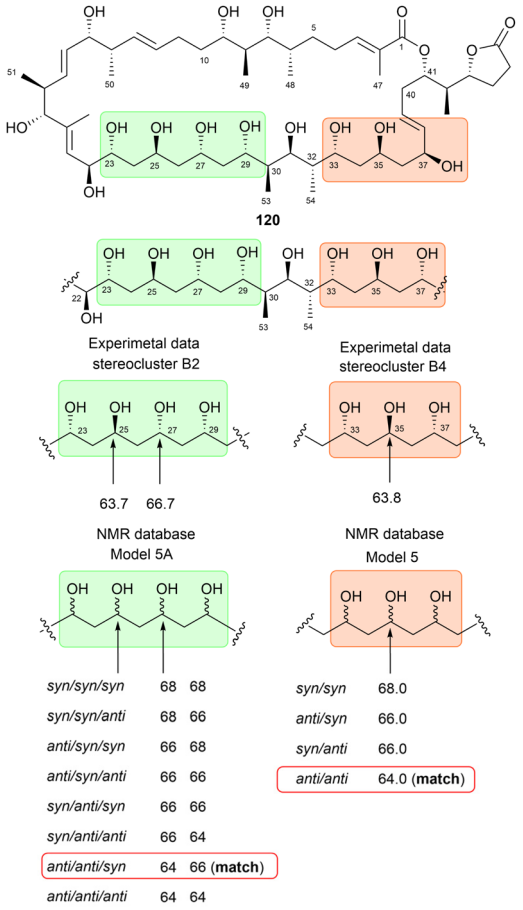

Fig. 69 Determination of the relative configurations of stereoclusters B2 (green box, from C23 to C29) and B4 (orange box, from C33 to C37) of **120**. NMR data were recorded in DMSO-d_6.

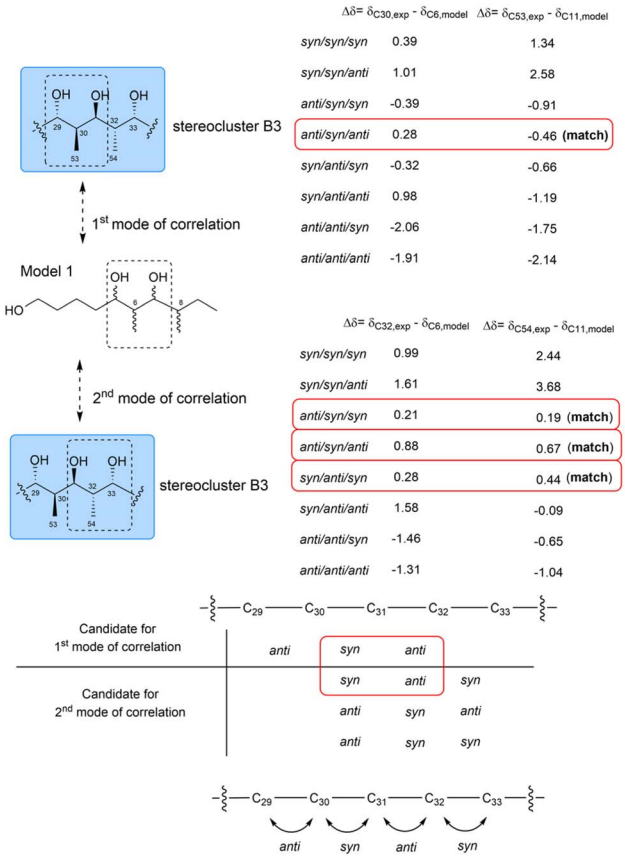

Fig. 70 Determination of the relative configurations of part B3 (blue box, C29 to C33). NMR data were recorded in DMSO-d_6.

C32 and C54 and the data of the corresponding carbons from Kishi's database suggested three possible relative configurations: *syn*/*anti*/*syn*, *syn*/*syn*/*anti* and *anti*/*syn*/*syn* (Fig. 70). Given that the configuration from C30 to C32 must be consistent across both correlation modes, only the *syn*/*anti*/*syn* isomer of the second mode met this requirement. Therefore, the relative configuration of part B3 was successfully assigned as *anti*/*syn*/*anti*/*syn* (Fig. 70).[87]

To determine the configuration of part B1, compound **122** was prepared through multiple steps of chemical degradation and modification of **120**. Model 4, which shares the α,β,γ,ε-tetraol peracetate partial structure of compound **122**, was also prepared to expand the database for assigning the relative configuration of C22 and C23 in part B1. The ^{13}C NMR chemical shifts of C21, C22, and C23 in compound **122** were similar to those of C1, C2, and C3, respectively, confirming the *anti*/*anti* orientation of substituents attached to C22, C23, and C25 (Fig. 71). Interestingly, the *anti* configuration of the two hydroxy groups at C23 and C25, determined through the analysis of model 2, aligns with the relative configuration of C23/C25 determined using model 5A (Fig. 69). This consistency across analyses utilizing Kishi's NMR database demonstrates the reliability and robustness of the method.[87]

The combined analysis of parts B1, B2, B3, and B4 enabled the researchers to determine the relative configuration of stereocluster B, as depicted in Fig. 67c. The ^{1}H NMR spectrum of compound **122** was compared with that of the degradation

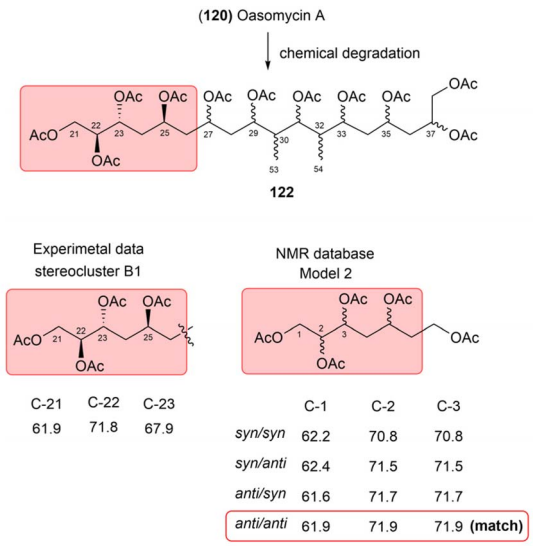

Fig. 71 Determination of the relative configurations of part B1 (red box, from C21 to C23). NMR data were recorded in $CDCl_3$.

product derived from natural oasomycin A, demonstrating excellent agreement with the configuration predicted using Kishi's NMR database.[88]

These successful case studies demonstrate that Kishi's NMR database is a powerful and straightforward tool for determining the relative configurations of polyketides, particularly polyols. Additionally, Kishi's database serves as a useful alternative to JBCA, especially when *J*-coupling values are altered or cannot be observed. However, this method has several limitations. First, it is applicable only to specific structural motifs, such as monomethylene-spaced polyols and allylic diols. Second, in numerous cases, Kishi's database cannot reliably distinguish between *syn*/*anti* and *anti*/*syn* isomers.[84] For instance, in the case of α,γ,ε-triols, the chemical shift of the internal carbon is approximately 66 ppm in both the *syn*/*anti* and *anti*/*syn* isomers. Finally, given that the NMR data included in Kishi's database have only been recorded in DMSO-d_6 and CD_3OD, this approach is not applicable to compounds that are insoluble in these solvents.

2.4.2. Application of chiral NMR solvents: Kishi's bidentate solvents. Bis-α-methylbenzylamines (BMBA), chiral NMR solvents, were developed to determine the absolute configurations of hydroxy groups separated by two carbon atoms. This approach relies on the formation of hydrogen bonds between the amino groups of BMBA and the hydroxy groups of alcohols, establishing a recognition mode (Fig. 72). To reduce the high viscosity of BMBA, a 5 : 2 mixture of BMBA-*p*-Me and an achiral solvent (such as $CDCl_3$, DMSO-d_6, pyridine-d_5, or CD_3OD) was used in the NMR experiments.[89] The absolute configurations of alcohols were assigned by analysing the chemical shift behaviors of the adjacent carbons in (*R*,*R*)- and (*S*,*S*)-BMBA-*p*-Me, following the empirical rule shown in Fig. 72c.[90] Notably, this

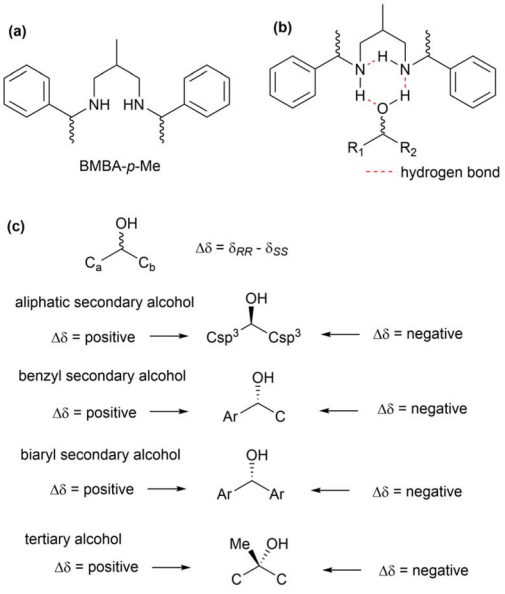

Fig. 72 (a) Structure of BMBA-*p*-Me. (b) Recognition mode between BMBA-*p*-Me and an isolated hydroxy group. (c) Empirical rule for determining the absolute configurations of alcohols using Kishi's bidentate chiral solvent.

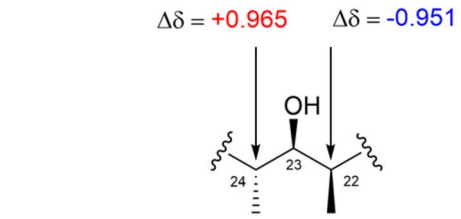

Fig. 73 Chemical shift differences of the carbon adjacent to C23 in pulvomycin B (**10**) observed in a 5 : 2 mixture of (*R*,*R*)- and (*S*,*S*)-BMBA-*p*-Me and $CDCl_3$.

method allows natural product chemists to determine the absolute configuration of hydroxy groups without requiring chemical derivatization, making Kishi's bidentate solvents a valuable alternative when the Mosher's method fails. Furthermore, each hydroxymethine unit can be analysed independently and simultaneously, simplifying the process of absolute configuration determination. This technique also has broad applications in determining the stereochemistry of a variety of alcohol types, including secondary, benzyl, biaryl, and tertiary alcohols.[89,90]

The absolute configuration of the hydroxy group at C23 in pulvomycin B (**10**) could not be determined using Mosher's method owing to the failure of MTPA derivatization by steric-hindrance. To address this problem, the ^{13}C NMR behavior of adjacent carbons in the presence of (*R*,*R*)- and (*S*,*S*)- BMBA-*p*-Me solvents was analysed, leading to the successful assignment of the C23 hydroxy group as an *S*-configuration (Fig. 73).[42]

Mohangic acids A–E (**123–127**), a series of *p*-amino acetophenoic acids, were isolated from *Streptomyces* sp. SNM31,

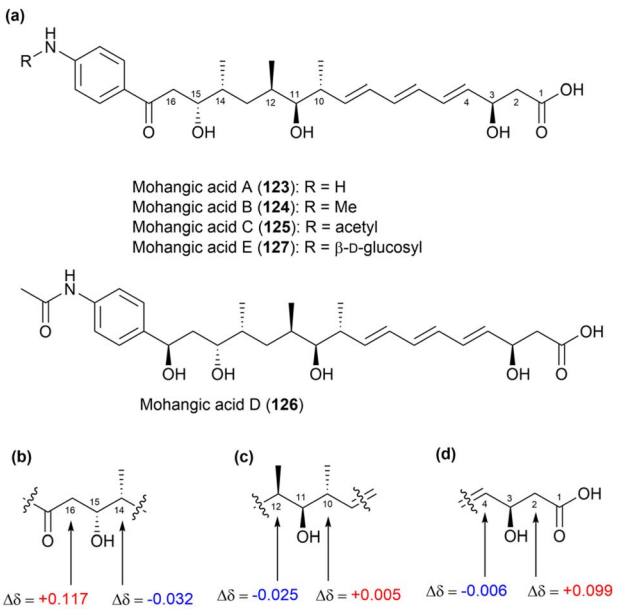

Fig. 74 (a) Structures of mohangic acids A–E (**123–127**). Chemical shift differences of the carbons adjacent to tertiary alcohols in mohangic acid A (**123**): (b) C15, (c) C11, and (d) C3, observed in a 5 : 2 mixture of (*R*,*R*)- and (*S*,*S*) BMBA-*p*-Me and pyridine-d_5.

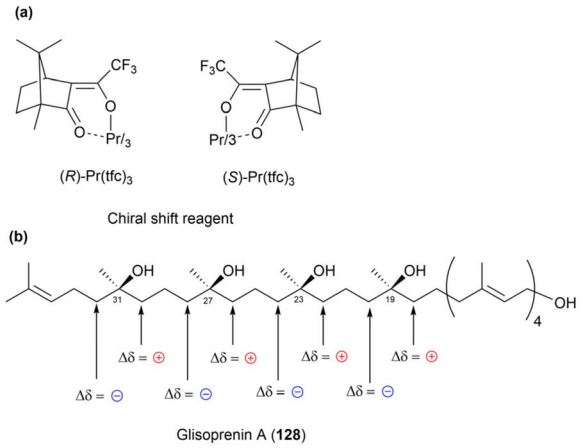

Fig. 75 (a) Structures of (*R*)- and (*S*)-Pr(tfc)$_3$, chiral shift reagents. (b) Structures and chemical shift differences of the carbons adjacent to the tertiary alcohols of glisoprenin A (**128**).

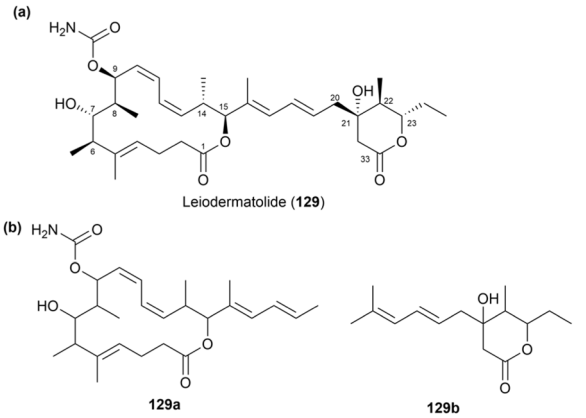

Fig. 76 (a) Structure of leiodermatolide (**129**). (b) Model structures **129a** and **129b** used in DP4 calculations for the macrolactone and δ-lactone parts, respectively.

a mudflat-derived strain. The ^{13}C NMR spectrum of mohangic acid A (**123**) was recorded in a 5 : 2 mixture of BMBA-*p*-Me and pyridine-d_5. Using Kishi's empirical rules, the three secondary alcohols in the alkyl chain of mohangic acid A were quickly assigned as 3*R*, 11*S*, and 15*R* without requiring chemical derivatization or degradation (Fig. 74). Owing to their shared biosynthetic origin and the similarities in the NMR data of the side chains, the absolute configurations of mohangic acids B–E (**124–127**) were also assigned as 3*R*, 11*S*, and 15*R*, consistent with those of mohangic acid A (**123**).[91]

Another successful application of Kishi's bidentate solvent was demonstrated with glisoprenin A (**128**). Glisoprenin A (**128**), a member of the polyprenol subclass isolated from the fungus *Gliocladium* sp. FO-1513, contains four stereogenic tertiary alcohols.[92] The initial attempt to assign the absolute configurations of the stereogenic centres was unsuccessful owing to overlapping ^{13}C NMR signals of adjacent carbons, recorded in (*R*,*R*)- and (*S*,*S*)-BMBA-*p*-Me, making it impossible to analyse their chemical shift behavior. This challenge was overcome by adding chiral shift reagents, (*R*)- and (*S*)-Pr(tfc)$_3$ (Fig. 75a), to the NMR mixture at a concentration of 25 mol% per hydroxy group in the structure of **128**. The addition of these reagents successfully spread out the ^{13}C resonances of all eight carbons adjacent to the tertiary alcohols, allowing for the detection of chemical shift differences between the α-carbons in (*R*,*R*)- and (*S*,*S*)-BMBA-*p*-Me. This analysis revealed that the absolute configurations of all four stereogenic centres were *S* (Fig. 75b). The assignment was further confirmed by comparing the ^{1}H NMR spectra of natural and fully synthetic glisoprenin A (**128**).[93,94]

2.4.3. Application of DP4, CP3 calculations and other related methods. The rapid development of computational tools has notably advanced stereochemical analysis of organic compounds. Among these, DP4 has become a popular tool for the stereochemical analysis of type-I PKS-derived polyketides. Another method, CP3, is often used in organic synthesis because it requires two sets of experimental NMR data, corresponding to two optical isomers or two structural variants. For example, CP3 is useful for determining the configurations of major and minor products from chemical synthesis, such as the total synthesis of isohasubanan alkaloids.[95] However, natural products are usually isolated as single isomers, yielding only one set of NMR data, which limits the application of CP3. In such cases, DP4 is preferred because it requires only one set of experimental NMR data. DP4 works by predicting the ^{1}H and ^{13}C NMR spectra of all possible conformers and comparing them statistically with the experimental NMR data. The relative configuration is then assigned as the conformer with the highest probability.[96]

Leiodermatolide (**129**), a 16-membered macrolactone connected to a δ-lactone *via* an alkenyl chain, was first isolated from the marine sponge *Leiodermatium* sp. by Amy E. Wright's research group. Intensive NMR data analysis determined the relative configuration of **129** (Fig. 76). However, Mosher's method failed to assign its absolute configuration. To address this, the DP4 methodology was applied. Model structures **129a** (corresponding to the marcolactone part) and **129b** (corresponding to the δ-lactone part) were used for the calculations. The experimental ^{1}H and ^{13}C NMR data of **129** and the DP4-predicted ^{1}H and ^{13}C NMR data of 622 conformers of **129a**, generated from 32 possible diastereoisomers, and 99 conformers of **129b**, generated from four possible diastereoisomers, were analysed. This analysis assigned the absolute configurations of the macrolactone core as (6*R*, 7*S*, 8*S*, 9*S*, 14*S*, and 15*S*) and the δ-lactone part as (21*S*, 22*S*, and 23*S*), with >99% probability. Given that Mosher's method failed to assign the absolute configurations, the final confirmation of these assignments required comparisons of NMR data and optical rotation between synthetic and natural leiodermatolide (**129**).[97] The macrolactone core of **129** and a non-natural isomer of **129** (6*S*, 7*S*, 8*R*, 9*S*, 14*S*, 15*S*) were synthesized independently by the research groups of Stephen M. Dalby and Martin E. Maier, respectively, confirming the DP4-predicted configuration for the macrolactone.[98,99] Finally, the proposed stereochemistry of the

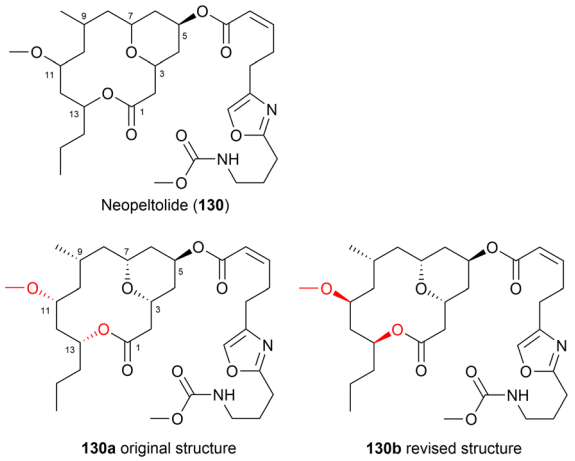

Fig. 77 Structures of the original (**130**) and modified neopeltolides (**130a** and **130b**).

δ-lactone part (21*S*, 22*S*, 23*S*) was validated by Alois Fürstner through total synthesis.[100]

Neopeltolide (**130**), a 14-membered macrolide, was isolated from a marine sponge belonging to the family Neopeltidae. The planar structure and relative configuration of neopeltolide were initially determined by 2D NMR data analysis (Fig. 77). However, owing to the limited quantity of **130**, its absolute configuration remained ambiguous.[101] Application of the DP4 method revealed that the correct configuration of neopeltolide was **130b**, the 11,13-*epi*-isomer of the originally proposed structure.

The absolute configurations of formicolides A (**2**) and B (**3**) were determined through a combination of 2D NMR, genomic approaches, and DP4 calculations.[36] For formicolide A (**2**), DP4 analysis was used to determine the absolute configurations at C5, C13, and C19. An analysis of the calculated ^{1}H and ^{13}C NMR data of the 50 conformers of two possible diastereomers (**2a** and **2b**) of **2** with the experimental NMR data of **2** led to the stereochemical assignment of C5, C13, and C19 as 5*R*, 13*S*, and 19*S*, with 100.0% probability. Meanwhile, for formicolide B (**3**), DP4 calculations focused on the side chain (C20 to C28). Using 17 conformers of two possible diastereomers, **3a** (19*S*, 20*S*, 21*R*, 22*R*, and 25*R*) and **3b** (19*S*, 20*S*, 21*R*, 22*R* and 25*S*), the side-chain configuration was determined as 19*S*, 20*S*, 21*R*, 22*R*, and 25*R* (Fig. 78).[36]

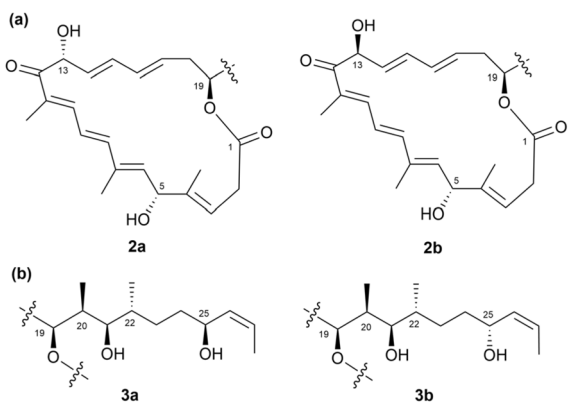

Fig. 78 (a) Two diastereomers considered in DP4 calculations for the macrolactone core of formicolide (**2**). (b) Two diastereomers considered in DP4 calculations for the side chain of formicolide B (**3**).

As mentioned in Section 2.3, the absolute configuration of C12 of arenicolide A (**59**) was unidentified although other chiral centers were assigned by combination of various methods such as JBCA, modified Mosher's method, and chemical modification. Recently, the stereocenter at C12 was assigned as 12-(*R*) with 100% probability by employing DP4. In total, 40 conformers of two C12-epimers of the macrolactone ring of **59** were considered for the calculation. Bioinformatic analysis revealed the absence of key tyrosine residue in the ER domain of module 12 of biosynthetic PKS genes, suggesting an *R* configuration of C12, which is consistent with the result from the DP4 calculation.[102]

Although DP4 is simple and robust aid for the determination of structure as well as configuration of a natural product, it has the common limitation of all comparison-based methods, where an incorrect structure may coincidentally match the experimental data more closely than the correct candidate.[103] There are several reasons for this problem, such as energy miscalculation, subtle differences in chemical shift between isomers, and the uncertain correctness of proposed structure candidates. To overcome this, Jonathan M. Goodman's group developed DP5 probability. Generally, DP5 is similar to DP4 in giving the probability that a proposed structure candidate is correct. However, the advancement of DP5 is that the structure candidates are proposed without any assumption about their correctness, since DP5 compares each proposed isomer to the chemical space, while DP4 compares each isomer against each other.[104] As of the drafting of this paper, DP5 has been available for only two years, so there are no case studies reporting the use of DP5 to determine the configuration of type-1 polyketide-derived natural products. In conclusion, both DP5 and DP4 each have their own unique advantages. DP5 shows higher reliability for cases where the proposed structures are of uncertain correctness, while DP4 is suitable for cases where the correctness of the structure candidates is guaranteed.[103,104] By understanding the strengths and limitations of each method, natural product chemists can choose the most appropriate method for each individual case to obtain a result with the highest probability.

2.5. Exploitation of chiroptical properties

2.5.1. Application of $[Mo_2(OAc)_4]$ in ECD experiments. Experimental ECD is a powerful technique for studying chiral molecules and their interactions with metal complexes, such as molybdenum diacetate ($[Mo_2(OAc)_4]$).[105] Notably, the $[Mo_2(OAc)_4]$ complex consists of two molybdenum atoms coordinated by four acetate groups. Its unique geometric arrangement can result in intriguing optical properties. Transition metal complexes can exhibit chirality if they adopt non-superimposable mirror image structures, with the arrangement of ligands around the metal centre playing a key role in

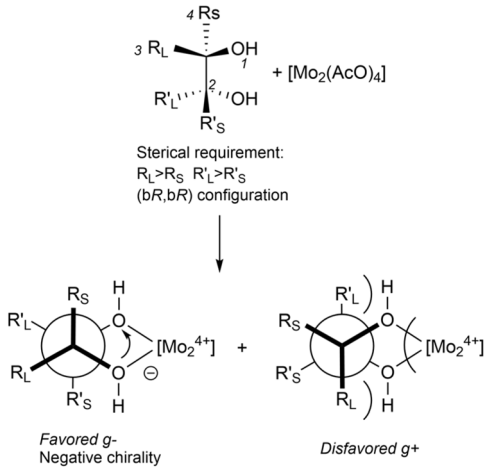

Fig. 79 Relationship between the steric configuration of the substrate and the sign of the O–C–C–O dihedral in the Cottonogenic derivative.

determining the chiral character. When a chiral ligand binds to $[Mo_2(OAc)_4]$, it can induce changes in the ECD spectrum by altering the electronic transitions owing to the new environment created around the metal centre (Fig. 79).

This phenomenon, known as induced ECD, occurs when an achiral complex, such as $[Mo_2(OAc)_4]$, interacts with a chiral environment, leading to the appearance of ECD signals. The presence of chiral substrates or solvents can induce ECD responses in the molybdenum complex, enabling stereospecific interaction analysis. The ECD spectrum of the $[Mo_2(OAc)_4]$ complex can be further analysed to identify the specific electronic transitions responsible for the observed circular dichroism. By comparing experimental ECD data with theoretical calculations, researchers can determine how the chiral ligand influences the complex's electronic structure. Specific peaks in the ECD spectrum correspond to different conformational states, providing insights into stereochemistry.

A practical application of this method was demonstrated in the study of dentigerumycin (**131**, Fig. 80), a type-I PKS-derived non-ribosomal peptide synthetase (NRPS) natural product produced by the bacterium *Pseudonocardia* associated with fungus-growing ants, such as *Apterostigma dentigerum*. These ants maintain a mutualistic relationship with the fungi they cultivate for food and actinobacteria that produce antibiotics, such as *Pseudonocardia*, which inhibit the parasitic fungus *Escovopsis* sp.[106] Molybdenum acetate $[Mo_2(OAc)_4]$ was used to determine the absolute configuration of dentigerumycin. The researchers determined the absolute configuration of the acyl side chain through the CD spectral analysis of the $[Mo_2(OAc)_4]$ complex with the 1,2-diol at positions C29 and C30. Following the empirical rule, the dentigerumycin complex displayed a negative sign at 305 nm in its induced CD spectrum, indicating that the C29 and C30 stereogenic centres adopt the 29*S* and 30*R* configurations if the 1,2-diol remains in its expected low-energy conformation.

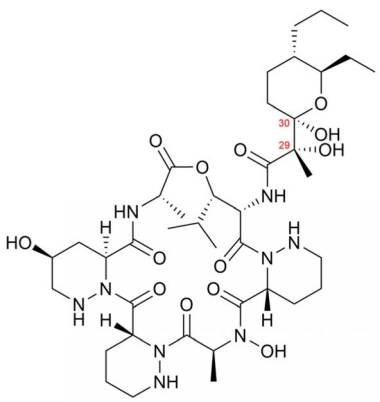

Fig. 80 Structure of dentigerumycin (**131**).

2.5.2. General aspects of ECD calculations for absolute configuration estimations. The determination of absolute configurations in natural products through ECD techniques has advanced with the application of time-dependent density functional theory(TDDFT) calculations.[107] Computational models allow researchers to predict ECD spectra, which can then be compared with experimental data to confirm the absolute configurations of natural products.

The process begins by identifying the potential conformers of the compound. This step is typically performed using Monte Carlo methods in combination with molecular mechanics (such as MMFF94) or semi-empirical approaches (*e.g.*, AM1) to estimate the relative energies of the conformers. Once identified, these conformers are further optimized using DFT techniques. In the next step, UV/ECD TDDFT calculations are performed on the optimized conformers using computational software such as Gaussian, TURBOMOLE, or NWChem.[107–109] The UV/ECD spectra of each individual conformer are then averaged using Boltzmann statistics to generate the final calculated ECD spectrum. The accuracy of these calculations depends on the choice of basis sets and functionals. Larger basis sets typically provide more accurate results but require more computational time. The level of ECD calculation is expressed as a combination of the functional and basis set used, indicating the methods employed at each stage. The TDDFT calculations yield key parameters, including excitation energies, oscillator strengths, and rotatory strengths. Oscillator strengths simulate the UV spectrum, while rotatory strengths are used to generate the ECD spectrum. The calculated rotatory strength values are converted into ECD curves using either a Gaussian or Lorentzian distribution function.

2.5.3. Case studies of ECD calculations. Spirosnuolides A–D (**132–135**), 18-membered macrolides characterized as a unique [6,6]-spiroketal structure, were identified from *Kitasatospora* sp. INHA29, a strain isolated from a termite nest (Fig. 81).[110] Among these four polyketides, the absolute configuration of compound **133** was solved by ECD calculation. A conformational analysis of compound **133** was conducted using MacroModel, integrated with Maestro. The study employed the Merck molecular force field (MMFF94) in the gas phase and a mixed torsional/low-mode sampling approach, applying a 20 kJ mol^{-1} energy cutoff, which identified 21 conformers. These conformers were subsequently optimized geometrically using DFT calculations with TmoleX 4.3.2 and Turbomole. The

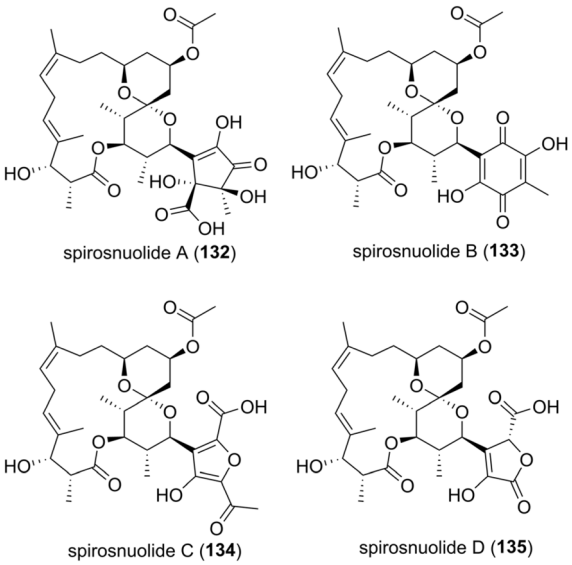

Fig. 81 Structures of spirosnuolides A–D (**132–135**).

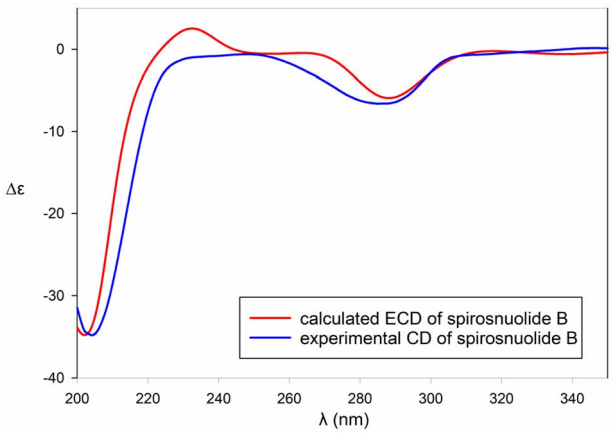

Fig. 82 Experimental ECD and calculated ECD spectra of spirosnuolide B (**133**).

optimization utilized the def-SV(P) basis set for all atoms and the B3LYP functional in the gas phase. From this, eight conformers with a Boltzmann population exceeding 1% were selected for ECD calculations. Simulated ECD spectra were generated using the TD-DFT method at the CAM-B3LYP/def2-TZVP level. Boltzmann-weighted ECD curves were produced with SpecDis 1.71 software, applying a sigma/gamma value of 0.24 eV and a UV correction of +20 nm to align with the experimental results. By comparing the experimental ECD spectrum with calculated ECD spectrum of compound **133**, its configuration was successfully determined (Fig. 82).[110]

In piceamycin (**52**) mentioned in Section 2.3.2,[72] the stereochemistry of the unprotonated C8 carbon of the cyclopentenone remained undetermined. Due to the inability to chemically derivatize this chiral centre for stereochemical analysis, ECD calculations were employed. To determine the stereochemistry, three-dimensional models representing the two possible

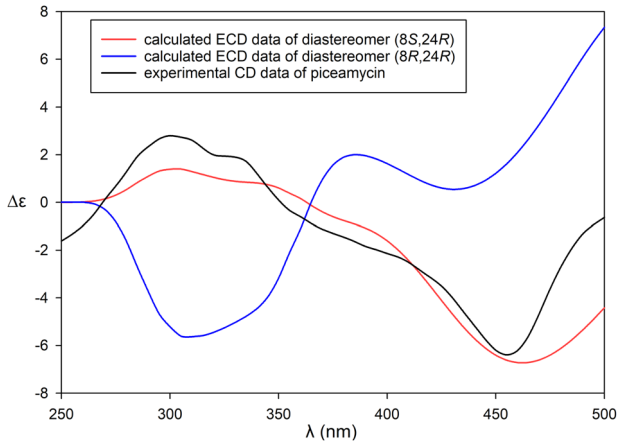

Fig. 83 Experimental ECD of piceamycin (**52**) and calculated ECD spectra of two possible diastereomers (8*S*/24*R* and 8*R*/24*R*).

diastereomers (8*S*/24*R* and 8*R*/24*R*) were constructed, and ECD spectra were calculated for both. The experimental ECD spectrum of piceamycin revealed a positive Cotton effect at 300 nm and a negative Cotton effect at 455 nm. Notably, the calculated ECD spectrum for the 8*S*/24*R* diastereomer closely matched the experimental data (Fig. 83). This alignment suggests that the C8 configuration of piceamycin is *S*.[72]

(+)-Phorbasides A (**136a**) and B (**136b**) are two macrolides structurally related to the rare callipeltosides, such as (−)-callipeltoside A (**137**). These compounds were isolated from a sponge of the *Phorbas* genus in Western Australia (Fig. 84).[111]

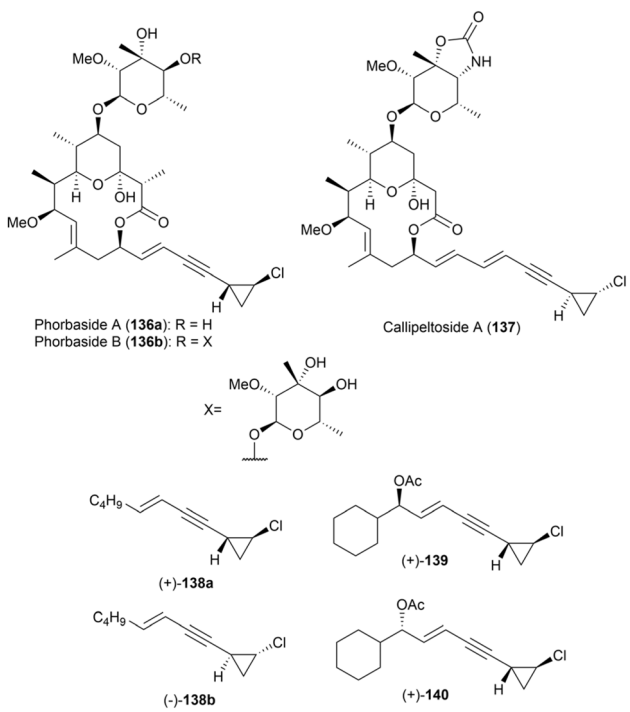

Fig. 84 Structures of (+)-phorbasides A and B (**136a** and **136b**), (−)-callipeltoside A (**137**), and synthesized enantiomeric models ((+)-**138a**, (−)-**138b**, (+)-**139**, and (+)-**140**).

The authors conducted a comprehensive configuration analysis of **136a** and **136b** using semi-quantitative CD analysis, leveraging the Cotton effect (CE) caused by hyperconjugation between the cyclopropyl ring's σ-like bonds and the extended ene-yne π system. This method revealed that the configuration of the *trans*-chlorocyclopropane ring in **136a** and **136b** is opposite to that in **137**.

The CD spectra of **136a** and **136b** are nearly identical, exhibiting a pronounced positive CE [λ_{max} 232 ($\Delta\varepsilon$ +9.1), 241 (+8.1)] and vibronic fine structure associated with the asymmetrically perturbed ene-yne chromophore. A red shift in the UV spectrum of **136a**, attributed to significant hyperconjugation with the chlorocyclopropane ring, supported these findings. The authors hypothesized that the sign of the CE would depend on the configurations of both the adjacent *trans*-chlorocyclopropane ring and the C13 acyloxy substituent.

To determine the configurations at C18 and C19 in **136a** and **136b**, the authors synthesized enantiomeric models (+)-**138a** and (−)-**138b** with defined chirality at the chlorocyclopropane rings (Fig. 84). CD spectral analysis confirmed that the observed CE arises from the asymmetry of the ene-yne chlorocyclopropane chromophore. The CE of **138a** aligned with that of (+)-**138a** and opposed that of (−)-**138b**. The acyloxy substituent at C13 affected the magnitude but not the sign of the CE, as demonstrated using models (+)-**139** and (+)-**140**. Consequently, the complete macrolide configurations of **136a** and **136b** were assigned as (2*S*, 3*S*, 5*S*, 6*R*, 7*R*, 8*R*, 9*R*, 13*R*, 18*R*, and 19*S*).

The stereochemical determination of long-chain natural product lipids is particularly challenging, especially for those with multiple hydroxy groups, such as caylobolide A, derived from the cyanobacterium *Lyngbya majuscula*.[112] These lipids, common in polyketides and glycolipids, present significant difficulties in elucidating the relative configurations of isolated stereogenic centres. Polyketides often contain segments with different glycol architectures (1,3-, 1,5-, or even 1,7-glycols), adding complexity to stereochemical analysis.

Several methodologies have been employed to resolve the configurations of 1,2- and 1,3-glycols, including ^{13}C NMR data analysis, exciton coupling circular dichroism (ECCD), *J*-based analysis, and the use of universal NMR databases. However, in acyclic chains or macrocyclic polyketides, hydroxy groups separated by four or more carbon–carbon (C–C) bonds often fail to provide meaningful configurational information through NMR or CD spectral properties. For example, the CD spectra of acyclic 1,5-glycol diarylcarboxylate esters in isotropic solutions typically show only baseline signals.

The authors proposed a solution involving the pre-alignment of long-chain lipids through partial ordering within the lipid bilayers. This approach allows for non-averaged orientations of chromophore charge-transfer dipole moments, facilitating the long-range transmission of stereochemical information within 1,n-glycol lipids (where n = 5, 7, and 9). The resulting data provide insights into the relative and absolute configurations of glycol molecules by analysing ECCD signals from their derived porphyrin carboxylate diesters encapsulated in submicrometer-sized liposomes.

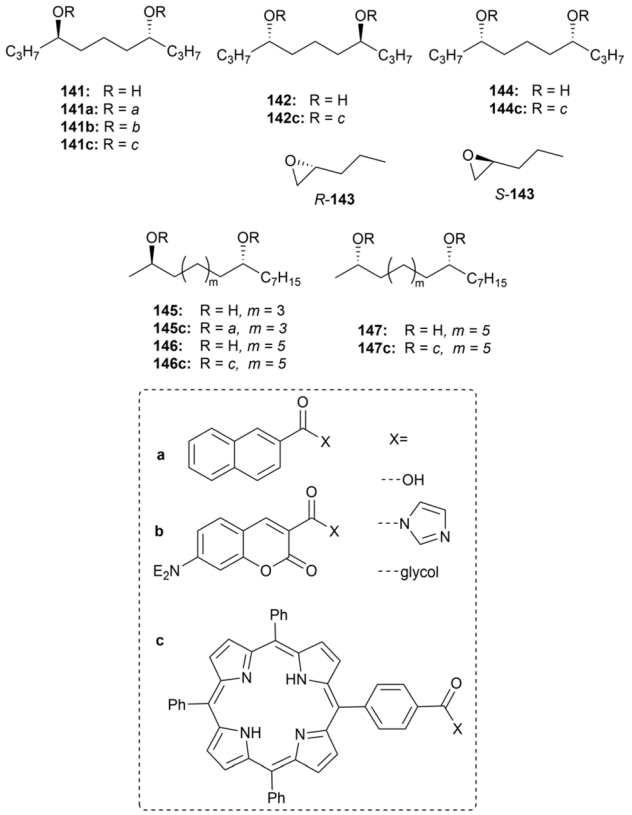

Fig. 85 Model glycols, esters, and chromophores.

A model study was conducted to validate the principles of ECCD. Enantiomeric C2-symmetric glycols, specifically (*R*, *R*)-**141** and (*S*, *S*)-**142**, with over 99% enantiomeric excess, were synthesized from (*R*)- and (*S*)-1,2-epoxypentane (Fig. 85). The *meso*-isomer, **144**, was separated from a by-product mixture through subsequent chemical reactions. These stereoisomers were acylated with carboxylic acids or *N*-acylimidazoles to yield purified diesters (**141a–c**, **142c**, and **144c**) (Fig. 85).

CD measurements revealed that (*R*, *R*)-**141a–c** in methanol or (*R*, *R*)-**141a–b** in liposomes produced baseline spectra. However, (*R*, *R*)-**141c** in liposomes displayed a pronounced positive bisignate signal owing to exciton coupling, with a λ_{max} of 430 nm and an intensity of +52. In contrast, the enantiomer (*S*, *S*)-**142c** exhibited a bisignate CD spectrum with inverted signs and magnitudes relative to (*R*, *R*)-**141c**. Conversely, the *meso*-**144c** ester produced only a baseline signal.

The signs of the bisignate CD spectra correlated with the extended conformational helicity of the lipid chains, highlighting the relationship between the observed CD signals and the helicity of the electric transition dipole moments of the coupled chromophores. The ECCD of (*R*, *R*)-**144c** exhibited nonlinear concentration dependence, with optimal signal detection occurring around 1 μM and a detection sensitivity of approximately 40 pmol. The authors also explored the distance dependence of ECCD in TPP diesters of acyclic 1,*n*-glycols. They observed that diastereomeric glycols with hydroxy groups at positions n = 7 (compound **145**) and n = 9 (compound **146**) adopted *anti* (pseudo-*C*2 symmetric) configurations, whereas the

glycol with $n = 9$ in compound **147** exhibited a *syn* (*pseudomeso*) arrangement. The CD spectra of (*R*, *R*)-**145c** and (*R*, *R*)-**146c** displayed strong positive bisignate signals with specific *A* values of 51 and 27, respectively. These signals decreased linearly with increasing *n* and the distance between ester oxygens, which was estimated to be around 10 Å for $n = 9$. In contrast, the *pseudomeso* form (**147c**) exhibited only a baseline signal. Based on linear extrapolation from their findings, the authors suggested that the ECCD detection limit could extend to $n = 13$, with an estimated interatomic distance of approximately 15 Å, as predicted by Chem3D modeling. In summary, the study demonstrated that ECCD signals in TPP diesters of acyclic 1,*n*-glycols are strongly dependent on the anti (*pseudo-C*2 symmetric) configuration of the glycols. The intensity of these signals decreases linearly with increasing interatomic distance, while the *pseudomeso* configuration produces only baseline signals.

The determination of the complete stereochemical structure of (−)-sagittamide A (**148**), a novel polyacetoxy long-chain α,ω-dicarboxylic acid extracted from a tropical didemnid tunicate, was challenging (Fig. 86).[113] Initial analyses using conventional 2D NMR techniques allowed for partial stereochemistry assignments. While the configurations of the terminal amino acids, L-ornithine and L-valine, were straightforward to identify, the central hexol region (C5–C10) posed significant challenges due to complex stereochemistry and difficulties in interpreting *J* couplings.

To address these challenges, the researchers employed a progressive-convergent methodology that combined three advanced techniques for comprehensive stereochemical analysis. First, *J*-based analysis predicted an all-*anti* configuration for C6–C9, narrowing the possible diastereomers from 32 to 4. Next, Kishi's universal database was used to compare the ^{13}C NMR chemical shifts of sagittamide A against predefined stereo-structured models (**149a–149h**) (Fig. 86).

The final step involved ECCD to determine the absolute stereochemistry. Molinsiki's group generated hexaol diastereomers corresponding to specific configurations (**149e** and **149f**) and converted them into per-benzoate ester derivatives (**150**, **151**, and **152**) (Fig. 86). CD spectra of these derivatives revealed opposite Cotton effects for compounds **150** and **151**, indicating that the absolute configuration of (−)-sagittamide A corresponds to the configuration of *ent*-**148**. Additionally, the authors validated their findings by comparing the CD spectra of *ent*-**151** with that of L-ribose, which provided a reliable reference point for confirming the stereochemical assignments. The relationship established between *ent*-**151** and the known structure of L-ribose helped validate their stereochemical assignments. Based on these analyses, they determined the complete configuration of (−)-sagittamide A as (5*S*, 6*S*, 7*S*, 8*R*, 9*R*, 10*S*).

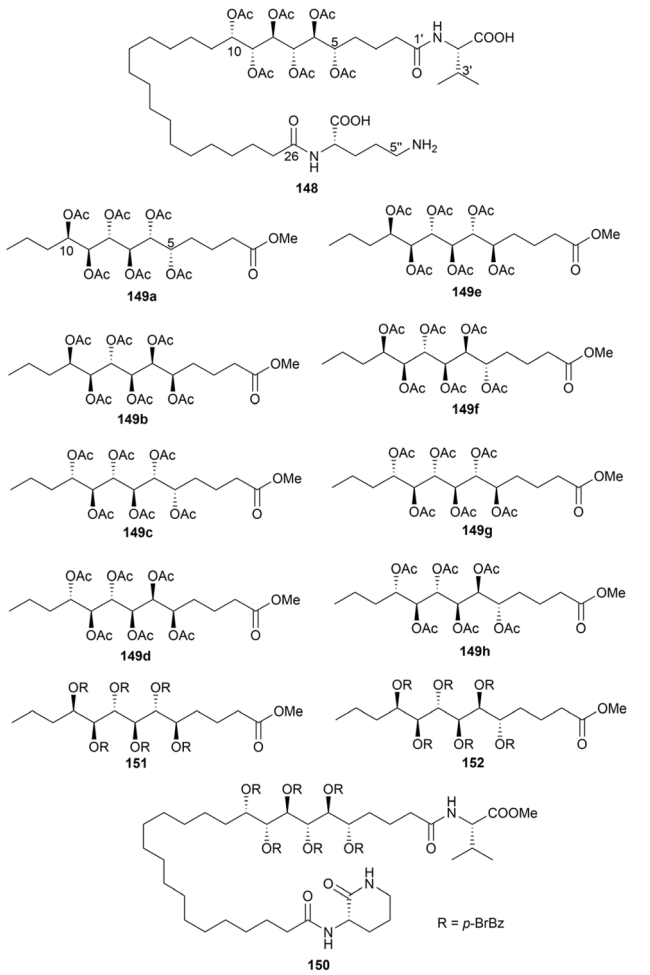

Fig. 86 Structures of (−)-sagittamide A (**148**), stereo-structured models **149a–149h**, and the per-benzoate ester derivatives (**150**, **151**, and **152**).

3. Conclusions and perspectives

The exploration of configurational analysis methods for type-I PKS-derived natural products remains a fundamental area of research in natural product chemistry. This review highlights a variety of strategies for determining stereochemistry, including JBCA, chemical derivatizations using auxiliary chiral reagents, chemical degradations, NMR chemical shift comparisons with universal databases, and chiroptical properties coupled with quantum mechanics-based calculations applied to type-I polyketides. Case studies illustrate the practical applications of these methodologies, emphasizing their importance in accurately determining absolute and relative configurations, which provides critical insights into the stereochemical structures of type-I PKS-derived natural products.

While current methodologies are highly effective, challenges persist. Complex natural products, particularly certain type-I PKS-derived polyketides, can pose significant difficulties, including low production yields, chemical instability, or the presence of unique functional groups for which established methods are unavailable. Looking forward, integrating chemical and spectroscopic techniques while accounting for the limitations of each method will provide more reliable and definitive stereochemical analysis. On the other hand, as bioinformatics analysis of polyketide synthases for configurational assignments, which can be complementary to chemical and spectroscopic analysis, continues to evolve,[114,115] reviewing the recent analysis of type-I polyketide BGCs in respect to

stereochemistry is required to address recent advancements and emerging challenges in this rapidly growing field. Complete stereochemical elucidation of bioactive type-I PKS-derived natural products will enable to provide accurate targets for total synthesis and enhance their potential applications in pharmaceutical development.

4. Data availability

No primary research results, software or code have been included, and no new data were generated or analysed as part of this review.

5. Author contributions

D.-C. O., H. C., S.-J. N., and K. M. participated in conceptualization. J. C., P. F. H., G. J. K. and T. T. M. B. were responsible for manuscript writing and preparation of graphical content. All authors participated in manuscript revising and editing.

6. Conflicts of interest

There are no conflicts to declare.

7. Acknowledgements

This work was supported by the National Research Foundation of Korea grants funded by the Republic of Korean Government (Ministry of Science and ICT) (RS-2024-00352229, NRF-2020R1A6A1A03044512, 2021R1A2C1010727, 2021R1C1C1009609, 2022R1A2C1011848, and 2022R1A4A3022401).

8. Notes and references

1 A. R. Carroll, B. R. Copp, R. A. Davis, R. A. Keyzers and M. R. Prinsep, *Nat. Prod. Rep.*, 2023, **40**, 275–325.
2 D. O'Hagan, *Nat. Prod. Rep.*, 1993, **10**, 593–624.
3 A. T. Keatinge-Clay, *Nat. Prod. Rep.*, 2012, **29**, 1050–1073.
4 C. Hertweck, *Angew. Chem., Int. Ed.*, 2009, **48**, 4688–4716.
5 T. R. Hoye, C. S. Jeffrey and F. Shao, *Nat. Protoc.*, 2007, **2**, 2451–2458.
6 W.-S. Li, Z. Luo, Y.-L. Zhu, Y. Yu, J. Wu and L. Shen, *Mar. Drugs*, 2020, **18**, 590–603.
7 N. Matsumori, D. Kaneno, M. Murata, H. Nakamura and K. Tachibana, *J. Org. Chem.*, 1999, **64**, 866–876.
8 M. Karplus, *J. Chem. Phys.*, 1959, **30**, 11–15.
9 G. Bifulco, P. Dambruoso, L. Gomez-Paloma and R. Riccio, *Chem. Rev.*, 2007, **107**, 3744–3779.
10 C. Nilewski, R. W. Geisser, M. O. Ebert and M. Erick, *J. Am. Chem. Soc.*, 2009, **131**, 15866–15876.
11 H. Choi, E. Mevers, T. Byrum, F. A. Valeriote and W. H. Gerwick, *Eur. J. Org. Chem.*, 2012, **2012**, 5141–5150.
12 C. Bassarello, G. Bifulco, A. Evidente, R. Riccio and L. Gomez-Paloma, *Tetrahedron Lett.*, 2001, **42**, 8611–8613.
13 C. Campagnuolo, C. Fattorusso, E. Fattorusso, A. Ianaro, B. Pisano and O. Taglialatela-Scafati, *Org. Lett.*, 2003, **5**, 673–676.
14 A. R. Pereira, T. Byrum, G. M. Shibuya, C. D. Vanderwal and W. H. Gerwick, *J. Nat. Prod.*, 2010, **73**, 279–283.
15 A. Aiello, E. Fattorusso, C. Imperatore, P. Luciano, M. Menna and R. Vitalone, *Mar. Drugs*, 2012, **10**, 51–63.
16 C. Dalvit and G. Bovermann, *Magn. Reson. Chem.*, 1995, **33**, 156–159.
17 K. Scott, J. Keeler, Q. N. Van and A. J. Shaka, *J. Magn. Reson.*, 1997, **125**, 320–324.
18 W. P. Aue, J. Karhan and R. R. Ernst, *J. Chem. Phys.*, 1976, **64**, 4226–4227.
19 K. Nagayama, P. Bachmann, K. Wuthrich and R. R. Ernst, *J. Magn. Reson.*, 1978, **31**, 133–148.
20 U. Piantani, O. W. Sørensen and R. R. Ernst, *J. Am. Chem. Soc.*, 1982, **104**, 6800–6801.
21 A. L. Davis, E. D. Laue, J. Keeler, D. Moskau and J. Lohman, *J. Magn. Reson.*, 1991, **94**, 637–644.
22 C. Griesinger, O. W. Sørensen and R. R. Ernst, *J. Am. Chem. Soc.*, 1985, **107**, 6394–6396.
23 C. Griesinger, O. W. Sørensen and R. R. Ernst, *J. Chem. Phys.*, 1986, **85**, 6837–6852.
24 C. Griesinger, O. W. Sørensen and R. R. Ernst, *J. Magn. Reson.*, 1987, **75**, 474–492.
25 M. Kurz, P. Schmieder and H. Kessler, *Angew. Chem., Int. Ed.*, 1991, **30**, 1329–1331.
26 W. Kozminski and D. Nanz, *J. Magn. Reson.*, 1997, **124**, 383–392.
27 A. Meissner and O. W. Sørensen, *Magn. Reson. Chem.*, 2001, **39**, 49–52.
28 S. Gil, J. F. Espinosa and T. Parella, *J. Magn. Reson.*, 2011, **213**, 145–150.
29 K. E. Kövér, V. J. Hruby and D. Uhrín, *J. Magn. Reson.*, 1997, **129**, 125–129.
30 J. Boyd, N. Soffe, B. John, D. Plant and R. Hurd, *J. Magn. Reson.*, 1992, **98**, 660–664.
31 A. Ross, M. Czisch, C. Ciselar and T. A. Holak, *J. Biomol. NMR*, 1993, **3**, 215–224.
32 G. W. Vuister, J. Ruiz-Cabello and P. C. M. Van Zijl, *J. Magn. Reson.*, 1993, **100**, 215–220.
33 V. V. Krishnamurthy, *J. Magn. Reson., Ser. A*, 1996, **121**, 33–41.
34 C. P. Butts, B. Heise and G. Tatolo, *Org. Lett.*, 2012, **14**, 3256–3259.
35 J. Sauri and T. Parella, *Magn. Reson. Chem.*, 2012, **50**, 717–721.
36 J. S. An, J. Y. Lee, E. Kim, H. Ahn, Y.-J. Jang, B. Shin, S. Hwang, J. Shin, Y. J. Yoon, S. K. Lee and D.-C. Oh, *J. Nat. Prod.*, 2020, **83**, 2776–2784.
37 F. Annang, G. Pérez-Moreno, V. González-Menéndez, R. Lacret, I. Pérez-Victoria, J. Martín, J. Cantizani, N. de Pedro, D. Choquesillo-Lazarte, L. M. Ruiz-Pérez, D. González-Pacanowska, O. Genilloud, F. Vicente and F. Reyes, *Org. Lett.*, 2020, **22**, 6709–6713.
38 M. C. Kim, H. Machado, K. H. Jang, L. Trzoss, P. R. Jensen and W. Fenical, *J. Am. Chem. Soc.*, 2018, **140**, 10775–10784.

39 M. Simone, S. Maffioli, A. Tocchetti, S. Tretter, M. Cattaneo, I. Biunno, E. Gaspari and S. Donadio, *J. Antibiot.*, 2015, **68**, 406–408.
40 S. X. Huang, X. J. Wang, Y. Yan, J. D. Wang, J. Zhang, C. X. Liu, W. S. Xiang and B. Shen, *Org. Lett.*, 2012, **14**, 1254–1257.
41 D.-G. Kim, K. Moon, S.-H. Kim, S.-H. Park, S. Park, S. K. Lee, K.-B. Oh, J. Shin and D.-C. Oh, *J. Nat. Prod.*, 2012, **75**, 959–967.
42 K. Moon, J. Cui, E. Kim, E. S. Riandi, S. H. Park, W. S. Byun, Y. Kal, J. Y. Park, S. Hwang, D. Shin, J. Sun, K.-B. Oh, S. Cha, J. Shin, S. K. Lee, Y. J. Yoon and D.-C. Oh, *Org. Lett.*, 2020, **22**, 5358–5362.
43 R. H. Contreras and J. E. Peralta, *Prog. Nucl. Magn. Reson. Spectrosc.*, 2000, **37**, 321–425.
44 I. E. Ndukwe, A. Brunskill, D. R. Gauthier Jr, Y. L. Zhong, G. E. Martin, R. T. Williamson, M. Reibarkh and Y. Liu, *Org. Lett.*, 2019, **21**, 4072–4076.
45 P. Cimino, G. Bifulco, A. Evidente, M. Abouzeid, R. Riccio and L. Gomez-Paloma, *Org. Lett.*, 2002, **4**, 2779–2782.
46 M. Menna, C. Imperatore, A. Mangoni, G. D. Sala and T. S. Orazio, *Nat. Prod. Rep.*, 2019, **36**, 476–489.
47 T. Kusumi, T. Ooi, Y. Ohkubo and T. Yabuuchi, *Bull. Chem. Soc. Jpn.*, 2006, **79**, 965–980.
48 J. A. Dale and H. S. Mosher, *J. Am. Chem. Soc.*, 1968, **90**, 3732–3738.
49 J. M. Seco, E. Quiñoá and R. Riguera, *Chem. Rev.*, 2004, **104**, 17–118.
50 M. J. Rieser, Y. H. Hui, J. K. Rupprecht, J. F. Kozlowski, K. V. Wood, J. L. McLaughlin, P. R. Hanson, Z. Zhuang and T. R. Hoye, *J. Am. Chem. Soc.*, 1992, **114**, 10203–10213.
51 T. Takeuchi, M. Hatano, M. Umekita, C. Hayashi, S. Wada, M. Nagayoshi, R. Sawa, Y. Kubota, M. Kawada, M. Igarashi and M. Shibasaki, *Org. Lett.*, 2017, **19**, 4207–4210.
52 M. Chinworrungsee, P. Kittakoop, M. Isaka, P. Maithip, S. Supothina and Y. Thebtaranonth, *J. Nat. Prod.*, 2004, **67**, 689–692.
53 T. H. Quang, D. C. Kim, P. V. Kiem, C. V. Minh, N. X. Nhiem, B. H. Tai, P. H. Yen, N. Ngan, H. J. Kim and H. Oh, *J. Anibiot.*, 2018, **71**, 826–830.
54 Y. Igarashi, H. Ogura, K. Furihata, N. Oku, C. Indananda and A. Thamchaipenet, *J. Nat. Prod.*, 2011, **74**, 670–674.
55 J. Park, Y.-H. Shin, S. Hwang, J. Kim, D. H. Moon, I. Kang, Y.-J. Ko, B. Chung, H. Nam, S. Kim, K. Moon, K.-B. Oh, J.-C. Cho, S. K. Lee and D.-C. Oh, *Angew. Chem., Int. Ed.*, 2024, **63**, e202402465.
56 T. Yabuuchi and T. Kusumi, *J. Org. Chem.*, 2000, **65**, 397–406.
57 K. Sasaki, M. Satake and T. Yasumoto, *Biosci., Biotechnol., Biochem.*, 1997, **61**, 1783–1785.
58 B. Reguera, M. García-Portela, E. Velasco-Senovilla, P. Rial, L. Escalera, P. A. Díaz and F. Rodríguez, *Front. Protistol.*, 2024, **1**, 1328026.
59 G. Yu, P. Sun, R. Aierken, C. Sun, Z. Zhang, Q. Che, G. Zhang, T. Zhu, Q. Gu, M. Li and D. Li, *Mar. Life Sci. & Technol.*, 2021, **4**, 237–244.
60 J. H. Im, S. Oh, E. S. Bae, S. Um, S. K. Lee, Y. H. Ban and D.-C. Oh, *J. Ind. Microbiol. Biotechnol.*, 2023, **50**, 1–10.
61 J. M. Seco, E. Quiñoá and R. Riguera, *Tetrahedron: Asymmetry*, 2001, **12**, 2915–2925.
62 K. M. Blazewska and T. Gajda, *Tetrahedron: Asymmetry*, 2009, **20**, 1337–1361.
63 S. K. Latypov, J. M. Seco, E. Quinoa and R. Riguera, *J. Org. Chem.*, 1995, **60**, 504–515.
64 S. Saito, Y. Xiaohanyao, T. Zhou, J. Nakajima-Shimada, E. Tashiro, D. W. Triningsih, E. Harunari, N. Oku and Y. Igarashi, *J. Nat. Prod.*, 2022, **85**, 1697–1703.
65 S. Porto, J. M. Seco, J. F. Espinosa, E. Quiñoá and R. Riguera, *J. Org. Chem.*, 2008, **73**, 5714–5722.
66 J. M. Seco, E. Quiñoá and R. Riguera, *Chem. Rev.*, 2012, **112**, 4603–4641.
67 T. F. Molinski and B. I. Morinaka, *Tetrahedron*, 2012, **68**, 9307–9343.
68 C. Imperatore, P. Luciano, A. Aiello, R. Vitalone, C. Irace, R. Santamaria, J. Li, Y.-W. Guo and M. Menna, *J. Nat. Prod.*, 2016, **79**, 1144–1148.
69 I. R. G. Thistlethwaite, F. M. Bull, C. Cui, P. D. Walker, S.-S. Gao, L. Wang, Z. Song, J. Masschelein, R. Lavigne, M. P. Crump, P. R. Race, T. J. Simpson and C. L. Willis, *Chem. Sci.*, 2017, **8**, 6196–6201.
70 Y. Morishita, H. Zhang, T. Taniguchi, K. Mori and T. Asai, *Org. Lett.*, 2019, **21**, 4788–4792.
71 Y.-H. Shin, J. Y. Beom, B. Chung, Y. Shin, W. S. Byun, K. Moon, M. Bae, S. K. Lee, K.-B. Oh, J. Shin, Y. J. Yoon and D.-C. Oh, *Org. Lett.*, 2019, **21**, 1804–1808.
72 Y.-H. Shin, S. Kang, W. S. Byun, C.-W. Jeon, B. Chung, J. Y. Beom, S. Hong, J. Lee, J. Shin, Y.-S. Kwak, S. K. Lee, K.-B. Oh, Y. J. Yoon and D.-C. Oh, *J. Nat. Prod.*, 2020, **83**, 277–285.
73 J. Shen, Y. Fan, G. Zhu, H. Chen, W. Zhu and P. Fu, *Org. Lett.*, 2019, **21**, 4816–4820.
74 P. G. Williams, E. D. Miller, R. N. Asolkar, P. R. Jensen and W. Fenical, *J. Org. Chem.*, 2007, **72**, 5025–5034.
75 R. Suo, K. Takada, H. Kohtsuka, Y. Ise, S. Okada and S. Matsunaga, *J. Nat. Prod.*, 2018, **81**, 1108–1112.
76 S. Rychnovsky, B. Rogers and T. Richardson, *Acc. Chem. Res.*, 1998, **31**, 9–17.
77 H. C. Kwon, C. A. Kauffman, P. R. Jensen and W. Fenical, *J. Org. Chem.*, 2009, **74**, 675–684.
78 K. Oguchi, M. Tsuda, R. Iwamoto, Y. Okamoto, J. Kobaysashi, E. Fukushi, J. Kawabata, T. Ozawa, A. Masuda, Y. Kitaya and K. Omasa, *J. Org. Chem.*, 2008, **73**, 1567–1570.
79 S. Hoshino, M. Okada, T. Wakimoto, H. Zhang, F. Hayashi, H. Onaka and I. Abe, *J. Nat. Prod.*, 2015, **78**, 3011–3017.
80 H. C. Kwon, C. A. Kauffman, P. R. Jensen and W. Fenical, *J. Am. Chem. Soc.*, 2006, **128**, 1622–1632.
81 J. Lee, Y. Kobayashi, K. Tezuka and Y. Kishi, *Org. Lett.*, 1999, **1**, 2181–2184.
82 D. Menche, *Nat. Prod. Rep.*, 2008, **25**, 905–918.
83 H. Seike, I. Ghosh and Y. Kishi, *Org. Lett.*, 2006, **8**, 3861–3864.

84 Y. Kobayashi, C. H. Tan and Y. Kishi, *Helv. Chim. Acta*, 2000, **83**, 2562–2571.
85 Y. Kobayashi, J. Lee, K. Tezuka and Y. Kishi, *Org. Lett.*, 1999, **1**, 2177–2180.
86 G. Kretzschmar, M. Krause and R. Lajos, *Tetrahedron*, 1997, **53**, 971–986.
87 Y. Kobayashi, C. H. Tan and Y. Kishi, *Angew. Chem., Int. Ed.*, 2000, **39**, 4279–4281.
88 C. H. Tan, Y. Kobayashi and Y. Kishi, *Angew. Chem., Int. Ed.*, 2000, **39**, 4282–4284.
89 Y. Kobayashi, N. Hayashi and Y. Kishi, *Org. Lett.*, 2002, **4**, 411–414.
90 Y. Kobayashi, N. Hayashi and Y. Kishi, *Tetrahedron Lett.*, 2003, **44**, 7489–7491.
91 M. Bae, K. Moon, J. Kim, H. J. Park, S. K. Lee, J. Shin and D.-C. Oh, *J. Nat. Prod.*, 2016, **79**, 332–339.
92 H. Nishida, X. H. Huang, H. Tomoda and S. Omura, *J. Antibiot.*, 1992, **45**, 1669–1676.
93 C. M. Adams, I. Ghosh and Y. Kishi, *Org. Lett.*, 2004, **6**, 4723–4726.
94 I. Ghosh, Y. Kishi, H. Tomoda and S. Omura, *Org. Lett.*, 2004, **6**, 4719–4722.
95 D. K. Nielsen, L. L. Nielsen, S. B. Jones, L. Toll, M. C. Asplund and S. L. Castle, *J. Org. Chem.*, 2009, **74**, 1187–1199.
96 S. G. Smith and J. M. Goodman, *J. Am. Chem. Soc.*, 2010, **132**, 12946–12959.
97 I. Paterson, S. M. Dalby, J. C. Roberts, G. J. Naylor, E. A. Guzmán, R. Isbrucker, T. P. Pitts, P. Linley, D. Divlianska, J. K. Reed and A. E. Wright, *Angew. Chem., Int. Ed.*, 2011, **50**, 3219–3223.
98 I. Paterson, K. K. H. Ng, S. Williams, D. C. Millican and S. M. Dalby, *Angew. Chem., Int. Ed.*, 2014, **53**, 2692–2695.
99 C. Rink, V. Navickas and M. E. Maier, *Org. Lett.*, 2011, **13**, 2334–2337.
100 J. Willwacher, N. Kausch-Busies and A. Fürstner, *Angew. Chem., Int. Ed.*, 2012, **51**, 12041–12046.
101 A. E. Wright, J. C. Botelho, E. Guzman, D. Harmody, P. Linley, P. J. McCarthy, T. P. Pitts, S. A. Pomponi and J. K. Reed, *J. Nat. Prod.*, 2007, **70**, 412–416.
102 S. Hwang, B. E. Heo, T. Q. Nguyen, Y. J. Kim, S. G. Lee, T. H. Huynh, E. Kim, S. I. Jo, M. J. Baek, E. K. Shin, J. Oh, C. Park, Y. J. Yoon, E. J. Park, K. T. Kim, S. Ryoo, D. G. Lee, C. Wood, M. Woo, D. D. Kim, S. Paik, E. K. Jo, J. Jang and D.-C. Oh, *Angew. Chem., Int. Ed.*, 2025, **64**, e202412994.
103 M. O. Marcarino, S. Cicetti, M. M. Zanardi and A. M. Sarotti, *Nat. Prod. Rep.*, 2022, **39**, 58–76.
104 A. Howarth and J. M. Goodman, *Chem. Sci.*, 2022, **13**, 3507–3518.
105 L. D. Bari, G. Pescitelli, C. Pratelli, D. Pini and P. Salvadori, *J. Org. Chem.*, 2001, **66**, 4819–4825.
106 D.-C. Oh, M. Poulsen, C. R. Currie and J. Clardy, *Nat. Chem. Biol.*, 2009, **5**, 391–393.
107 A. E. Nugroho and H. Morita, *J. Nat. Med.*, 2014, **68**, 1–10.
108 X.-C. Li, D. Ferreira and Y. Ding, *Curr. Org. Chem.*, 2010, **14**, 1678–1697.
109 G. Bringmann, T. Bruhn, K. Maksimenka and Y. Hemberger, *Eur. J. Org Chem.*, 2009, **17**, 2717–2727.
110 T.-H. Huynh, S. C. Jang, Y. H. Ban, E.-Y. Lee, T. Kim, I. Kang, J. S. An, S. Kang, J. Han, Y. Kwon, D. Oh, H.-G. Park, J.-C. Cho, J. Jang, K.-B. Oh, S.-J. Nam, S. K. Lee and D.-C. Oh, *JACS Au*, 2024, **4**, 4821–4832.
111 C. K. Skepper, J. B. Macmillan, G.-X. Zhou, M. N. Masuno and T. F. Molinski, *J. Am. Chem. Soc.*, 2007, **129**, 4150–4151.
112 J. B. MacMillan and T. F. Molinski, *J. Am. Chem. Soc.*, 2004, **126**, 9944–9945.
113 S. C. Lievens and T. F. Molinski, *J. Am. Chem. Soc.*, 2006, **128**, 11764–11765.
114 D. H. Kwan and F. Schulz, *Molecules*, 2011, **16**, 6092–6115.
115 A. T. Keatinge-Clay, *Nat. Prod. Rep.*, 2016, **33**, 141–149.

